

AFIT/GE/ENG/99M-26

ANTENNA GAIN ENHANCEMENT USING A PHOTONIC
BAND GAP REFLECTOR

THESIS

Karl C. Schloer, Captain, USAF

AFIT/GE/ENG/99M-26

Approved for public release; distribution unlimited

J 19990413 087 3

REPORT DOCUMENTATION PAGE			Form Approved OMB No. 0704-0188	
Public reporting burden for this collection of information is estimated to average 1 hour per response, including the time for reviewing instructions, searching existing data sources, gathering and maintaining the data needed, and completing and reviewing the collection of information. Send comments regarding this burden estimate or any other aspect of this collection of information, including suggestions for reducing this burden, to Washington Headquarters Services, Directorate for Information Operations and Reports, 1215 Jefferson Davis Highway, Suite 1204, Arlington, VA 22202-4302, and to the Office of Management and Budget, Paperwork Reduction Project (0704-0188), Washington, DC 20503.				
1. AGENCY USE ONLY (Leave blank)		2. REPORT DATE March 1999		3. REPORT TYPE AND DATES COVERED Master's Thesis
4. TITLE AND SUBTITLE ANTENNA GAIN ENHANCEMENT USING A PHOTONIC BAND GAP REFLECTOR			5. FUNDING NUMBERS	
6. AUTHOR(S) Karl C. Schloer, Captain, USAF				
7. PERFORMING ORGANIZATION NAME(S) AND ADDRESS(ES) Air Force Institute of Technology 2950 P Street WPAFB OH 45433-7765			8. PERFORMING ORGANIZATION REPORT NUMBER AFIT/GE/ENG/99M-26	
9. SPONSORING/MONITORING AGENCY NAME(S) AND ADDRESS(ES) Dr. Stephen W. Schneider AFRL/SNRP 2241 Avionics Circle Suite 16 WPAFB OH 45433-7318 (937) 255-6127 x4230			10. SPONSORING/MONITORING AGENCY REPORT NUMBER	
11. SUPPLEMENTARY NOTES Advisor: Peter J. Collins, Major, USAF (937) 255-6565 x4304 e-mail: Peter.Collins@afit.af.mil				
12a. DISTRIBUTION AVAILABILITY STATEMENT Approved for public release; distribution unlimited			12b. DISTRIBUTION CODE	
13. ABSTRACT (Maximum 200 words) Scientists have long known that periodic structures can filter electromagnetic (EM) waves. In the last decade, extension of one- and two-dimensionally periodic structures into a third periodic dimension has produced photonic band gap (PBG) structures. A PBG structure is characterized by its omnidirectional stop band at a set of frequencies determined by the structure's periodicity and permittivity. In the present research, we investigate such a structure as an antenna reflector. We aim to develop a modeling approach that provides accurate computations of PBG behavior without relying on massively parallel processing. We also construct and measure the bulk reflection and transmission properties of a PBG structure, then use it as a planar reflector for a two-arm spiral antenna. We measure the same antenna's radiation properties when mounted above an absorber loaded cavity and a conducting ground plane to determine whether the PBG reflector provides gain enhancement. This comparison of a PBG reflector's performance against standard mounts for a practically useful broadband antenna is unique in PBG research.				
14. SUBJECT TERMS Photonic Band Gap, Photonic Crystal, High Gain Antenna, Antenna Reflector, Periodic Structure, Frequency Selective Surface, PARANA, Finite Element Method, Computational Electromagnetics			15. NUMBER OF PAGES 118	
			16. PRICE CODE	
17. SECURITY CLASSIFICATION OF REPORT Unclassified	18. SECURITY CLASSIFICATION OF THIS PAGE Unclassified	19. SECURITY CLASSIFICATION OF ABSTRACT Unclassified	20. LIMITATION OF ABSTRACT UL	

The views expressed in this thesis are those of the author and do not reflect the official policy or position of the Department of Defense or the U.S. Government.

ANTENNA GAIN ENHANCEMENT USING A PHOTONIC BAND GAP REFLECTOR

THESIS

Presented to the faculty of the Graduate School of Engineering
of the Air Force Institute of Technology

Air University

In Partial Fulfillment of the
Requirements for the Degree of
Master of Science

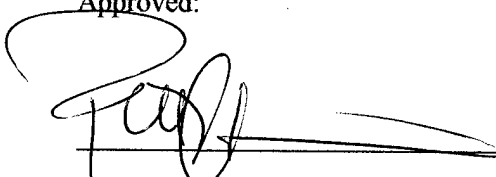
Karl C. Schloer, B. S.
Captain, USAF

March, 1999

ANTENNA GAIN ENHANCEMENT USING A PHOTONIC BAND GAP REFLECTOR

Karl C. Schloer, B. S.
Captain, USAF

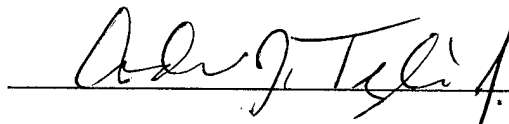
Approved:



Chairman

11 MAR 99

Date



Member

11 Mar 99

Date



Member

11 Mar 99

Date

Acknowledgements

My sincere gratitude goes to my advisor, Major Peter J. Collins, whose enthusiasm for this topic often provided the motivation needed to overcome setbacks. His unfailing willingness to answer questions and provide guidance and assistance was an invaluable asset on more occasions than I want to admit. I also thank the other members of my committee, Dr. Vittal P. Pyati and Dr. Andrew J. Terzuoli, for their time and input as the project evolved.

Thanks are also due to my sponsor, Dr. Stephen W. Schneider, for providing extensive material support and asking challenging questions throughout the process. Mr. Jim Mudd and Dr. John Mehr were also vital allies. Without them, I would have been unable to construct, mount, or measure the antenna and reflector combinations. I also could not have measured bulk properties without the expertise and assistance of Dr. John Schultz and Mr. Stan Bashore at AFRL/XPB.

Accolades for customer service go out to Russell M. Hastings, Condie L. Inman, and Jan A. LeValley of the AFIT Model Shop, who always responded to unreasonable student work requests with a smile and an excellent product delivered quickly. Similar recognition goes to Mr. Rick Patton of the AFIT Microwave and Observables Laboratories for his continuing support with the tools, workbenches, and other details in which the devil usually resides.

For repeatedly serving as sounding boards and idea filters, I thank Captains Grayson Cochran, Matt Craig, Bob Eigel, and Art Ford.

Finally, the most important person I need to thank is my wife, Trina Roberts-Schloer. No new bride ever endured being a 'school widow' better than she.

Karl C. Schloer

Table of Contents

<u>Acknowledgements</u>	iii
<u>List of Figures</u>	vii
<u>List of Tables</u>	ix
<u>Abstract</u>	x
<u>I. Introduction</u>	1
<u>II. Background</u>	3
Basic Theory and Categories of PBG Structures	4
Waves in Periodic Media	4
Early Development and the First PBG Structure	5
Metallic PBG Structures and Wire Meshes	9
The Effective Reflection Plane Concept	13
Effective Medium Theory and the Plasma Frequency	15
Metallodielectric PBG Structures	17
PBG Structures for Radio Frequency Antenna Applications	20
PBG Materials as Planar Antenna Substrates	21
PBG Materials as Antenna Reflectors	23
<u>III. Methodology</u>	28
Review of Research Goals	28
Designing the PBG Reflector	29

Antenna	29
Qualitative Choices - Development of Hybrid Design.....	30
Quantitative Choices - Design Parameters.....	32
Material Selection.....	32
Pattern Dimensions.....	36
Fabrication Procedure and Final Product.....	37
Computational Approach.....	38
Desktop Design: I-DEAS & PARANA	38
Test & Measurement.....	40
Reflection/Transmission Measurement Setup	40
Antenna Patterns.....	43
<u>IV. Results</u>	47
'Desktop Design' Process	47
Modeling and Design Portability (I-DEAS)	47
Computational EM (PARANA).....	48
Focused Arch Measurements	50
First Variable: Frequency	51
Second Variable: Incident Angle	53
Third Variable: Polarization (TE vs. TM)	55
Antenna Patterns.....	57
Ground Plane.....	57
Absorber Loaded Cavity.....	57
PBG Reflector.....	59
<u>V. Analysis & Conclusions</u>	60
'Desktop Design' Approach.....	60
Reflection & Transmission Analysis.....	61

Band Edge/Cutoff Frequency	61
Polarization Effects	62
Effective Reflection Plane Analysis	64
Antenna Gain Pattern Analysis.....	69
Conclusions.....	70
<u>VI. Suggestions for Further Work</u>	72
Characterization and Refinement of the AFIT PBG Structure	72
Defect Studies	72
Effective Reflection Plane Engineering	73
Method of Assembly.....	73
Minimum Size Requirement	74
Antenna Type and Mounting.....	74
Computational Electromagnetics	75
<u>Appendix A. Reflection/Transmission Data</u>	76
<u>Appendix B. Antenna Pattern Cuts</u>	87
<u>Appendix C. Gain Enhancement Contours</u>	91
<u>Appendix D. Effective Reflection Plane Analysis</u>	94
<u>Bibliography</u>	101
<u>Vita</u>	106

List of Figures

Figure 1. Yablonovite - First Successfully Fabricated PBG Structure	8
Figure 2. Metallic PBG Structure Fabricated from Printed Circuit Boards	11
Figure 3. UCLA Metallodielectric Photonic Crystal	19
Figure 4. Geometry for Poilasne's Reflection Plane Analysis	26
Figure 5. Two-Arm Spiral Antenna Used in Present Work	29
Figure 6. AFIT Photonic Crystal Design	32
Figure 7. Leung's Diamondlike PBG Crystal	33
Figure 8. GTRI Focused Arch Measurement System	41
Figure 9. Top View of Focused Arch System	42
Figure 10. Vacuum Bagging Schematic for Focused Arch Measurements	43
Figure 11. Antenna Test Body Configuration for PBG Reflector Measurements	44
Figure 12. Geometry for Azimuth and Elevation Angles	51
Figure 13. AFIT PBG Structure in Transmission, Normal Incidence, Various Polarizations	52
Figure 14. AFIT PBG Structure in Reflection, Normal Incidence, Various Polarizations	53
Figure 15. Effects of Changing Incident Angle with Constant Azimuth and TE Polarization	54
Figure 16. Effects of Changing Incident Angle with Constant Azimuth and TM Polarization	55
Figure 17. Effects of Changing Polarization with Constant Incident Angle	56
Figure 18. Ground Plane Backed Antenna Pattern, 90° Azimuth, TE Polarized	58
Figure 19. Absorber Loaded Cavity Backed Antenna Pattern, 0° Azimuth, TE Polarized	58
Figure 20. PBG Reflector Backed Antenna Pattern, 45° Azimuth, TE Polarization	59
Figure 21. AFIT Photonic Crystal Without Vias, Showing First 2 1/2 Layers of Atoms	63

Figure 22. SCHERPA Output for Normal Incidence, Zero Azimuth, Vertical Polarization.....	65
Figure 23. Comparison of SCHERPA Prediction with Measured Relative Gain at Normal Incidence.....	67
Figure 24. Contour Plots of PBG Reflector Performance.....	68

List of Tables

Table 1. Reflection Properties Test Matrix	42
Table 2. Antenna Pattern Test Matrix	46
Table 3. PARANA Solution Performance on UCLA MDPC Design.....	49

Abstract

Scientists have long known that periodic structures can filter electromagnetic (EM) waves. In the last decade, extension of one- and two-dimensionally periodic structures into a third periodic dimension has produced photonic band gap (PBG) structures. A PBG structure (PBGS) is characterized by its omnidirectional stop band at a set of frequencies determined by the structure's periodicity and permittivity. In the present research, we investigate such a structure as an antenna reflector. We aim to develop a modeling approach that provides accurate computations of PBG behavior without relying on massively parallel processing. We also construct and measure the bulk reflection and transmission properties of a PBGS, then use it as a planar reflector for a two-arm microstrip spiral antenna. We measure the same antenna's radiation properties when mounted above an absorber-loaded cavity and a conducting ground plane to determine whether the PBG reflector provides gain enhancement. This comparison of a PBG reflector's performance against other mounts for a practically useful broadband antenna is unique in PBG research.

ANTENNA GAIN ENHANCEMENT USING A PHOTONIC BAND GAP REFLECTOR

I. Introduction

In 1987, a laser researcher at Bell Communications Research (Bellcore) suggested that an artificial analog of a natural crystal structure might function as an omnidirectional spatial filter for EM radiation (Yablonovitch, 1987). Since then, researchers from such disparate backgrounds as quantum physics, computational electromagnetics, materials science, and electrical engineering have come to collaborate in the development of a growing subject known as photonic band gap, or PBG, engineering. Simply defined, a PBG crystal is a man-made object with a periodic structure such that it prevents the propagation of certain EM modes in all possible directions within its bulk. It can be dielectric, metallic, or a mix of both. Properly designed, it can have the same degree and type of controllability for EM wave propagation that a doped semiconductor has for electronic propagation.

Such a structure could clearly have a host of uses. Any application requiring a broad, uniform, omnidirectional frequency stop band is a candidate application for a PBG structure (PBGS). In the radio frequency (RF) arena, applications might include antenna substrates and reflectors, radomes, waveguides, high-Q cavities, and various low observable applications.

In the present work, we investigate the use of a PBGS as a planar RF antenna reflector. Our practical goal is twofold. First, develop a design and modeling procedure that allows the PBG problem to be kept at the workstation level without relying on parallel computing resources

to get accurate results. Second, construct, measure, and install a PBG structure that enhances a practical antenna's gain across multiple octaves. We follow a standard approach to this problem, beginning with an introduction to the basic theory and a survey of the relevant work performed to date. We then detail our research goals and our methods for accomplishing them, including a discussion of the design process itself. After a top-level review of our major results, we proceed to a more detailed analysis of the finer points demonstrated in our work. A final review of the useful lessons from our research leads to notes on potential areas for further study.

In the course of this research, we break with the majority of PBG research and focus our measurement efforts on reflected magnitude and phase information rather than just transmitted magnitude. This decision comes from the requirement that we accurately characterize the complex reflected fields in order to develop a PBG reflector of practical interest.

Throughout this work, several terms are used interchangeably. Photonic crystal, photonic band gap structure (PBGs), and PBG material are among the most frequently used, and the reader should not be confused by the varied terms. We provide further explanation in any cases where a change in terminology is significant.

II. Background

While active research into PBG structures developed only in the last decade, the theory predicting the existence of PBGs will be familiar to researchers in fields as diverse as crystallography, optics, and radome design. This is because the PBG problem is a matter of solving the macroscopic Maxwell's equations for wave propagation in periodic media. Indeed, the first hypothesis describing PBG behavior referred to an "electromagnetic band gap" rather than a photonic band gap (Yablonovitch, 1987: 2059). One wonders whether the original usage -had it survived - might have promoted more 'crosstalk' between the physicists performing most early PBG research and the microwave engineers who, it now appears, will likely see the first practical PBG applications.

The mathematical description of the PBG problem is this: media with periodic changes in potential impose periodic boundary conditions on propagating EM modes. Electromagnetic waves not matched to those boundary conditions cannot propagate. This holds true for interactions between x-rays and crystals, visible light and multilayer films, or microwaves and periodic dielectrics. Thus, the underlying mathematical problem is one that has been addressed in several other fields; Yablonovitch identifies work in 1914 on the dynamic theory of x-ray diffraction as the earliest antecedent to modern photonic band theory (Yablonovitch, 1993:286). One can even argue that the broad familiarity of the concepts underlying PBG design has accelerated progress in the field by allowing a synergy to develop between researchers with very different backgrounds. Presumably, the U.S. Army Research Office wanted such an effect when it established a Multidisciplinary University Research Initiative (MURI) for Photonic Band

Engineering. The results have clearly shown that PBG materials present unique opportunities, with at least ten PBG-related patents issued in the United States since 1992 (Moore *et al.*, 1997:1; U.S. Army Research Office, 1999:6).

This chapter consists of two major sections. In the first, we deal with the theory and broad categories of PBG materials and structures. We start with a very brief description of wave motion in periodic media. We then trace the evolution of PBG structures from the proposal of their existence in 1987 to the fabrication of the first, all-dielectric, photonic crystals. We then introduce the next type of photonic crystal, the metallic PBG (MPBG) structure, and discuss three important aspects of its analysis: the effective reflection plane, effective medium theory, and the plasma frequency. We close the first half of the chapter with a description of a third and final category, metallodielectric photonic crystals (MDPC). The second half of the chapter explores the state of the art in development of PBG materials for microwave and millimeter-wave antenna applications, covering both planar antenna substrates and antenna reflectors. This sequence provides the reader the framework for understanding the present work. The reader should note that while existing PBG literature uses both empirical and purely theoretical approaches, this work emphasizes the former type. This is because ours is primarily 'engineering' research, with an emphasis on construction and characterization of an experimental structure. For the reader more interested in the mathematical-theoretical aspects of PBG research, works described below as 'theoretical' or 'mathematical' provide good starting points for a broader literature review.

Basic Theory and Categories of PBG Structures

Waves in Periodic Media. Brillouin's work in the 1940s demonstrated that a periodic lattice imposes restrictions on energies propagating within it (Brillouin, 1946). His

approach was to begin with familiar one-dimensional problems and extend them to two and three dimensions, demonstrating in each case that certain basic requirements exist for wave propagation. While Brillouin focused on mechanical waves in crystal lattices and analogous frequency domain behavior of electric filters, some of his fundamental concepts relate directly to the PBG problem. First, he determined that only frequencies with an appropriate relationship to the lattice constant could propagate through the medium. Specifically, the allowed frequencies f are restricted to values satisfying a periodic function F such that $f = F(k)$ with F having a period of $1/a$, where a is the lattice spacing and k is the wavenumber (*ibid.*:18). While the above result is from the one-dimensional derivation, the same result applies in expanded form for two or three dimensions. Second, he introduced the notion that all possible wave vectors could be reduced to equivalent vectors contained within the "fundamental interval" or unit cell of the lattice. The most common explanation of this reduction relies on a transformation to reciprocal space (a concept carried over from solid state physics and crystallography) and is beyond the scope of this work. The reader seeking such a detailed explanation is referred to Joannopoulos (1995:112-114). Finally, Brillouin noted that frequencies outside the pass bands of a given filter (mechanical or electrical) decay exponentially within the medium (*ibid.*:25).

Early Development and the First PBG Structure. Since Brillouin's time, the notion of a 'band gap' of forbidden energies has become a familiar part of solid state physics. Physicists, materials scientists, and electrical engineers have made an art of engineering electronic band gaps to tailor materials to various applications (Solymar and Walsh, 1988). In optics, one-dimensionally periodic multilayer structures of alternating high and low dielectric constant are the basis for antireflection coatings and Fabry-Perot filters (Hecht, 1987:368-378). In the late 1980s, Eli Yablonovitch, working at Bell Communications Research (Bellcore),

hypothesized that macroscopic dielectric structures with a periodic variation in electrical permittivity could exhibit band gaps of forbidden frequencies:

In wave optics, layered structures (interference coatings) in which the index of refraction alternates from high to low every quarter wavelength have also become indispensable. The periodic spatial modulation opens up a forbidden gap in the electromagnetic dispersion relation, at least for light propagating perpendicular to the layers. . . We can anticipate, then, that full three-dimensional spatial periodicity of $\lambda/2$ in the refractive index can result in a forbidden gap in the electromagnetic spectrum near the wavelength λ *irrespective of propagation direction*, just as the electronic spectrum has a band gap in crystals. (Yablonovitch, 1987:2059)

Yablonovitch examined the symmetry groups of natural crystals to find potentially useful lattice structures. His early work focused on the face-centered cubic (fcc) structure because it has the most nearly spherical Brillouin zone (BZ) of any lattice. This maximizes the probability of finding a band gap which "overlaps" all the zone's surfaces in reciprocal space (Yablonovitch, 1993: 286). The BZ is the region of reciprocal space that is closer to a given reciprocal lattice point than to any other reciprocal lattice point. By developing a structure with a band gap over the entire BZ in reciprocal space, one also achieves a band gap in all possible propagation directions in real space. The PBG literature refers to such an omnidirectional band gap as a 'complete' band gap. Fortunately, the present research does not require any detailed use or understanding of reciprocal lattices or BZs. While important in the theoretical development of PBG structures, they are beyond the scope of this research and the interested reader is referred elsewhere for more thorough treatments (Bouckaert *et al.*, 1936; Brillouin 1946:131-139; Joannopoulos *et al.*, 1995:112-120).

While initial experimental results appeared promising (Yablonovitch and Gmitter 1989), independent calculations eventually showed that the fcc lattice did not possess a complete band gap (Leung and Liu 1990, Zhang and Satpathy 1990). By accounting for the vector nature of EM

fields rather than relying on scalar wave approximations, both groups independently determined that along two specific propagation directions, the fcc lattice showed a symmetry-induced degeneracy between two pass bands. This was qualitatively equivalent to discovering a semiconductor with no energy gap in certain directions, and indicated that the fcc lattice might not be the best choice for PBG structures.

As a next step, researchers sought another lattice with the desirable BZ shape of the fcc lattice but with a symmetry group different enough to remove the fcc degeneracies. They settled on the diamond lattice, which is actually two interpenetrating fcc lattices and hence has exactly the same BZ. In late 1990, both theory and experiment turned up structures that did possess complete band gaps. Ho, Chan, and Soukoulis, at Ames Laboratory and Iowa State University, were first to publish calculations showing that a diamond lattice structure should possess a complete gap with a fractional bandwidth as high as 28.8% (Ho *et al.*, 1990). Almost simultaneously, Yablonovitch, Gmitter, and Leung were measuring a complete band gap with a fractional bandwidth of 19% in a modified fcc structure with nonspherical 'atoms' at the lattice positions (Yablonovitch *et al.*, 1991). They lifted the symmetry-induced fcc degeneracy by altering the symmetry of the atoms themselves. They first masked the top surface of a dielectric slab with a triangular array of holes, then drilled through each hole three times at 35.26° off normal and with a 120° spacing in azimuth (Figure 1). The result was a fcc array of odd-shaped voids or air "atoms" that has since been dubbed "Yablonovite" (Joannopoulos *et al.*, 1995:81).

Yablonovitch *et al.* next explored the effects of introducing various defects into a PBG structure (Yablonovitch *et al.*, 1991b). They found effects similar to those associated with donor and acceptor defects in a semiconductor, introducing narrow bands of allowed modes within the band gap. These results, combined with their earlier work, allowed them to describe the following

basic properties of all-dielectric photonic crystals. First, the forbidden gap of a lattice with lattice constant a is centered on a frequency f_0 proportional to c/a , where c is the speed of light. The size of a dielectric photonic crystal is therefore dictated by the desired stop band location. Second, in-gap modes decay exponentially with increasing depth into the structure, exactly as predicted by Brillouin. This has the convenient side effect that PBG attenuation can typically be expressed in terms of dB per unit cell. Third, lattice defects can introduce localized modes within the

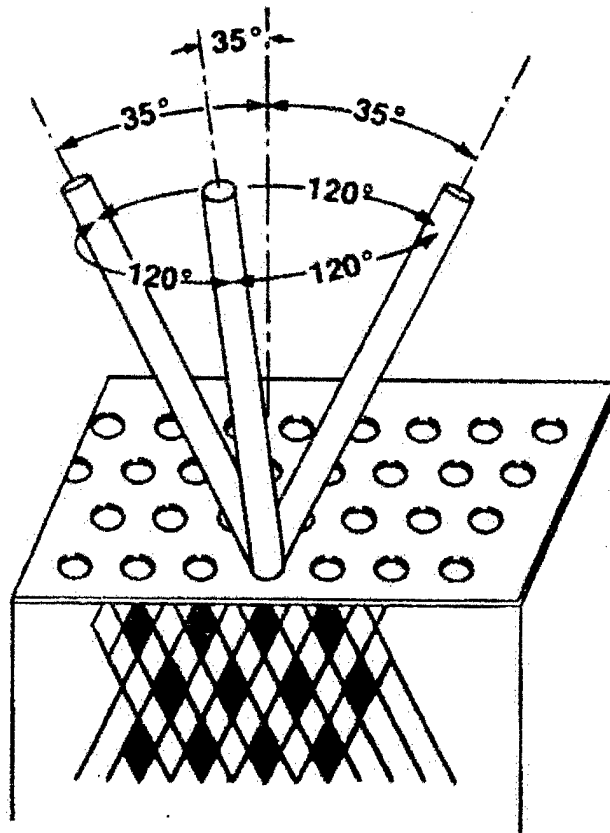


Figure 1. Yablonovite - First Successfully Fabricated PBG Structure
(reproduced from Yablonovitch *et al.*, 1991a:2296)

forbidden gap. In a thin enough PBG, or for a series of defects, this can allow frequency-selective propagation through the structure even within the forbidden gap.

More work, primarily dealing with dielectric PBG structures and aimed at optical and laser applications, followed quickly from a broad spectrum of researchers. Within 14 months, the scope of research warranted publication of a survey article in Optics & Photonics News and a special feature of 18 articles in the Journal of the Optical Society of America B (Everitt 1992, Bowden *et al.*, 1993). These consisted of a mix of both application- and theory-oriented research, with the bulk of the applications still aimed at lasers. In less than six years, PBG study had passed from pure theory into development of multiple applications.

Metallic PBG Structures and Wire Meshes. One of the challenges in developing PBG structures for use at optical and infrared (IR) wavelengths is the difficulty of fabricating structures at such small sizes. PBG applications in the microwave regime, on the other hand, have almost the opposite problem. Here, while easy to fabricate, the PBGS must be unreasonably large to accomplish the field rejection levels most applications require. Özbay *et al.* have pointed out that with a typical rejection of 3-4 dB per layer, an all-dielectric photonic crystal would need to be around 10 layers thick to achieve a 40 dB depth in the stop band. Furthermore, an all-dielectric PBGS with a stop band at 2 GHz would need to be about a meter square (Özbay *et al.*, 1996:3797). This problem arises from the fundamental requirement that an all-dielectric PBGS have a lattice constant on the order of one wavelength at the desired center frequency. These size considerations and the weight problems they imply have been major factors in the decision to develop metallic PBG structures.

By 1996, several articles had reported both theoretical and experimental results of metallic PBG (MPBG) research. Sigalas *et al.* at Ames Lab/Iowa State reported calculations indicating that a 3D MPBG structure would show qualitatively different stop band behaviors depending on the topology of the scatterers (Sigalas *et al.*, 1996). Specifically, a "cement"

topology of isolated metallic scatterers exhibited behavior similar to a dielectric PBG structure, with stop bands related to the electrical size of the unit cell. For a "network" scattering topology however, the 3D structures exhibited a cutoff frequency, f_c , below which calculations indicated the MPBG structure would have near zero transmission. Furthermore, increasing the lattice constant led to a decreasing absorption of EM energy so that they predicted essentially lossless behavior at radio frequencies. Their results indicated that for cylindrical rods in simple cubic and diamond lattices with lattice constant a , f_c fell at $0.44 c/a$ and $0.7 c/a$, respectively. Thus, stop band behavior could be obtained at a low operating frequency f_0 with a metallic photonic crystal having f_c well above f_0 and thus having a much smaller unit cell than would be required for an all-dielectric PBGS. Even allowing for the use of many unit cells in each direction, this could allow a significant size reduction compared with dielectric photonic crystals.

The same group of researchers published experimental results for a 2D metallic PBG design the following year (McCalmont *et al.*, 1996). Their design consisted of stacked metallic grids in a dielectric medium, fabricated by etching the desired grid pattern onto printed circuit boards (PCBs). To an electrical engineer, their design looks much like a resonant metallic radome (Figure 2). The difference is that the MPBG structure is periodic in the z direction and produces a stop band rather than a pass band. Their structure showed stop band transmission 35 dB down from the band edge for a structure only three unit cells thick.

Another point only peripherally addressed in McCalmont *et al.*'s paper is the fact that the cutoff frequency is dependent in part on the permittivity of the dielectric PCB substrate. Specifically, this relates back to our earlier statement that f_c is proportional to the speed of light, c . To state the point explicitly, c is the speed of light *in the medium containing the PBG structure*. This means that the cutoff frequency is proportional to the speed of light in a vacuum, c_0 , divided

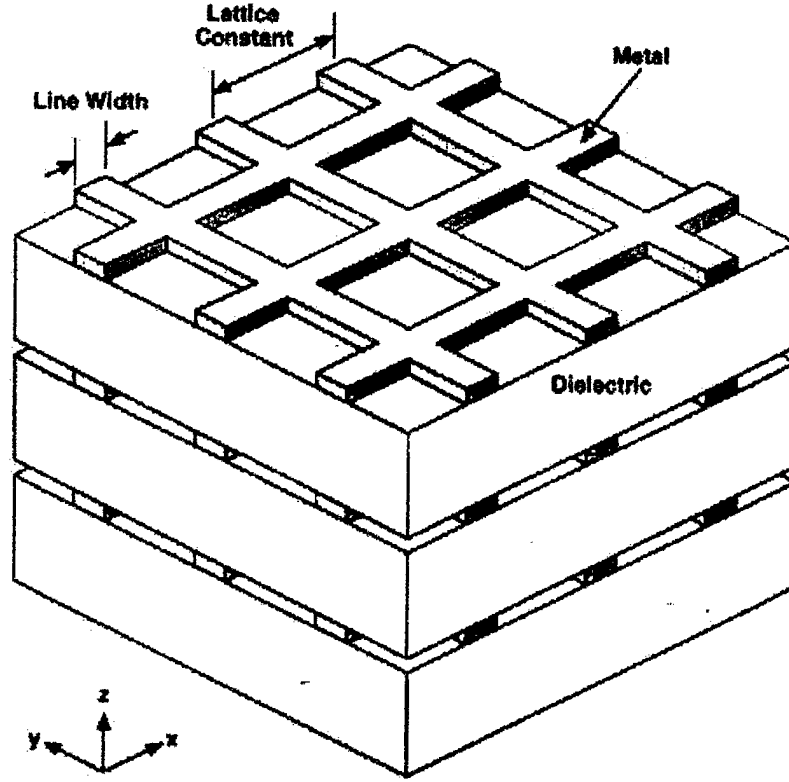


Figure 2. Metallic PBG Structure Fabricated from Printed Circuit Boards
(reproduced from McCalmont *et al.*, 1996:2759)

by the index of refraction of the medium. In practice, this means a designer can achieve the same cutoff frequency in a smaller structure by building the MPBG lattice in a high-permittivity medium. Since we return to this concept later, we summarize it here with the following equation for the cutoff frequency f_c of a metallic PBG structure:

$$f_c = K \frac{c_0}{a\sqrt{\epsilon_r}} \quad (1)$$

where c_0 is the speed of light in vacuum, a is the lattice constant, and ϵ_r is the relative permittivity of the medium. The final term, K , is a proportionality constant accounting for the symmetries of both the lattice and the scattering elements. The reader should note that we have introduced the K parameter as a matter of convenience for comparing different MPBG designs. It is useful as a

figure of merit in low-frequency PBG selection, since a higher K allows a higher cutoff frequency for a given structure size and permittivity. Alternatively, a higher K allows a smaller structure to achieve a given cutoff frequency. While useful for comparing designs with empirically measured cutoff frequencies, K is not a tool for analytically predicting a cutoff frequency. Best viewed in the same light as an automotive mileage rating; it is not readily calculated from first principles, but once measured does provide a comparison between models.

In an experimental analog to Sigalas *et al.*'s 1995 calculations for a diamond network of metallic scatterers, Sievenpiper *et al.* (at UCLA under a relocated Yablonovitch) measured the transmission properties of such a wire mesh (Sievenpiper *et al.* 1996). Their measurements showed a stop band extending from a cutoff frequency of 6.5 GHz down at least to the limit of their reported data at 1 GHz. Sievenpiper and his associates considered this low frequency stop band the dominant electromagnetic feature of the mesh.

Özbay and Temelkuran further extended the body of work on layer-by-layer MPBG crystals in two papers with the Ames Laboratory/Iowa State group. The first of these two papers focused on defect structures in photonic crystals (Özbay *et al.* 1996). The results showed the same low-frequency "metallicity gap" reported in earlier MPBG work. In their layer-by-layer structures, they also showed that a metallic photonic crystal could achieve power rejection levels of 7-8 dB per layer in transmission, a significant improvement over the typical 3-4 dB per layer attenuation associated with all-dielectric designs (Özbay *et al.*, 1996:3798). The second paper (Temelkuran *et al.* 1998) is of greater importance to the present research for two reasons. First, it is one of the few to report reflection magnitude and phase instead of transmission data. In the present research, where we envision using a PBG structure as an antenna reflector, this reflection-

oriented analysis provides a more relevant perspective. Second, the paper uses an "effective reflection plane" analysis of the penetration of EM fields into the PBG structure. Researchers at the Georgia Institute of Technology and the Georgia Tech Research Institute (GTRI) developed this approach, and its importance to our research merits presentation in a separate section here.

The Effective Reflection Plane Concept. Kesler *et al.* originated the effective reflection plane (ERP) concept in 1996 (Kesler *et al.*, 1996); it will appear again in Smith *et al.*, 1999. By measuring the complex electric field reflected from a PBGS, one can extract phase information. Using a perfectly electrically conducting (PEC) plane at the same position as the surface of the PBG provides a phase reference. Calibration with this reference gives data representing the phase accrual in one round trip from the crystal's surface to an effective reflection plane within the PBGS and back to the surface. At normal incidence, the depth L_{eff} of the reflection plane below the crystal's surface as a function of the frequency f and phase ϕ of the reflected field is

$$L_{eff} = \frac{c_0}{2f\sqrt{\epsilon_r}} \left(\frac{\phi - 180^\circ}{360^\circ} \right) \quad (2)$$

where c_0 is the speed of light in vacuum and ϵ_r is the relative permittivity of the crystal (Temelkuran *et al.*, 1998:364). The GTRI group's presentation of the above equation uses complex exponential notation; we have chosen Temelkuran's form for its simplicity and its direct relevance to our own code used in Chapter V.

It is important to note that the ERP concept does not fully describe the scattering from a PBG structure, nor does it pretend to. Rather, it is a simplification describing the total effect of the reflected fields at a particular frequency. When applied to measured data, it effectively sums whatever more complicated scattering processes are at work into a single value for the depth an

EM wave seems to penetrate into the PBG material before reflection. If one is interested in describing the far-field electromagnetic 'appearance' of a PBG material, particularly for measured data, the ERP is a valid description of the bulk material's behavior. If one is instead interested in the details of interaction between layers in the material, as in studies of defect structures, the ERP may not serve so well. This may also be a problem in our research, where the reflector is clearly in the near field of the antenna. With that cautionary statement in mind, we will still use ERP analysis to obtain a rough prediction of the behavior of our PBG reflector.

At normal incidence, placing an antenna a distance $\lambda_0/4$ above a PEC plane causes perfect constructive interference between the direct and reflected wave components at a frequency f_0 . Movement away from normal incidence or to a frequency other than f_0 results in less constructive interference and eventually to destructive interference between direct and reflected waves. For an ideal broadband planar antenna reflector, we must satisfy two requirements: perfect reflection and perfect positioning. Perfect reflection is straightforward; the goal is to double the field strength in the forward direction by recovering the energy initially radiated toward the reflector. Assuming a PBG material is not lossy (i.e., non-absorbing), its near-zero transmission within the band gap implies that it is a nearly perfect reflector. Perfect positioning requires that the reflector move relative to the antenna to maintain quarter-wavelength spacing at frequencies other than f_0 . This requirement is clearly not achievable with a stationary ground plane reflector. A PBG substrate, with its frequency-dependent effective reflection plane, might satisfy this condition. If the effective reflection plane moves at an appropriate rate, it will maintain a quarter-wave spacing over a finite bandwidth, thus providing the broadband field enhancement we seek. Practically, there will be limits on the reflection efficiency, the stop band width, and the ability of the reflection plane to move at precisely the right rate. Still, by matching these parameters reasonably well to the desired values, we should obtain field enhancement over a large fractional bandwidth.

We will return to this discussion and present the necessary condition for broadband gain enhancement in the 'PBG Materials as Antenna Reflectors' section.

Effective Medium Theory and the Plasma Frequency. One additional piece of theoretical material deserves mention here. The 1996 UCLA paper on wire meshes also introduced effective medium theory into photonic crystal analysis (Sievenpiper *et al.*, 1996:2482). This theory predates PBG research by decades, with significant work appearing in the early 1970s (Kirkpatrick, 1971; Vassallo, 1972) which in turn references work from as early as 1935. The research in the 1970s focused on calculating an effective dielectric tensor $\overline{\epsilon_{eff}}$ that accounts for variations in the constitutive properties of inhomogeneous media. To paraphrase Sievenpiper *et al.*, effective medium theory indicates that when $a \ll \lambda$, the wire mesh and surrounding air form an effectively homogeneous medium with a frequency-dependent permittivity $\epsilon_{eff}(f)$. They go on to state that such a medium can have a negative, predominantly real permittivity in the microwave regime. One finds an explicit statement of the functional dependence of ϵ_{eff} on f in Sigalas *et al.* 1995 and Pendry *et al.* 1996. We reproduce it here for reference:

$$\epsilon_{eff}(f) = 1 - \frac{f_p^2}{f(f + i\gamma)} \quad (3)$$

Here, f_p is the "plasma frequency" of the metal and γ is an absorption coefficient. As an explanation, we will now summarize the descriptions of f_p and γ found in Pendry *et al.*, 1996.

Under excitation by a time-varying electric field, the "electron gas" associated with a metal undergoes a collective oscillation called a plasmon; f_p is the frequency of this plasmon. The absorption coefficient describes the dissipation of the plasmon's energy into the metal. For metals, γ is typically orders of magnitude smaller than f_p . This implies that the magnitude of ϵ_{eff} increases

rapidly for decreasing frequency below f_p . Metals tend to have plasma frequencies on the order of thousands of terahertz. Thus, at microwave frequencies of several gigahertz, metals have permittivities with extremely large magnitudes. Such large values, substituted into the equation for the Fresnel reflection coefficient Γ at a metal-air interface,

$$\Gamma = \frac{1 - \sqrt{\epsilon_r}}{1 + \sqrt{\epsilon_r}} \quad (4)$$

yield reflection coefficients on the order of $\Gamma = -0.999 + 0.001j$. This is in effect the electric field reflection coefficient of -1.0 for a PEC, familiar from introductory electromagnetics courses.

Careful consideration of Equation (3) reveals that for frequencies sufficiently far below f_p , the dielectric function becomes predominantly imaginary. In mentioning a predominantly real ϵ_{eff} , Sievenpiper implicitly assumes that the wire mesh's plasma frequency has been lowered several orders of magnitude from its normal value. Pendry differs on this subject, arguing that reducing the plasma frequency to such a degree requires the large self-inductance of extremely thin wires. If correct, Pendry's argument implies that the MPBG cutoff frequency is not analogous to a plasma frequency. Sievenpiper acknowledges this possibility by stating that f_c may instead be analogous to the cutoff frequency in a metallic waveguide. Sigalas' group used a similar waveguide model for first-order approximations of f_c in both 2D and 3D MPBG structures; their results agreed well with their own more rigorous computations (Sigalas *et al.* 1995).

From the preceding discussion, we conclude that effective medium theory provides useful insight on the behavior of wire meshes. The effective medium is intuitively satisfying because of the small electrical size of the mesh in the $a \ll \lambda$ regime. The frequency-dependent dielectric function in Equation (3) produces results consistent with the observed behavior of metals as

microwave reflectors. The question of whether the MPBG cutoff frequency f_c is more analogous to a waveguide cutoff or a plasma frequency remains unanswered.

Metallodielectric PBG Structures. Having reviewed the development of pure dielectric and metallic PBG structures along with some of the relevant theoretical topics, we now encounter the final class of PBG structures: metallodielectric photonic crystals (MDPCs). As the name implies, these structures incorporate both dielectric and metallic components as significant parts of the design. Note that the classification of a photonic crystal as 'metallic' or 'metallodielectric' is arbitrary and may differ between authors. We follow the convention, established by Brown and McMahon in the first published metallodielectric design, that a metallodielectric's "stop band characteristics depend strongly on the [metallic elements] as well as the support dielectric constant" (Brown and McMahon, 1995:2138). For this choice of terminology, PBG structures exhibiting only the 'metallicity gap' below f_c , without a separately tunable lower band edge, are metallic PBG structures, even if the metal resides in a dielectric medium. Hence the circuit-board based design described earlier is classified as a metallic PBG structure even though most of its volume is dielectric (McCalmont *et al.*, 1996:2760). We reserve the 'metallodielectric' designation for band gap structures that use both dielectric and metallic components as integral parts with unique contributions to the stop band behavior.

As mentioned above, Brown and McMahon at MIT Lincoln Laboratory published the first metallodielectric photonic crystal (MDPC) research in 1995. They measured transmission characteristics of metal spheres supported by dielectric in a face-centered-cubic lattice - a simple 'metal atoms, dielectric medium' structure. The two most important aspects of their results were the measured stop band widths and their explanation of the band locations. For a structure less than two unit cells thick, they reported a stop band roughly 10 dB deep and extending from

9 GHz to 22 GHz for a remarkable 84% fractional bandwidth. This eclipsed all previously published results for broad stop bands in PBG structures. The second important result was their conclusion that while the electrical size of the lattice determined the stop band center frequency, the electrical size of the spheres determined the lower band edge. Specifically, they noted that the lower band edge very nearly matched the Mie condition for maximum scattering cross section of a sphere, namely, that $\pi D \approx \lambda$, where D is the sphere diameter and λ is the wavelength in the surrounding medium (Brown and McMahon, 1995:2140).

These results highlighted perhaps the most useful engineering aspect of the MDPC - the ability to independently tune the band edges. This provides control over both band positioning and bandwidth that is absent from the previously discussed PBG structures. In a low observables application, one might use a PBG structure to match the band edges to the desired operating range of a broadband antenna for field enhancement within the stop band. Outside the stop band, the structure could transmit energy into an absorbing medium to reduce radar cross section. Recalling the introduction of donor and acceptor modes into a PBG structure through defect formation (Yablonovitch *et al.*, 1991b), we can now envision MDPCs with a *photonic* band gap controllability that approaches the *electronic* band gap controllability of doped semiconductors. Such media would constitute the revolutionary engineering materials envisioned by some PBG researchers (Everitt, 1992:20; Joannopoulos *et al.*, 1995:94).

Additional Lincoln Lab researchers went on to develop MDPCs that were among the first to demonstrate PBG behavior at infrared wavelengths (McIntosh *et al.*, 1997). These small (4cm^2) structures shared their larger cousins' very broad fractional bandwidth (up to 83%) and independent scattering influences on the upper and lower band edges (*ibid.*:2938).

A third metallodielectric crystal developed at UCLA uses isolated metallic scatterers with strong capacitive coupling through a dielectric medium (Sievenpiper *et al.*, 1998). Printed circuit boards, aligned with their pattern elements (the metallic islands) forming a diamond lattice and separated by thin dielectric films, form the structure (Figure 3). Metallic islands are the 'atoms'

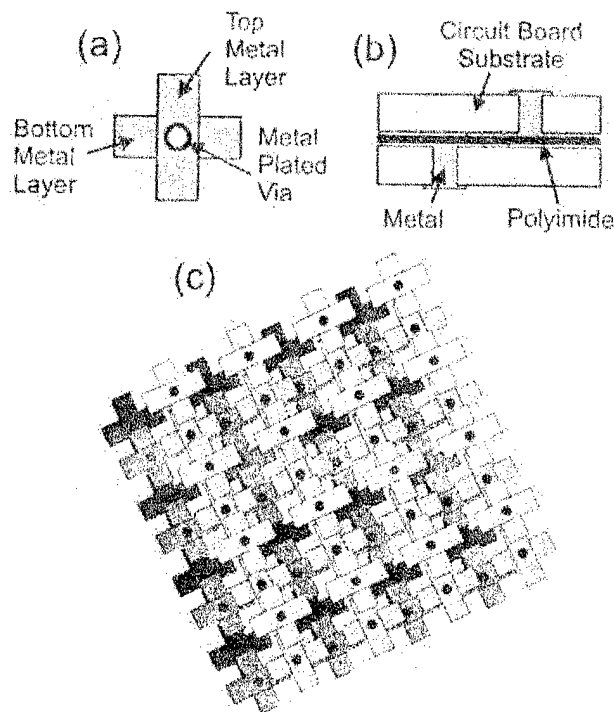


Figure 3. UCLA Metallodielectric Photonic Crystal, Showing (a) Metallic Island, (b) Single Circuit Board Cross-Section, and (c) Stack of Four Circuit Boards Forming One Unit Cell (reproduced from Sievenpiper *et al.*, 1998:2830)

whose spacing determines the upper band edge. Capacitive coupling between islands simulates the carbon-carbon bonds of the diamond structure and is the dominant factor in determining the lower band edge. The lower edge in frequency is given by $1/(LC)^{1/2}$, where L is the inductance and C the capacitance between islands (*ibid.*:2829). This structure exhibits another very broad - 86% fractional bandwidth - stop band, further strengthening the resemblance to the Lincoln Lab

structures' behavior. UCLA has refined the capacitive MDPC design as part of the Photonic Band Engineering MURI's High Impedance Ground Plane project, filing for a U.S. patent and collaborating with four companies to commercially develop such structures (U.S. Army Research Office, 1998).

Metallodielectric photonic crystals are clearly the most advanced PBG structures reported to date. The author is unaware of any other single type or combination of photonic crystals that simultaneously shows such strong rejection per unit cell, extremely wide fractional bandwidth, and independent tunability of the band edges. The aggregation of these characteristics in a single structure presents tantalizing possibilities to the researcher willing and able to explore them.

PBG Structures for Radio Frequency Antenna Applications

Now that the reader is familiar with dielectric, metallic, and metallodielectric PBG structures along with some of the supporting theory, we will review the state of research on using PBG components in radio frequency (RF) antenna systems. We have already alluded to the fact that the PBG idea was born out of semiconductor laser research (Yablonovitch, 1987). A review of the first two major survey articles on the subject reveals that references to laser applications outnumber proposed microwave applications by a margin of better than four to one (Everitt, 1992; Bowden *et al.*, 1993). Ironically, Yablonovitch's first measured band gap was located in the K_u -band (12-18 GHz) because fabrication was most practical at microwave length scales (Yablonovitch *et al.*, 1991a and 1991b). Radio frequency antenna-oriented PBG research began appearing in 1993 and expanded rapidly from 1996 onward. We will now survey this antenna-related research, beginning with the use of PBG substrates for planar antennas and concluding with an examination of PBG structures as antenna reflectors.

PBG Materials as Planar Antenna Substrates. Jasper and Tran provide a succinct statement of the reason for exploring PBG substrates:

Planar antennas fabricated on conventional dielectric substrates . . . are highly inefficient radiators. This inefficiency is due primarily to the fact that the antennas radiate much more efficiently into the dielectric substrate than into air. Energy radiated into the substrate is lost to surface-wave and leaky-wave excitation, which causes coupling to other components of the circuit and generates cross-talk and noise. A PBG substrate is an excellent planar antenna substrate, since radiation is not allowed to couple into the substrate over the band gap, leading to a significant enhancement in radiation efficiency. (Jasper and Tran, 1996:80)

The first major article on antenna applications of PBG materials reported Lincoln Laboratory's use of a planar bow-tie antenna on a photonic crystal substrate fabricated at Bellcore (Brown *et al.*, 1993). The published results showed a dramatic rejection of the antenna radiation from the substrate side of the antenna. The energy dissipated into a uniform dielectric substrate was virtually eliminated when using the PBG substrate. To address the possibility that the difference in radiated power might arise from differing input impedance for the two substrates, the researchers reported power reflected back into the signal generator. They found less than 10% of the power was reflected for the uniform dielectric while about 10% reflection accompanied the PBG substrate. In follow on work, they examined the effects of surface composition and antenna placement on the field pattern of a dipole atop the same type of 'Yablonovite' substrate (Brown *et al.*, 1994). This second experiment showed the same tendency of the PBG substrate to eliminate most of the radiation in the rearward hemisphere. The patterns in the forward hemisphere were significantly different from that of a dipole in free space, with asymmetric spikes appearing in both the E-plane and H-plane patterns. Placing the antenna at different symmetry points on the substrate lattice also changed the patterns, though the authors considered these changes qualitatively minor. The more significant factor was surface composition,

apparently because of the different mode structures supported by the two different surfaces tested (*ibid.*: 3347). After offering the surface mode explanation, the authors still concluded that the problem was "a complex issue involving electromagnetic interaction between metals and dielectrics that may warrant theoretical investigation" (*ibid.*). Next, University of New Mexico researchers joined the Lincoln Lab effort by designing an ultrawideband (UWB) photonic crystal as a possible broadband antenna substrate (Agi *et al.*, 1994). In this work, they stacked three photonic crystals with different but overlapping stop bands to achieve a 44% fractional bandwidth centered on 20.5 GHz. This initial group of three antenna-related experiments indicated that PBG substrates might allow significant gain improvement for planar antennas by overcoming the problem of power loss into a homogeneous substrate. Wideband enhancement also appeared possible, but there were unresolved questions concerning both the effect of a PBG substrate on an antenna's pattern shape and the sensitivity of antenna performance to placement relative to the PBG lattice.

Two years later, despite such concerns, Ellis and Rebeiz at the University of Michigan were the first to report using PBG substrates to improve the commercial viability of a particular type of antenna (Ellis and Rebeiz, 1996). As they pointed out, the tapered slot antenna (TSA) is a form of microstrip antenna usually limited to use on substrates between 0.005 and 0.03λ thick. Throughout much of the millimeter wave band, this results in unreasonably thin substrates. By fabricating the TSA on a dielectric substrate drilled with a hexagonal lattice of holes, Ellis and Rebeiz completely overcame the performance penalties normally associated with mounting a TSA on a thick dielectric substrate. In fact, they also improved antenna directivity by 30%, raised the main beam efficiency 14%, and reduced cross-polarization by 75% compared with a TSA on a normal thin dielectric substrate (*ibid.*: 1159).

In the last two years, researchers at UCLA, the University of California at Irvine, and the University of Illinois have presented both measurements and calculations of the behavior of PBG substrates with simple antennas. Coccioli, Deal, and Itoh used a PBG substrate to achieve a 10 dB reduction in the sidelobes caused by surface waves emanating from a microstrip patch (Coccioli *et al.*, 1998). Yang, Alexopoulos, and Yablonovitch calculated a 15 dB power gain over a narrow angular region for a Hertzian dipole with both PBG substrates and superstrates (Yang *et al.*, 1997). They also noticed significant positioning sensitivity of the antenna relative to the PBG lattice. Further computations of substrate and superstrate combinations with a patch antenna predicted a 2-5 dB peak gain over the same antenna backed by a uniform dielectric loaded cavity (Zhang *et al.*, 1998). Clearly, researchers have decided that PBG structures' transmission characteristics are worth exploring for RF sidelobe and backlobe suppression and gain enhancement in microstrip antennas. This leads naturally to the central question in the present research: Can a PBG used as a broadband reflector compete with existing antenna reflectors?

PBG Materials as Antenna Reflectors. In the previously described work, PBG substrates are integrated directly as the substrates on which microstrip antennas are fabricated. Some researchers have also explored the use of PBG materials as antenna reflectors separated from the radiating element. Such work falls into two broad categories. In the first, completely separate PBG structures serve as planar reflectors for radiating elements. In the second, the PBG reflector and radiating element are both fabricated within the same block of material in a monolithic design.

The 'separate-reflector' category comprises the majority of published work in this area. Kesler *et al.* at GTRI and Georgia Tech published the first significant article on this implementation of a PBG reflector three years ago (Kesler *et al.*, 1996). This work introduced the

effective reflection plane concept. The primary focus was on development and validation of that concept by measuring the patterns generated from dipole antennas placed in front of 2D and 3D dielectric PBG reflectors. Experimental results showed behavior similar to that of the same dipole placed in front of a PEC reflector. These results also agreed well with numerical predictions. This provided an initial validation of the relatively simple ERP model for describing the observable effect of the scattering from a PBG reflector. In work pending publication as of this writing, Smith, Kesler, and Maloney have also used the effective reflection plane model as part of a detailed study of a "woodpile" PBG reflector with a monopole antenna (Smith *et al.*, 1999). This work examines gain, field patterns, and input impedance as functions of frequency and position for the monopole-reflector combination. Both calculation and measurement indicate that the PBG reflector allows a maximum gain of nearly 6 dB relative to the isolated monopole. The ERP model again shows good agreement with more rigorous FDTD calculations. As for the impact of this research on 'real' antennas, Georgia Tech Research Corporation is the assignee for a patent on a complete antenna, reflector, and transmission line system utilizing PBG materials (Moore *et al.*, 1997).

Sigalas *et al.* at Ames Laboratory, already familiar from their work with metallic PBG structures, conducted another pair of experiments exploring the effect of antenna positioning relative to a PBG reflector (Sigalas *et al.*, 1997; Leung *et al.*, 1997). Working with another dielectric layer-by-layer or 'woodpile' PBG structure, they experimented with both dipole and slot antennas. For the dipole, calculation and measurement showed significant improvement in directivity for the dipole with reflector versus the free space dipole. Patterns were, however, strongly dependent on two positioning factors. Antenna height and the resulting phase relation between the direct and reflected waves was one factor. Antenna position in the unit cell and its effect on the dipole interaction with the strongly position-dependent E field at the PBG surface

was the second factor, though its importance decreased as the antenna was raised further above the reflector (Sigalas *et al.*, 1997). The slot antenna placed on the PBG reflector showed an average gain of 2-3 dB over the free slot for a 14% fractional bandwidth, with positional dependence similar to that shown by the dipole. The slot did hold one distinct advantage over the dipole in that it showed none of the dipole's tendency to form strong sidelobes in the forward hemisphere. The authors attributed this to the effective electrical isolation of the two hemispheres by the metallic plane containing the slot itself (Leung *et al.*, 1997). Both experiments showed that while a PBG reflector could improve antenna radiation characteristics, a poor choice of position could actually degrade antenna performance.

The final group with published research on PBG reflectors is located at the Université de Rennes in France. In the first of two papers, Poilasne *et al.* investigated the use of a planar MPBG reflector with dipole and square spiral antennas (Poilasne *et al.* 1997). Their measurements of the spiral antenna's radiation showed that depending on frequency, their structure could either degrade or enhance the region over which the polarization remained circular.

They also performed a simple ray-optics analysis of a point source above a dielectric-coated reflection plane to derive two necessary and sufficient phase conditions for wideband constructive interference (Figure 4). Cast in terms of the variables used in the present work, these conditions are:

$$\frac{4\pi f d \sqrt{\epsilon_r}}{c_0} \cos(\theta_2) = -\Phi(f, \theta_2) + 2n\pi \quad (5)$$

$$\frac{4\pi d \sqrt{\epsilon_r}}{c_0} \cos(\theta_2) = -\frac{\partial}{\partial f} \Phi(f, \theta_2) \quad (6)$$

where d is the distance to the reflection plane, θ_2 is the angle of the refracted ray within the dielectric, and n is any integer. The other variables are by now self-explanatory.

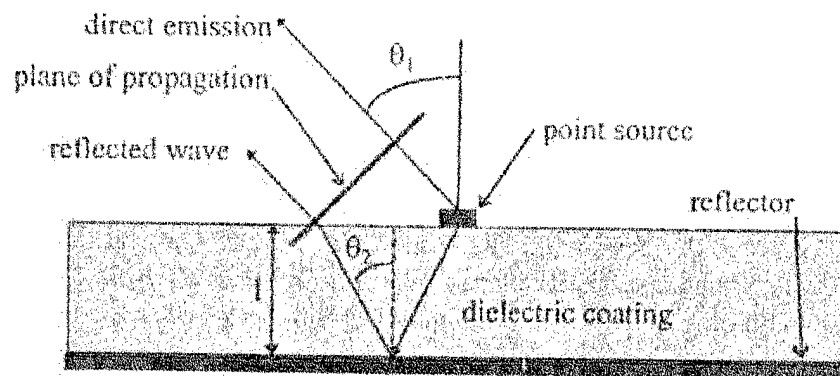


Figure 4. Geometry for Poilasne's Reflection Plane Analysis
(reproduced from Poilasne *et al.*, 1997:385)

Equation (6) shows that for a given incident angle, a linearly decreasing phase presents the possibility of matching these criteria. The GTRI researchers had already observed a tendency for their PBG structure to show a linearly decreasing reflected phase within the band gap (Kesler *et al.*, 1996). Poilasne's group showed that their reflector should also have the required linear phase behavior at normal incidence, but did not report any attempt to maximize the measured band of constructive interference. Measuring and exploiting this linear phase change for broadband gain enhancement is a primary goal of the present research.

In their second experiment, Poilasne's group altered a dipole's radiation pattern using MPBG reflectors (Poilasne *et al.*, 1998). Compared with the beamwidth of a dipole in front of a planar PBG reflector, they increased the 3 dB beamwidth 64% by using a MPBG corner reflector. They further suggested such a configuration might be useful in suppressing grating lobes for a dipole array.

Ten different papers on antenna applications of PBG materials appeared in a special session of the International Union of Radio Science's National Radio Science Meeting in June,

1998 (Yang and Agi, 1998). These included four papers on the use of PBG substrates for microstrip antennas, two on other PBG-antenna combinations, and four on more general theoretical issues. While the information provided in the conference digest is not detailed enough to support an extensive review here, it does indicate that PBG substrates and reflectors are potentially useful for improving antenna gain, efficiency, and directivity. These papers, along with the tangible results developing from the USARO MURI effort mentioned at the start of the chapter, demonstrate that PBG materials in antenna systems are a growing research area. With the current state of PBG research, it is hard to imagine that we would not see practical use of RF PBGs in the near future.

In this chapter, we have reviewed research on the use of PBG materials as both substrates and reflectors for microwave and millimeter wave antennas. Experimental results clearly show that photonic crystals can improve the radiation properties of several types of antennas. Of particular relevance to the present work are the recent results showing that PBG reflectors may provide substantial gain enhancement over useful bandwidths. We have reviewed criteria which, combined with the effective reflection plane model, provide a simple analytical method for designing an antenna-reflector combination for broadband gain enhancement. With this background in place, we will now describe our research goals and the design of our experiment.

III. Methodology

Review of Research Goals

Now that the reader is familiar with the basic theory and current research on PBG materials, we will review the goals of the current work and point out how they will advance the state of the art. Broadly stated, the goals are 'broadband gain enhancement' and 'desktop design.' First, we want to develop a PBG material with a complete band gap covering the S -, C -, X -, and K_u -bands (2-18 GHz). Second, using the PBG as an antenna reflector, we want to demonstrate a power gain of at least 3 dB across the operating bandwidth of a practical antenna matched to the PBG stop band. The gain comparison will be against an absorber-loaded cavity in place of the PBG reflector, since this would be a typical mounting surface for a broadband antenna (Balanis, 1997:554). This combination constitutes a goal which, to our knowledge, has not been achieved: a practically useful RF gain enhancement across a multiple octave bandwidth. Finally, we want to demonstrate a design technique that keeps the entire design process from computer-aided design (CAD), through numerical analysis and up to fabrication, on a desktop workstation. Again, we are unaware of other work which would allow a design team to draw a PBG model in a CAD program, export it to an accurate workstation-based electromagnetic code for iterative design, and hand the final design to a production team in a format that lends itself to automated production. We feel that achieving these goals will make a new and substantial contribution to PBG research and the development of practical PBG antenna systems.

We will detail our approach to this work in three stages. First, we will discuss how we selected a specific photonic crystal design to meet our gain enhancement goals. We will then describe the technique we developed to meet the 'desktop design' goal. Finally, we will present the experimental techniques we used to evaluate whether our PBG-antenna combination met our stated goals.

Designing the PBG Reflector

Antenna. The starting point for our PBG design was the antenna. As stated before, we wanted to demonstrate gain enhancement for a broadband antenna rather than a dipole or other simple radiator. The sponsor provided the two-arm spiral microstrip antenna shown in Figure 5. The substrate was $762\text{ }\mu\text{m}$ (.030") FR-4 glass-fiber-reinforced epoxy printed circuit board material, which we assumed to have a relative dielectric constant of 4.6. The antenna was assumed to have a usable operating band from 2-18 GHz.



Figure 5. Two-Arm Spiral Antenna Used in Present Work (Scale in cm)

Qualitative Choices - Development of Hybrid Design.

Our most basic consideration was the need for a broad stop band at centimeter-scale wavelengths in a structure of reasonable size. This pointed toward either a metallic structure used below the plasma frequency or a metallodielectric design with very strong capacitive or inductive coupling. Dielectric PBG structures, with a unit cell size of around 7.5 cm at the low frequency end of our design range, would be too large to achieve many repetitions in the space available. This would reduce their size to only a few unit cells in the surface plane and probably less than two unit cells in depth. These size constraints, imposed by the cavity in our antenna test body (45.7 cm x 45.7 cm x 15.2 cm), implied a rejection of only 6-8 dB, which we considered insufficient for our purposes.

Due to time constraints, manufacturing needed to be relatively simple and quick. With both a printed circuit board (PCB) milling machine on loan from our sponsor and PCB manufacturers in the local area, the means were at hand for producing PCB designs of practically any type. Precedents for both metallic and metallodielectric designs using PCBs already existed (McCalmont *et al.*, 1996; Sievenpiper *et al.*, 1998). Thus we focused our attention on a PCB-based, metallic or metallodielectric design.

This still left other important variables undetermined. Lattice structure presented several choices, with published research on metallic designs using simple cubic, diamond, and tetragonal lattices (Pendry *et al.*, 1996; Sievenpiper *et al.*, 1996; 1998; Leung 1997; Özbay *et al.*, 1996; Temelkuran *et al.*, 1997). Topologically speaking, these designs used capacitively coupled as well as electrically conducting arrays of scatterers. We chose a diamond lattice structure because of its well-established property of a complete band gap. Among MDPC designs, a strongly coupled 'cement' topology like Sievenpiper *et al.*'s (1998) would provide a tunable lower band edge to match the antenna's. Unfortunately, calculations based on Sievenpiper *et al.*'s research (see p. 18)

indicated that on-hand materials would not provide strong enough coupling to push the band edge down to the desired 2 GHz. A metallic structure with a network topology, on the other hand, would form a stop band with a low frequency limit due only to the use of a finite structure. Since our structure would be roughly the size of the cavity in the test body (45 cm square), we calculated this would allow us to push the lower band edge to 1 GHz or lower.

With a conducting diamond lattice design as a general framework, all that remained in the qualitative description of our structure was the form of the individual network elements. An abortive earlier attempt at sketching an inductive network provided a starting point. By straightening out the meandering elements of the inductive sketch, we produced the element shown in Figure 6a. For comparison with the diamond lattice of Figure 6b, the 'atom' is the horizontal cross at the center of the pattern element. In practice, we would print the orthogonal arms on separate circuit boards, then align them properly to produce the cross. The 'bonds' are the plated vias, extending through the two separate circuit boards. A translated repetition of the design on the opposite surface of each board formed the neighboring 'atoms' (Figure 6c). The face of any circuit board would correspond to a crystal plane with Miller indices of (100). This provided a metallic network with a diamond bonding structure and which we expected would produce the desired low frequency 'metallicity' stop band. While the design borrowed fabrication methods from Sievenpiper *et al.*, 1998 and McCalmont *et al.*, 1996, and a wire mesh network topology from Sievenpiper *et al.*, 1996, the 'hybrid' PCB-based wire mesh was a structure we considered original. We later found that Leung had produced a very similar structure (Figure 7), but in an all-dielectric form without the plasma frequency behavior we expected for our metallic structure (Leung, 1997).

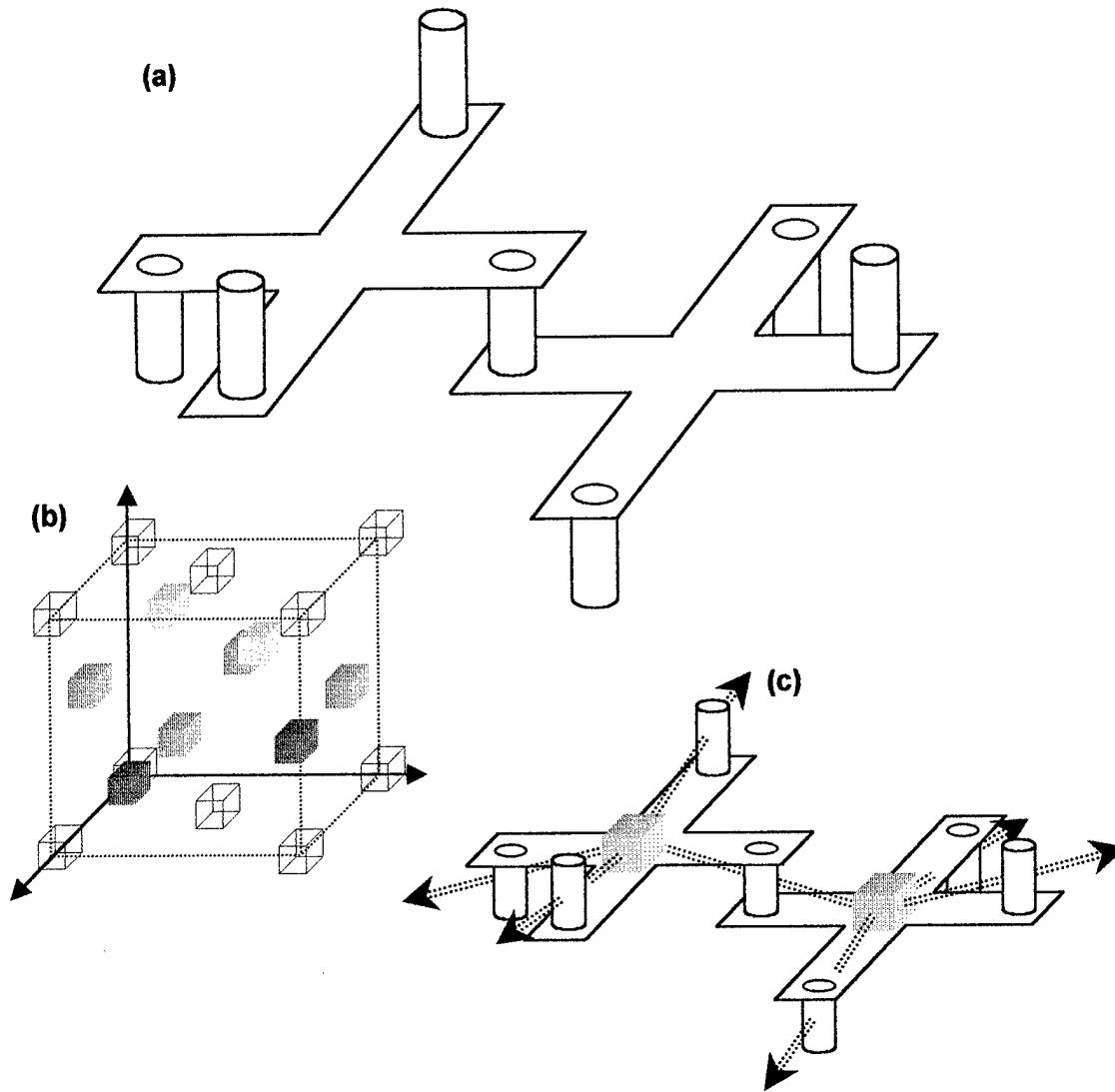


Figure 6. AFIT Photonic Crystal Design. (a) Two Metallic Pattern Elements (b) Generic Diamond Lattice Structure (c) Neighboring Pattern Elements with Diamond Bond Structure Overlay

Quantitative Choices - Design Parameters.

Material Selection. We chose the substrate material for our structure by referring to design equations presented in the work of Sievenpiper *et al.* (1996, 1998). These indicated that a conducting mesh with a diamond lattice exhibited a cutoff frequency f_c of

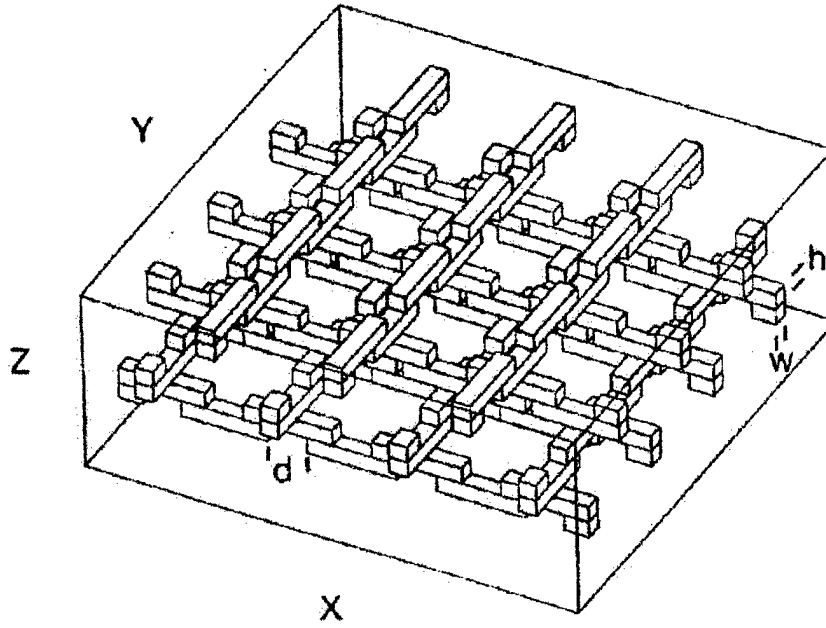


Figure 7. Leung's Diamondlike PBG Crystal (reproduced from Leung, 1997:3517)

$$f_c \approx \frac{c_0}{2a\sqrt{\epsilon_r}} \quad (7)$$

where c_0 is the speed of light in vacuum, a is the lattice constant, and ϵ_r is the relative permittivity of the medium containing the mesh. For a given f_c , Equation (7) shows that a large dielectric constant will provide the smallest possible lattice constant and thus the smallest structure. This also means that for a given structure size, a high permittivity medium will contain a larger number of unit cells and should produce a sharper stop band than a low permittivity medium. The medium in our design is simply the circuit board substrate, so this factor dictated that we choose the highest practical dielectric constant. The four-layer design of the unit cell required that each circuit board be a quarter unit cell thick, so the minimum available board thickness placed an upper limit on the allowable f_c for a material. This also imposed a restriction based on the desire to avoid distorting the lattice: a material with an ϵ_r satisfying the requirements above would be

useless to us unless it was available in a thickness of $a/4$. We chose to avoid any major lattice distortion to remove a variable from the problem space. For an example of a metallodielectric photonic crystal with a 'compressed' lattice, see McIntosh *et al.*, 1997.

Several additional concerns influenced our material choice. One relates to manufacturing. In choosing a broad material category (i.e., glass fiber reinforced polymer, ceramic, thermoplastic, etc.) we considered the board fabricator's ability to work with the board material. For example, the chosen design relies on good electrical conductivity throughout the structure, which in turn requires a high degree of reliability in the plated vias. Thus we restricted ourselves to materials that our chosen fabricator was accustomed to handling. Furthermore, we wanted a material that was nondispersive and effectively lossless across the desired operating range. The dispersion requirement was meant to keep our analysis simple, while the low loss requirement was intended to ensure that energy would be reflected, not absorbed, by the PBG structure. For a detailed treatment of dispersive and lossy materials in PBG structures, see Sigalas *et al.*, 1994. To increase the number of unit cells in our structure, we sought to at least double the electrical size of our mesh as compared with an air medium. This implied a need for a relative permittivity of at least 4. Finally, cost and ready availability also factored into the final choice of board material. We found a local circuit board manufacturer with ample stocks of Allied Signal ED130UV epoxy laminate, which they indicated had a dielectric constant of 4.6 at an unspecified frequency. From Equation (7), this meant that a cutoff frequency of 18 GHz would require individual boards about 1 mm thick. A 1.041 mm (.041") board was the closest available thickness. With a 0.035 mm layer of copper (after plating the vias) on each side of the board, this gave a quarter-unit-cell length of 1.111 mm. Substituting into Equation (7), this implied a cutoff frequency of 15.7 GHz, which we found acceptably close to the desired value of 18 GHz. Since our measurements were

equipment-limited to an upper end of 18 GHz, this slight depression of the cutoff frequency would also allow us to investigate the behavior of the structure in transition across the band edge.

It is worth noting one consideration that did not significantly influence our choice of dielectric constant. The Fresnel reflection coefficient Γ at the interface between two nonmagnetic, dielectric half-spaces is (at normal incidence)

$$\Gamma = \frac{\sqrt{\epsilon_{r1}} - \sqrt{\epsilon_{r2}}}{\sqrt{\epsilon_{r1}} + \sqrt{\epsilon_{r2}}} \quad (8)$$

where the 1 and 2 subscripts refer to the incident and transmitted sides of the boundary, respectively. When the incident medium is air, a large ϵ_{r2} produces a large reflection coefficient due solely to the air-dielectric interface, reducing the relative depth of the band associated with the structure internal to the dielectric medium. The reflected field undergoes a 180° phase shift upon reflection from the higher-index medium. Thus if the antenna-reflector distance is less than $\lambda/8$, the reflected field will destructively interfere with the directly radiated field. In our setup however, the incident medium is not air, it is the antenna substrate. Keeping the dielectric constant of the PCB substrate below the value of the FR-4 antenna substrate would theoretically avoid the 180° phase shift and potentially allow some constructive interference. However, our assumption that the dielectric-metal combination would be described by the effective medium theory dictated that the PBG medium's permittivity would be much larger than the antenna substrate's. Recall that the effective medium theory applies to photonic crystals where $a \ll \lambda$ if λ is the vacuum wavelength (Sievenpiper *et al.*, 1996:2482). In our case, $a = 4.4$ mm, while λ at 18GHz is 16.6 mm. While this is not as high a ratio as we would have liked, we decided that the effective medium theory applied well enough that the reflector permittivity would effectively be well above that of the antenna substrate. Instead of further considering Fresnel reflection

separately, we will turn to an effective reflection plane analysis that simply deals with the total observed reflection from the structure.

Pattern Dimensions. The calculations above highlight one implication of Equation (7); namely, that choosing a particular board material and thickness uniquely determines the structure's cutoff frequency. The only way to change f_c given a material and thickness is to use a structure with a different symmetry. For example, one might choose a tetragonal structure, which can be repeated with only two layers, in order to halve the lattice constant (Temelkuran *et al.*, 1998).

With our lattice constant determined, it was a matter of simple geometry to calculate the nearest-neighbor distance D in the $\langle 110 \rangle$ crystal direction as 3.141 mm. This would be the appropriate lateral separation for the pattern rows in our design as well as the correct distance between the centers of two successive pads in the same row. To generate the appropriate 'atom' spacing in successive layers, each row on one face of a circuit board had a replica of itself translated 1.570 mm along the length of the row on the opposite face of the board. Placing vias to form 'bonds' midway between 'atoms' on the upper and lower board surfaces fixed the via centers at 0.785 mm from the pad centers. Per the PCB fabricator's recommendation, we kept the via aspect ratio to about 4:1, setting their diameters at .254 mm. Leaving a margin of at least one via radius around the via set the size of the pads at 2.057mm by 0.508 mm.

This finalized the dimensions and spacing of all the array elements. The last remaining variable was the size of the array as a whole. Based on much of the existing research, we felt that three unit cells of depth would likely provide significant stop band behavior (Sievenpiper *et al.*, 1996; 1998; Temelkuran *et al.*, 1998). As far as lateral extent was concerned, we were limited to a 45 cm square by the size of the antenna test body. Within this constraint, we wanted to create as

large a reflector as we could afford in order to minimize the effects of finite size. In the end, cost was the primary consideration and we limited ourselves to a patterned area 27.94 cm square, corresponding to an array of some 3950 square unit cells. In free space, this size would correspond to a frequency of about 1 GHz; thus our structure's finite size would not introduce any strong resonances until well below the frequency band of interest.

Fabrication Procedure & Final Product. With the dimensions of our structure set, fabrication was straightforward. The raw board material was purchased directly from Circuit Center, Inc. of Kettering, Ohio. Because of the simplicity of the pattern, CCI produced the artwork for the boards in addition to conducting the etching, drilling, and plating on all 12 boards. We were able to reduce the fabrication cost almost 50% by accepting boards without alignment holes, since reusing the same artwork for all four alignments meant no retooling costs and a per unit price break. Instead, we ensured that the pattern was etched with respect to a reference corner that we then used to orient the boards ourselves. Careful inspection of the design will show that the same board pattern can be used to produce each layer's alignment through a straightforward combination of 90° rotations and lateral translations. After realigning the boards, we used a circuit milling machine to drill a pair of 0.32 cm diameter pinning holes in each set of three boards. The pinning holes' positions relative to the patterned area ensured that each board would align properly with its neighbors. The boards were pinned using 1/8" Acetron GP rods, chosen for their ready availability and dielectric constant of 3.7 (at 60 Hz), which was well enough matched to the ED130 board material for our purposes. The uneven edges of the boards were trimmed to produce a final structure 29.2 cm square and 1.33 cm thick. Upon final assembly, a visual check was made to see how well the boards aligned. Limitations in the pinning hole accuracy meant that any given pair of boards showed relative misalignments of up to about 17% of the nearest-

neighbor distance. This was not enough to change the topology between any two layers and appeared to have no major effect in our low-frequency operating regime. This appears to support the hypothesis that within an effective medium, the local geometry is not as important as in a dielectric photonic crystal (Sievenpiper *et al.*, 1996:2482). Since we did not collect data above 18 GHz, we cannot say whether the misalignment has any significant impact at the lattice constant-associated band gap frequency of 33 GHz for this structure. With the structure as built, we were satisfied that we would be likely see significant stop band behavior over most of our desired operating range.

Computational Approach

Desktop Design: I-DEAS & PARANA. As mentioned previously, the second major goal at the outset of this research was demonstration of a design, modeling, and prediction process. We planned to use computer aided design (CAD) software to construct a reflector model and export it to a computational electromagnetic (CEM) code for analysis. After using the CEM results to refine the design, we would use the final CAD model as our input to the fabrication process. To make the process practical, we also hoped to confine the entire process to workstations and avoid any supercomputing (i.e., massively parallel processing) requirements.

The choice of both the CEM and CAD programs was simple. Because it was readily available and designed for periodic structure work, we would use the government-owned Phased ARray ANTenna Analysis (PARANA Version 2.1) software as the CEM code. PARANA includes code and procedures for reading in geometry data from Structural Dynamics Research Corporation's I-DEAS™ CAD software, making it the natural choice as our CAD tool. As

outlined in the User's Manual, PARANA is a hybrid Finite Element Method - Boundary Integral Equation (FE-BIE) code written in FORTRAN-77 (McGrath, 1997). With approximately 30% of the papers reviewed for this work using similar FEM or hybrid FEM methods, we were optimistic that the code would be well suited to PBG analysis. PARANA accepts input geometry files in ASCII text format, and can compute solutions for a wide variety of geometries and materials. Along with the input geometry, PARANA requires a 15-line ASCII text input file with instructions on frequency, angle, polarization, mode limits, and other similar problem parameters. PARANA handles PBG structures as periodic radiation boundaries and computes transmitted and reflected field strength and polarization. For such problems, some matrix entries are angle dependent, necessitating a new solution for each incident angle. As a frequency-domain code, PARANA must also compute a new solution for every requested frequency (McGrath, 1997: 1). We compiled and ran the code on Sun UltraSPARC workstations.

The I-DEAS™ Master Series 6 CAD/CAM software was our modeling and geometry pre-processing tool. Its main purpose in our work was to output a finite element mesh that we could import into PARANA. A secondary but still important aim was to produce an output file usable in the fabrication process. In the case of our chosen design, this would mean a file usable by the average printed circuit manufacturer.

The procedure we used came straight from the PARANA User's Manual's appendix on "Preprocessing in I-DEAS Master Series™" (McGrath 1997:58-69). The major steps are:

- (1) Create a model of the PBG structure in the CAD program, with all dielectric regions and conducting surfaces explicitly identified.
- (2) Generate a finite element mesh on the CAD model.
- (3) Translate the mesh file into a format usable in PARANA.

- (4) Create and execute the PARANA instruction file that identifies the problem parameters and calls the appropriate mesh geometry for solution.

We would validate PARANA as a prediction tool by modeling the capacitively coupled MDPC of Sievenpiper *et al.*, 1998 and comparing the results against the published data.

Assuming the CEM results proved accurate, we would repeat the above procedure as many times as necessary to produce a PBG design that met our performance requirements. We would then export or translate the CAD model into a format that would fit the requirements of whatever fabrication technique we chose. To our knowledge, this would be the first demonstration of an iterative PBG design process, carried from modeling all the way through fabrication to measurement, which did not rely on fabrication of each new structure to determine a usable configuration.

Test & Measurement

Reflection/Transmission Measurement Setup. We performed bulk transmission and reflection measurements using a focused arch measurement system developed by the Georgia Tech Research Institute and located at the Air Force Research Laboratory's Signature Technology Branch (Figure 8). The system consists of two booms, each supporting a horn and a dielectric lens. Between the two lenses, above the pivot point that connects the booms, is a rotating frame in which a sample is placed during measurement. The lenses focus the radiation emitted by one horn into a Gaussian beam. The Gaussian profile is the same type seen in lasers, and has the very useful property that it possesses a planar phase front at its most tightly focused location or 'beam waist' (Verdeyen, 1995:63-80). In the focused arch system, the surface of the sample under test is placed at this beam waist, resulting in plane wave illumination. The

focusing power of the lenses is such that the beam waist is approximately 12 inches in diameter at 2 GHz, allowing measurement of relatively small samples with minimal 'contamination' from illumination of mounting fixtures and the support structure (Schultz, 1998).

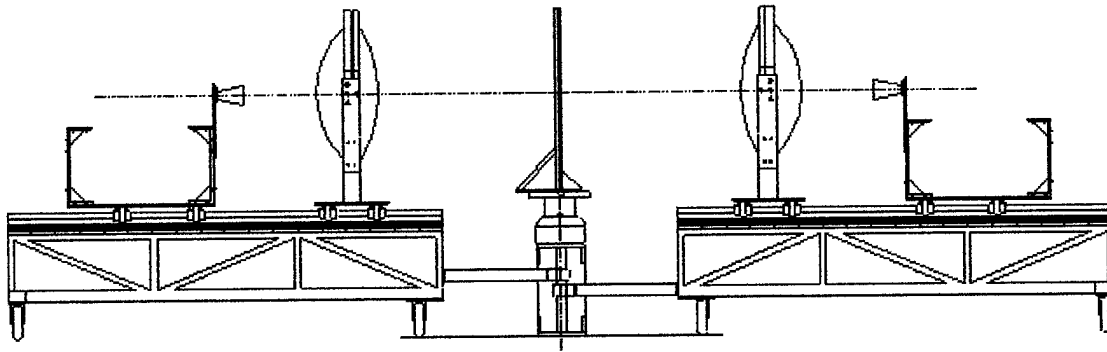


Figure 8. GTRI Focused Arch Measurement System (reproduced from Schultz, 1998:1)

In addition, the twin-boom configuration allows not only transmission and monostatic reflection measurements, but also bistatic reflection measurements (Figure 9). The low-incidence angle limit is determined by the size of the lenses, while the grazing incidence angle is limited by the beam waist size relative to the projected area of the sample under test. The ability to collect bistatic reflection data was attractive because the PARANA software gives the specular (i.e., bistatic) reflection coefficient for array problems (McGrath, 1997:10). This is also the type of data required for a ray-optic reflection plane analysis like that of Poilasne *et al.*, 1997:385. To get some idea of whether our structure possessed a complete band gap, we developed the reflection test matrix shown in Table 1. Azimuth is the angle of the bottom edge with the horizontal, where 0° places the edge parallel to the floor and the pattern elements on the front face in a vertical position. Elevation is the angle between the propagation direction and the normal to the front face of the sample. For transmission, we measured at normal incidence only, in horizontal and vertical polarizations and for both azimuth angles. All measurements were co-polarized, performed over a

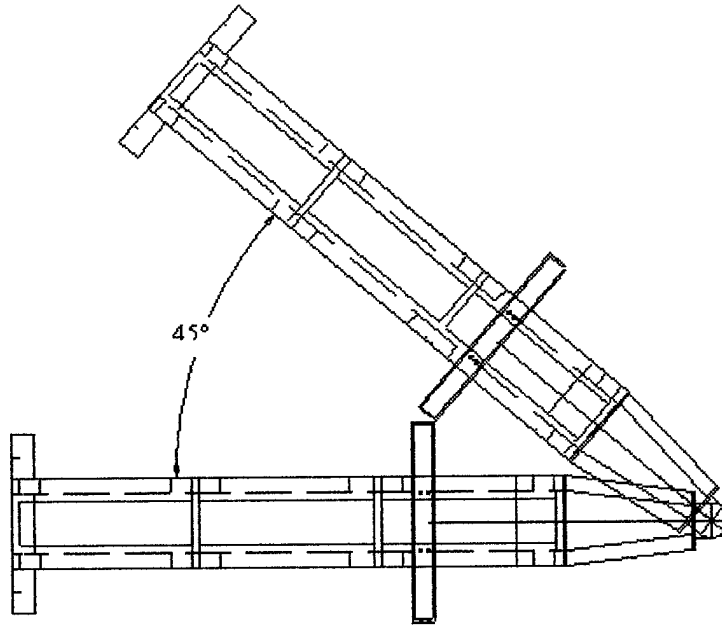


Figure 9. Top View of Focused Arch System (reproduced from Schultz, 1998:2)

range of 2.0-18.0 GHz and sampled every 20 MHz. While these measurements cannot prove the existence of a complete band gap in our structure, they give an indication of whether there are gross variations in the stop band across a range of angles and polarizations (H = TM, V = TE).

Table 1. Reflection Properties Test Matrix

Variable	Number of values	Values
Azimuth	2	0°, 45°
Elevation	5	0°, 35°, 45°, 55°, 65°
Polarization	2	HH, VV*

*Note - No VV measurement at 45° azimuth - degenerate case

To ensure electrical contact between the circuit board layers, we needed to keep pressure across the entire board surface throughout the measurement process. We sealed the stack of circuit boards in a bag made of two 89 μm plastic sheets, along with thin cotton-like sheets to permit air flow within the bag, and held the entire assembly under vacuum (Figure 10). The

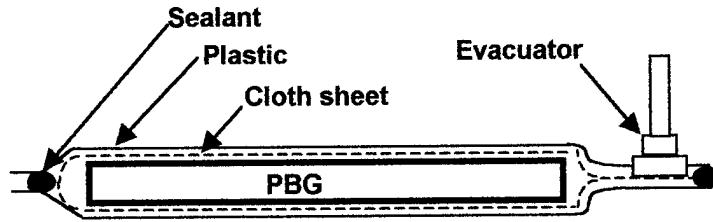


Figure 10. Vacuum Bagging Schematic for Focused Arch Measurements

pressure of the bag walls on the boards held them tightly together. In another side benefit of the focused arch system, the vacuum fittings, hose, and bag sealant were all located well outside the beam waist except at the very lowest frequencies and grazing angles.

Antenna Patterns. After measuring the bulk properties of our structure in the focused arch, we prepared for the antenna pattern measurements that were the focus of the entire work. The goal, the reader will recall, was to demonstrate that the PBG reflector could substantially enhance the antenna gain over a wide operating band. The two 'control' cases for comparison with the PBG reflector were a conducting plane reflector and an absorber loaded cavity.

The first significant adjustment we made in setting up the antenna experiment was drilling a 7/32" hole through the center of the PBG reflector in order to feed the antenna from inside our test body (Figure 11). With the hole drilled in the reflector, we fed two .086" coaxial cables through and soldered the center conductors onto the two arms. The outer conductors were taped together with copper tape immediately below the antenna substrate. The two pieces of coax were carefully cut and bent to keep the feed balanced. The coax leads were connected with the network analyzer through a 50-Ohm power splitter.

We set the reflector-antenna combination into an aluminum 'picture frame' insert which filled the space between the reflector and the test body cavity walls. We used more of the vacuum cloth and plastic from the focused arch setup to seal the entire rear surface of the reflector to the

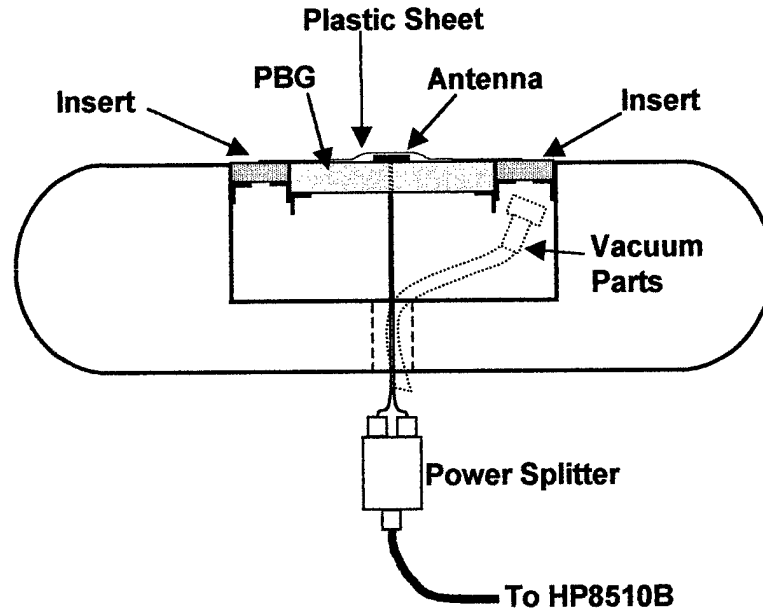


Figure 11. Antenna Test Body Configuration for PBG Reflector Measurements (Cross Section)

back of the insert, leaving a 'tab' in one corner to attach the vacuum fitting. The insert had angle aluminum on all four sides to support the reflector and was itself supported by angle aluminum on the test cavity walls. We adjusted the angle aluminum so that the reflector, insert, and test body surfaces were coplanar. We then covered seams at the junction of the insert with the copper and copper-painted test body with copper tape for improved continuity. A second piece of vacuum plastic was then laid on the front surface of the antenna and reflector and taped onto the insert. At this point, the entire test body assembly was placed onto a rotating foam support in an anechoic chamber. With the vacuum hose tucked away beneath the absorber along the chamber wall, we turned on the vacuum pump, ensured that neither feed line nor vacuum hose was entangled in the rotator, and were ready for measurements.

The test configuration was similar for the ground plane and absorber backed measurements. For the ground plane, we covered the bottom of the antenna substrate with copper

tape and mounted the antenna on a sheet metal insert matched to the test body cavity opening. The insert had a hole slightly smaller than the antenna itself cut out, and the antenna was placed so that it rested on the hole's rim. For the absorber loaded cavity measurements, we cut a block of broadband microwave absorber 5 1/4" thick (the cavity was 6" deep) that filled the entire lateral extent of the 18" square cavity. We removed the copper tape from the antenna substrate and placed the antenna on top of the sheet metal with the hole again, thus providing a way for radiation from the back of the antenna to be 'dumped' into the absorber.

For the measurements themselves, we used an HP8510B network analyzer to measure the antenna's response to excitation by a standard gain horn. Applying the theorem of reciprocity, we used this data to produce antenna pattern plots. Due to software limitations in the AFIT antenna chamber, data collection was an all-manual affair: position the rotator, conduct a frequency sweep, and read and save the data from the network analyzer using DOS-based interface software on a desktop PC. Based on the time intensive nature of this type of data collection, we decided to collect a minimal set of data that would still provide some insight on the performance of the reflector. For each of the three test body configurations (PBG reflector, ground plane, and absorbing cavity), we measured patterns for two polarizations every 5° in elevation. We performed these measurements at 0°, 45°, and 90° azimuth, with zero defined as the position with the front face pattern elements in a vertical position. We performed 801-point frequency sweeps to match the focused arch data. For the three configurations combined, we took 342 frequency sweeps, producing the test matrix shown in Table 2.

The PBG reflector work we summarized in Chapter II explored many variables, including antenna type, reflector shape and structure, antenna-substrate separation, and antenna position and orientation relative to the PBG unit cell. Reported results include polarization effects, gain/directivity enhancement, and input impedance for various antenna-reflector combinations.

Table 2. Antenna Pattern Test Matrix

Variable	Number of Values	Values
Test Body Configuration	3	PBG reflector Ground plane Absorbing cavity
Azimuth	3	0°, 45°, 90°
Elevation	19	0°-90° every 5°
Polarization	2	HH, VV

Within the limits of our available resources, we attempted to investigate many of these variables to at least a small extent. The modest size of our test matrices compared with the size of the problem space means there are many aspects of the AFIT PBG reflector experiment that we cannot adequately explore in the present work. Still, the results in the next chapter and the analysis in Chapter V will show that we have constructed an experiment that makes a unique contribution to the PBG literature. More importantly, in the spirit of scientific and engineering progress, our experience helps us identify in Chapter VI several research avenues that would provide greater insight into PBG reflectors.

IV. Results

In this chapter we present an overview of our results, reserving detailed analysis for Chapter V. We begin with the outcome of the proposed 'desktop design' process, since it was the first portion of the research we actually executed. We then discuss the measurements we performed in the focused arch system, examining the structure's behavior with respect to the variables of frequency, incident angle (both azimuth and elevation), and polarization. The chapter concludes with a look at the gross features of the pattern types associated with each of our antenna measurement configurations (reflecting plane, absorbing cavity, and PBG reflector). Graphics presented both here and in Chapter V are representative, not exhaustive, in nature; the reader wishing to see the full body of data is referred to the Appendices.

'Desktop Design' Process

Modeling and Design Portability (I-DEAS™). We found the CAD process very powerful for preparing virtual models of various PBG structures. We were able to produce drawings of the most complicated published PBG structures such as those recently fabricated at UCLA (Sievenpiper *et al.*, 1996; Sievenpiper *et al.*, 1998). After overcoming the initial 'learning curve' challenge of a high-end CAD package, we found the 3D-friendly nature of the software very useful. The ability to draw a symmetric portion of a unit cell then manipulate it to build up the model of the entire cell was very convenient. Also helpful was the ability to copy and assemble several unit cells to visualize the changing appearance of a PBG structure with varying incident angle. The one task requiring special attention was the process of identifying and

grouping conducting surfaces in a complicated unit cell structure. The program's tendency to split surfaces along every edge or junction sometimes required great vigilance to ensure that all the appropriate surfaces were 'tagged.'

The I-DEAS™ Master Series software, like all other major CAD packages, provided many options for exporting the drawings. We used the "I-DEAS™ Universal File" format, an ASCII text file that was the input to the PARANA translator program. With fields using FORTRAN-style formatting, this particular output format is ready-made for FORTRAN processing. Conversion into a CEM input is a matter of identifying the fields needed in the CEM calculations and reading them into a new file suited to the specific CEM code in use. As for the matter of having a file format usable in the fabrication process, our decision to use PCB fabrication techniques imposed a unique restriction: the majority of systems used in circuit board manufacturing require a Gerber formatted input file. I-DEAS™ does not directly export a Gerber format. A check of resources available from the Internet did not reveal any public domain translators that would convert any of the I-DEAS™ outputs to Gerber files, but several manufacturers listed proprietary packages for sale. In our case, the simplicity of the patterns we needed was such that the PCB fabricator was willing to draw the artwork in-house from sketches we provided. This limitation is more a problem of the PCB fabrication than one with I-DEAS™, but researchers wishing to use this approach need to consider whether a particular CAD program will meet all their needs in a 'desktop design' approach.

Computational EM (PARANA). We encountered difficulty reading the I-DEAS™ Universal Files into the PARANA translator. This problem was especially vexing because earlier AFIT research had used the I-DEAS™/PARANA combination without difficulty. After determining that the problem arose from changes to some of the I-DEAS™ Universal File field

designators in the current version of the CAD program, we modified the translator and succeeded in running some simple test cases provided with the PARANA code.

Our focus then shifted to validating the use of PARANA for complex PBG predictions. Earlier AFIT work had obtained good agreement between PARANA outputs and the measured results for a simple 2D square lattice of dielectric rods in air published in Kelly *et al.*, 1994. We would put PARANA to the test by predicting the results for the recently developed UCLA metallodielectric photonic crystals (Sievenpiper *et al.*, 1998:2831). We chose this design because of its relevance to our research and the richness of the unit cell structure. With two different dielectric media, conducting islands, strong capacitive coupling, and several electrically small features to be preserved in the finite element mesh, we felt the design was a good 'acid test' of PARANA's practicality for advanced PBG solutions.

Unfortunately, our use of PARANA on a Sun UltraSPARC workstation was not up to the task. We started with one of the UCLA circuit boards, then proceeded to two, four, and finally twelve boards stacked in the appropriate alignment. Times required for matrix solutions and even reading in the problem geometry skyrocketed (Table 3). Our projections and two abortive attempts indicated that the twelve-layer problem was practically unsolvable on the workstations, due largely to memory limitations.

Table 3. PARANA Solution Performance on UCLA MDPC Design

	1 Layer	2 Layers	4 Layers	12 Layers (est.)
Edges in FE mesh	18,500	34,000	66,000	212,000
Time to read geometry file (minutes)	4.5	12	83	---
Number of iterations per freq or angle step	500	900	1300	4200
Solve time per freq or angle step (minutes)	43	48	75	300

To see whether PARANA could compute the problem at all, we obtained a later version of the code (PARANA Version 2.1P) that had been developed for parallel processing. Working through the Aeronautical Systems Center's Major Shared Resource Center (ASC MSRC), we attempted to run the code on an IBM SP2 parallel computer. We were unable to execute the program in the parallel operating environment and did not obtain any results from this effort.

Thus our efforts at desktop design were partially successful. We found that integrating CAD made the modeling process relatively user-friendly. Our chosen package offered an output format that interfaced well with FORTRAN, making it well suited to CEM geometry preprocessing. It also offered a broad enough spectrum of output formats that we were reasonably confident a match could be found for most potential fabrication processes. PARANA was capable of solving simple or limited spatial domain PBG problems, but was unable in the desktop environment to produce a useful prediction of a complicated PBG design's behavior. When this final point became clear we proceeded, without any numerical modeling, to develop the metallic PBG structure described in Chapter III and measured its bulk transmission and reflection properties. These measurements are the subject of the next section.

Focused Arch Measurements

The data as presented here are relative to a metal plate calibration target. Thus the power levels for transmission and reflection have theoretical maxima of zero decibels. For the measurement setup used here, negative phase in reflection corresponds to a reflection distance greater than that for the metal plate, i.e., a reflection plane somewhere within the PBG structure. Figure 12 shows the test geometry with the appropriate angle variables labeled. On the left is a front view, with the plane of incidence corresponding to a horizontal plane, perpendicular to the

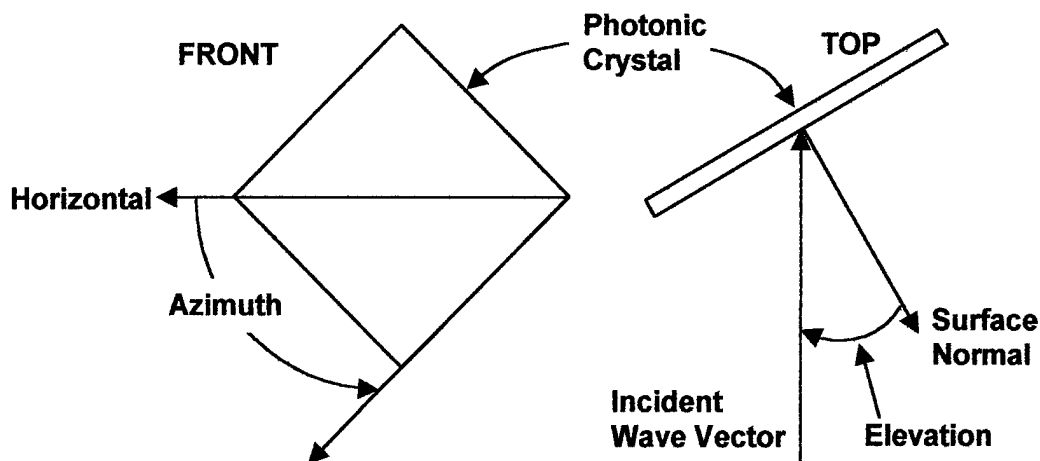


Figure 12. Geometry for Azimuth and Elevation Angles

page. On the right is a top view, with the page itself constituting the plane of incidence. Several of the plots for variable incident angle include a diagram showing the orientation of the structure and the pattern elements on the incident face. Note that while the vertical (V) and horizontal (H) polarizations are degenerate at 45 degrees azimuth and normal incidence, they are not the same for the off-normal case. In off-normal measurements, since the horizontal plane is the plane of incidence, V polarization is the TE or orthogonal case and H is TM or parallel polarization. Finally, recall that data below about 4 GHz is somewhat suspect because of the relatively large beam waist at the longer wavelengths.

First Variable: Frequency. Our first measurements were of the PBG structure's transmission (Figure 13). Recall from our earlier calculations that we expected a stop band edge at about 15.7 GHz (p. 32). In good agreement with the expected behavior, there is a pronounced drop in transmission at frequencies below 14.5 GHz. The -10 dB bandwidth extends all the way across the S , C , X , and lower K_u bands, indicating a fractional bandwidth of at least 150% in

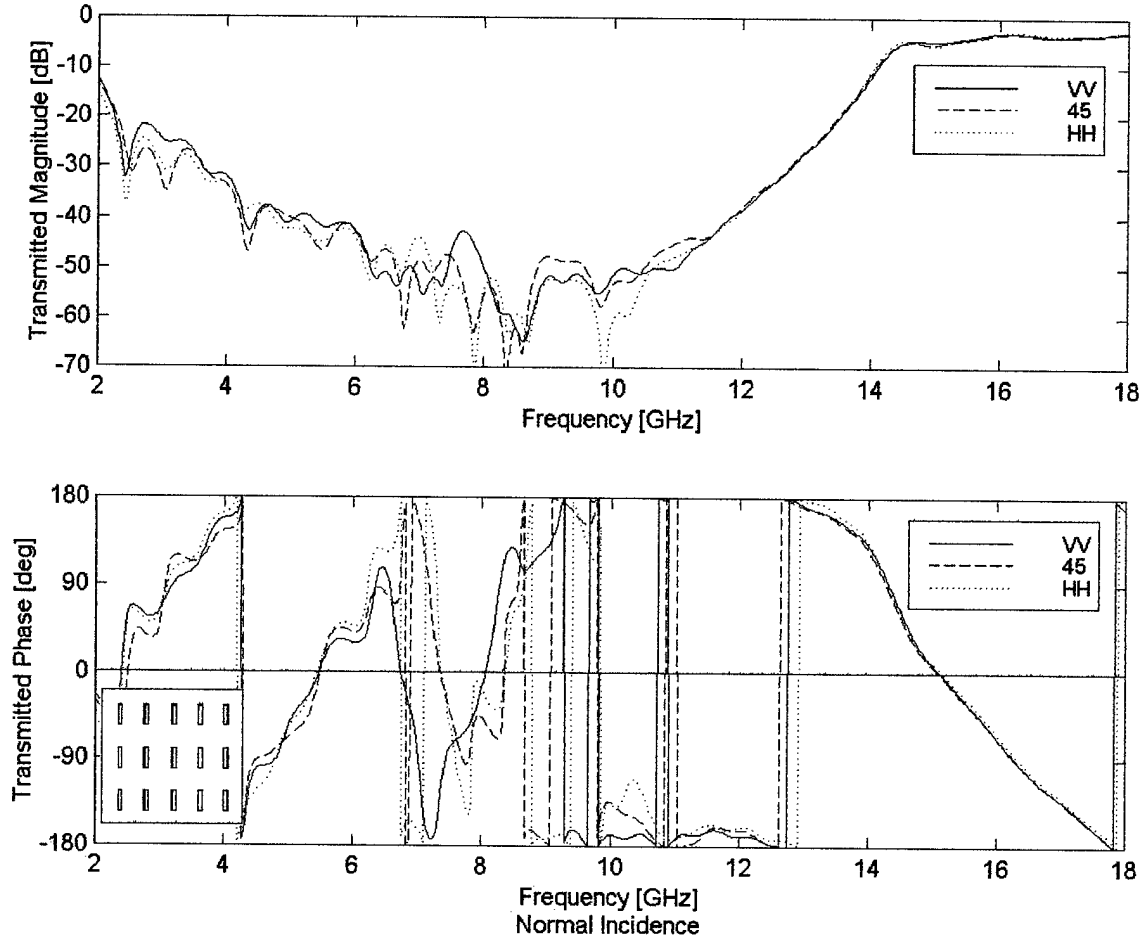


Figure 13. AFIT PBG Structure in Transmission, Normal Incidence, Various Polarizations

transmission. The transmission phase measurement within the stop band is suspect because of the extremely low power level.

Figure 14 shows the anticipated complementary behavior in reflection, with near unity reflection in the stop band and a rapid decrease at frequencies outside it. The phase rate is approximately linear with negative slope across the bandgap, indicating that the structure may meet Poilasne *et al.*'s criteria for wideband constructive interference. The small positive values around 13 GHz are a measurement artifact, probably arising from the time gating used in the

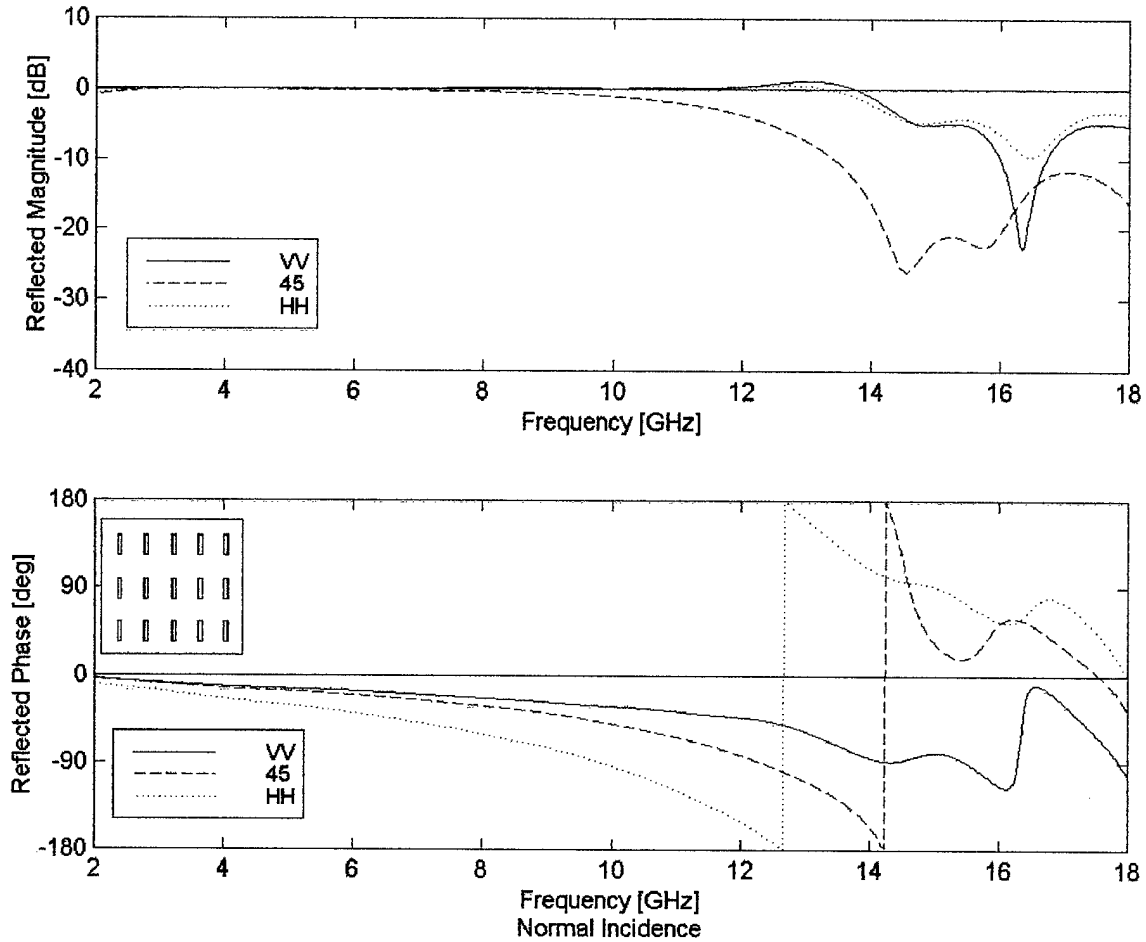


Figure 14. AFIT PBG Structure in Reflection, Normal Incidence, Various Polarizations

measurements. Similar features are visible in all of our reflection data, and could not be entirely eliminated despite our attempts to do so by varying the collection time gate.

Second Variable: Incident Angle. Our measurements for off-normal incidence were for reflection only, since that is the primary consideration in our proposed antenna reflector application. Assuming the structure is nearly lossless, one could infer approximate transmission behavior from the reflection data. This would, however, fail to account for reflection in any direction other than the specular. Figure 15 shows reflection behavior at the five incident angles we measured. This particular plot is for the zero azimuth, TE polarized case, but the overall

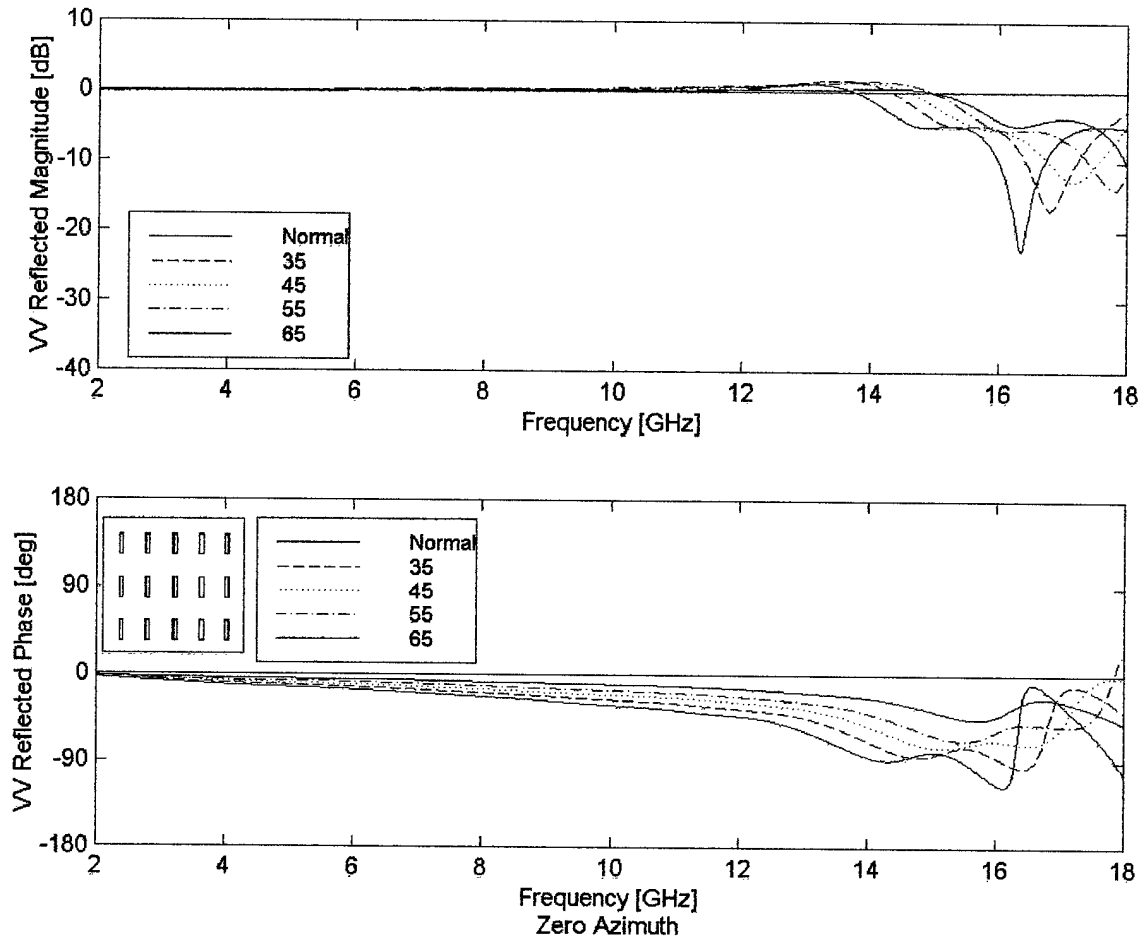


Figure 15. Effects of Changing Incident Angle with Constant Azimuth and TE Polarization

behavior of the 45° azimuth TE plot is similar. The only significant difference is that the 45° TE case shows a more rapid phase rolloff approaching the band edge. Incident angle shows practically no effect on reflected power magnitude. However, there is a slight but steady blue shift of the band edge with increasing incident angle. The phase slope is approximately halved when going from normal to 65° incidence. The TM polarized case is shown in Figure 16, and shows one significant change. Here, the magnitude of the phase slope *increases* with increasing incident angle, providing a strong motivation for examining the behavior with respect to polarization at a set incident angle.

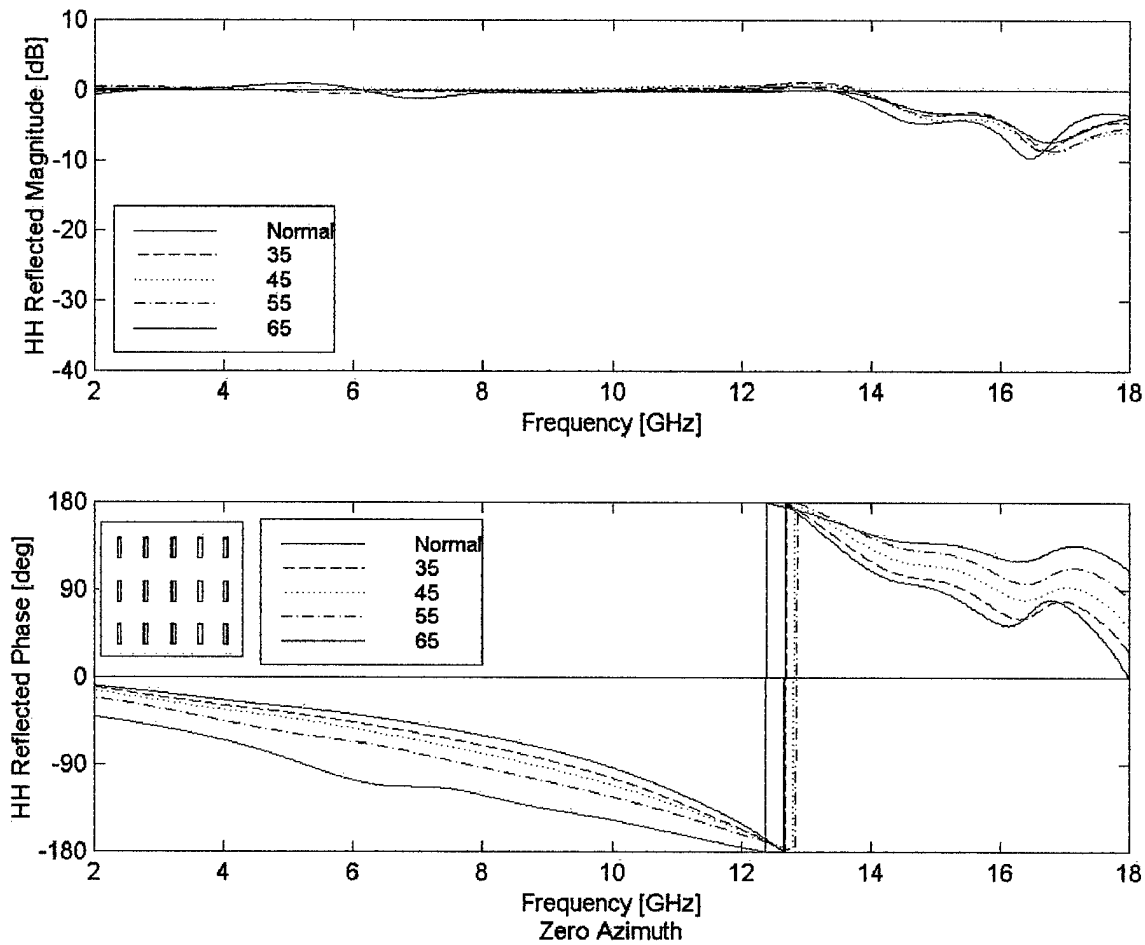


Figure 16. Effects of Changing Incident Angle with Constant Azimuth and TM Polarization

Third Variable: Polarization (TE vs. TM). The final variable we consider here is the polarization of the incident wave. Its effects are shown in Figures 13 and 14. In transmission, polarization has no significant impact. In reflection, on the other hand, polarization has a marked quantitative effect on the frequency response. In the magnitude plot of Figure 14, the reflected power rolls off more rapidly when the incident field 'bisects' the pattern. Phase behavior, on the other hand, shows a steady increase in the phase slope as the polarization moves from vertical to horizontal. While TE and TM distinctions disappear at normal incidence (because of the lack of a

uniquely defined plane of incidence), the lines in Figure 14 are still limiting cases of true off-normal TE and TM waves. This point becomes more significant upon examination of Figure 17, which shows data for 65° off normal incidence. Here we see that the two TE polarized (V pol) cases share a shallow phase slope while the TM (H pol) cases are steeper. Careful review of the figures presented here shows that while moving toward normal incidence causes the TE (shallow) and TM (steep) curves to move toward one another, they only converge for the 45° azimuth case. The zero azimuth case remains strongly polarization sensitive at normal incidence.

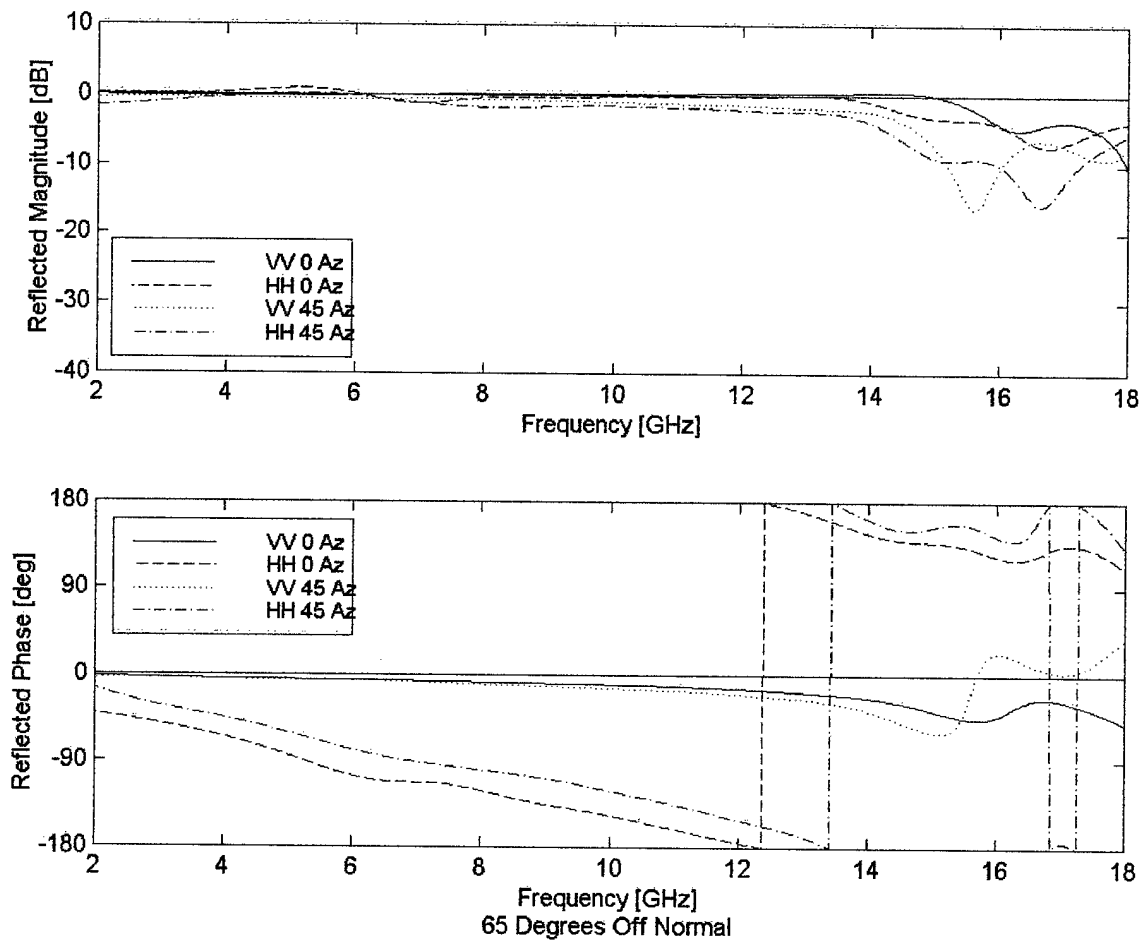


Figure 17. Effects of Changing Polarization with Constant Incident Angle

Antenna Patterns

The antenna patterns presented have had two steps of post processing applied. First, the data was calibrated with a standard gain horn measurement to get values in dBi. After the calibration, the data was still very noisy, so we averaged across a sliding three-point window in the frequency domain. This made the data far easier to read without altering any of the significant features. Note that the geometry is still the same as for the bulk properties, so that 'zero elevation' corresponds to normal incidence.

Ground Plane. Our measurements of the antenna above the PEC plane were the least successful of the three antenna configurations. We had decided early to mount the antenna directly onto the various surfaces without any additional dielectric spacers. Since the substrate was less than 1mm thick, it was electrically less than 0.1 wavelengths thick even at the high frequency end of our measurements. The shorting effect of the ground plane therefore affected the antenna so strongly that much of the data ended up in the system noise below -70 dB. A typical ground plane pattern appears in Figure 18.

Absorber Loaded Cavity. The absorber-loaded cavity, on the other hand, provided higher gain and smoother measurements. A typical pattern (Figure 19) features a wide, flat main lobe centered on approximately 45 degrees elevation. This may indicate that the antenna is excited in a higher-order mode, since the expected pattern in the fundamental mode would be centered about 0 degrees elevation (i.e., broadside). Frequency response is reasonably flat except at the extreme frequency limits. At the low frequency end, this is attributable to interference effects from the rim supporting the antenna, returns from the test body, and possibly cutoff of the antenna itself. At high frequencies, there is likely an observable effect due to damage done to the antenna during mounting - the center of one spiral arm partially delaminated from the epoxy

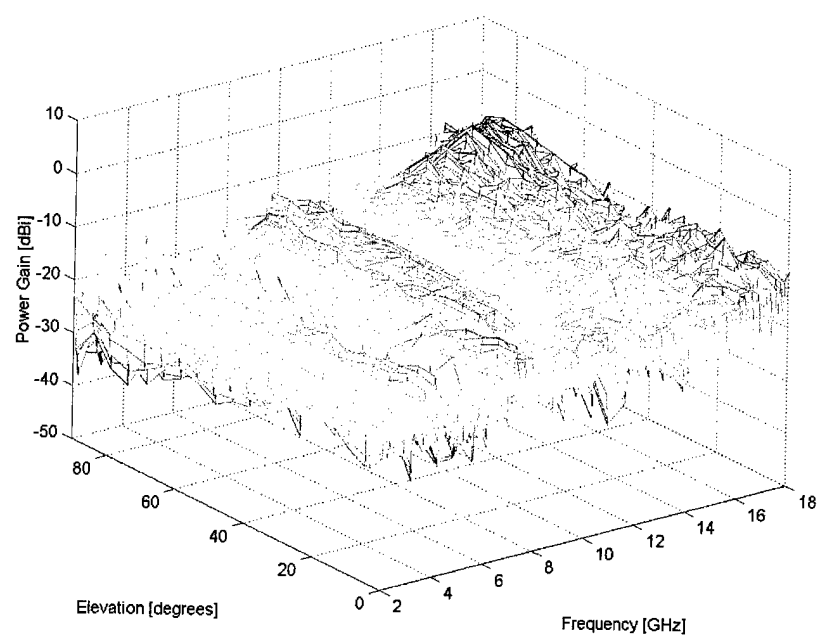


Figure 18. Ground Plane Backed Antenna Pattern, 90° Azimuth, TE Polarized

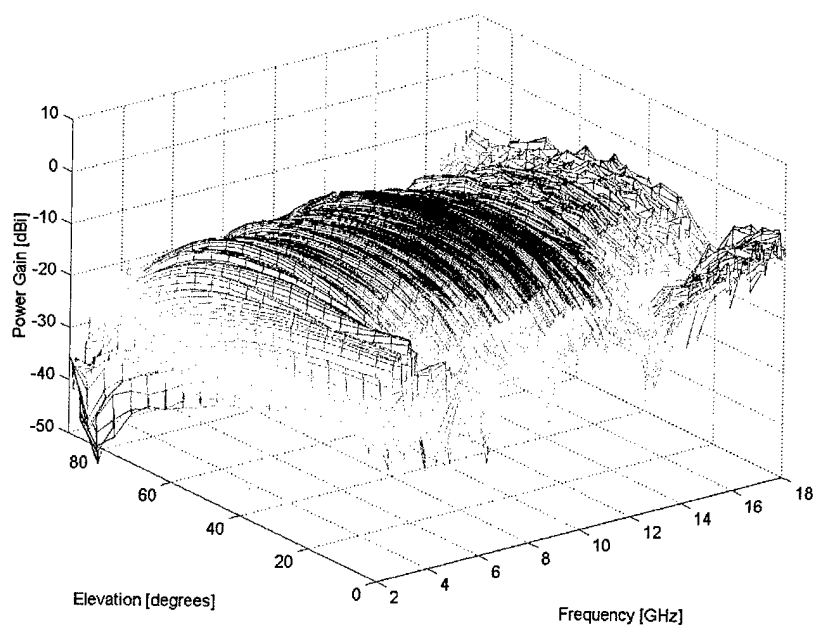


Figure 19. Absorber Loaded Cavity Backed Antenna Pattern, 0° Azimuth, TE Polarized

substrate during soldering of the coaxial feed. While there are minor variations in the pattern for the six different measurement cases, the overall similarity was enough to convince us that our measurement procedure was sound.

PBG Reflector. The PBG reflector measurements presented an intermediate case compared with the other two configurations (Figure 20). Not plagued by noise problems to the same extent as the ground plane arrangement, the PBG reflector still lacked the smoothness of the absorber loaded cavity measurements. The overall magnitude tends to fall above the ground plane and below the absorbing cavity case, indicating mixed success in achieving our gain enhancement goal. The behavior shown here, where gain decreases with frequency, is typical of this configuration. Readers wishing to examine all of the antenna patterns are referred to Appendix B.

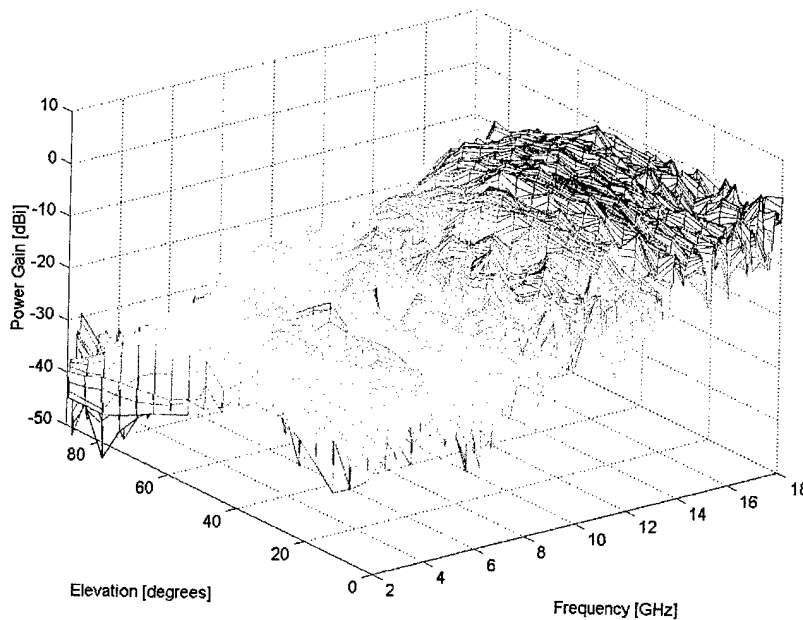


Figure 20. PBG Reflector Backed Antenna Pattern, 45° Azimuth, TE Polarization

V. Analysis & Conclusions

'Desktop Design' Approach

It is clear from the results we described in the previous chapter that the design approach we had hoped to implement ran into some difficulties. However, PARANA has proven usable for analysis of simpler PBG structures, and the parallel code has been implemented on an IBM SP2 workstation. Further consultation with the staff at the MSRC would probably allow a successful run of the code on the parallel computer. This, however, would not meet our original goal of using techniques that are practical in a desktop environment.

Still, the desktop design concept appears viable when we consider the use of other CEM codes. Several of the works cited in this thesis, particularly those dealing with metallic PBG structures, describe the use of a transfer-matrix method (TMM) developed by Pendry and MacKinnon (Pendry and MacKinnon, 1992). They describe it as "in essence a finite-element method in which space is divided into a set of small cells with coupling between neighboring cells. For most materials ϵ can be treated as diagonal in real space and hence complex structures can readily be incorporated into this methodology, even those including regions where $\epsilon=0$ " (*ibid.*:2772). They go on to state that for a square array of dielectric cylinders - the same structure for which PARANA has previously proven adequate - the technique "was fast enough that the band could easily be calculated on a personal computer. Moving the codes to our RISC workstations provides us with an extremely powerful desktop vehicle for investigation of photonic band structure" (*ibid.*:2774). This would give the computational flexibility we sought at the outset of this work, and we believe it is the best candidate for realizing the desktop design

goal. While many other codes exist, the successful use of Pendry's TMM approach in other research (Ho *et al.*, 1995; McCalmont *et al.*, 1996; Özbay *et al.*, 1996; Temelkuran *et al.*, 1998) makes us optimistic that it is particularly well suited to the PBG problem. Regardless, the most recent progress report on the Photonic Band Engineering MURI makes clear the challenge in meeting the objective of

computationally analyz[ing] some of the new PBG structures which are being developed in the optical and microwave regimes. Mainly this is for the purpose of guiding design. . . In addition we have the goal of design automation, or solving the inverse problem, in the form of genetic algorithms, for example. This goal is very computationally intensive, however, and most of our practical work is not automated and still has humans in the loop, making decision [*sic*] on how to modify certain designs (U.S. Army Research Office, 1998:19).

Reflection & Transmission Analysis

Band Edge/Cutoff Frequency. There is little to analyze here; the structure behaves essentially as expected. Our predicted band edge of 15.7 GHz agrees reasonably well with the observed value of 14.5 GHz in transmission, certainly within the expected error of the approximate relationship used for the original estimate (Equation (7)). Considering the variations we see in the band edge in reflection, there are likely some propagation directions in which a particular polarization can propagate, lowering the band edge slightly as in the UCLA MDPC (Sievenpiper *et al.*, 1996). Still, these are only minor perturbations to the overall behavior, and it appears that the AFIT photonic crystal has a cutoff frequency in the lower end of the K_u -band. Alternatively, the shift in the band edge may also come from misalignments between layers of the crystal. These misalignments, arising from the limited accuracy of our pinning hole placements, might represent a 'blurring' of the lattice structure, making it appear slightly larger and thus moving the associated band edge to a slightly lower frequency. This explanation would tend to

run counter to the effective medium hypothesis described earlier (pp. 15ff.), and further research would be required to determine which is the more reasonable explanation.

Polarization Effects. As mentioned earlier, there is a marked difference in the structure's reflection magnitude and phase as a function of incident wave polarization. This is readily explained by considering the relationship between the incident electric field and the metallic pattern elements of the mesh structure.

At normal incidence, we see a difference between the aligned (V and H) polarizations' reflected magnitude and that of the 45° (bisecting) polarization. When aligned, the field encounters pattern elements in every 'atomic' plane which are co-polarized with the incident wave. There are thus strong interactions between the two and the wave is strongly backscattered. In the bisecting polarization, the field is as far as possible from being aligned with any pattern element, the interaction with the cross-shaped 'atoms' is weaker, and the reflected magnitude decreases more rapidly as the frequency increases.

The phase relationship, on the other hand, is different and is best understood with reference to Figure 21. Here, for propagation in the $-z$ direction, a V-polarized field incident on the vertical elements of the front face immediately undergoes strong scattering and achieves the least penetration into the reflector. The 45° polarization is less closely aligned with the first plane of half-atoms and propagates further before undergoing reflection. The H-polarized wave does not encounter strong scattering until the first full layer of atoms, where it encounters horizontal pattern elements. Because of the extra plane of half-atoms on the surface of the crystal, we see an asymmetry-induced polarization dependence of the pattern.

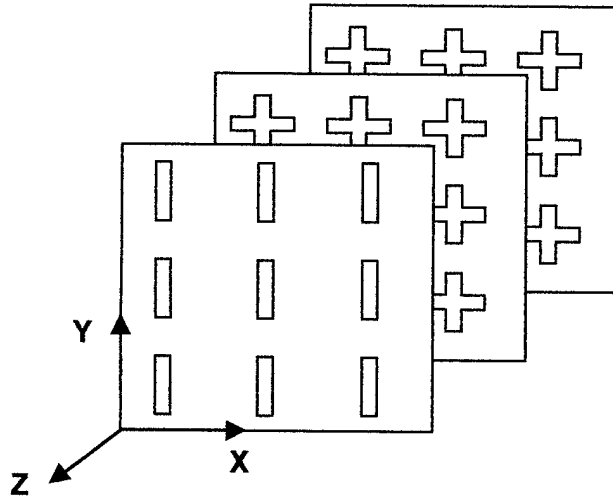


Figure 21. AFIT Photonic Crystal Without Vias, Showing First 2 1/2 Layers of Atoms

At off-normal incidence, a different concern comes into play. Here, the important factor is not the aligned or bisecting orientation, but rather the orientation of the E field within or orthogonal to the plane of incidence. TE radiation will interact primarily with the crosses that make up the 'atoms'. TM radiation, on the other hand, will excite a response on the plated via 'bonds'. As in the UCLA case, our slight reduction of the diamond symmetry (by introducing planar atoms) has split what would be a degeneracy in true diamond structure into distinguishable polarization cases (Sievenpiper *et al.*, 1998:2832). The only way to restore the degeneracy and improve the directional stability of the reflector's behavior is to make the structure fully replicate the diamond symmetry in all three dimensions.

If the above analysis is correct, one would expect the polarization effects to become more pronounced at higher frequencies, where the structure begins to look less like an effective medium and more like an array of discrete scatterers. The measured data show precisely this effect, with the phase separation between different polarizations growing steadily with increasing frequency (see Figures 14-16).

Effective Reflection Plane Analysis. To estimate the frequency span over which we would expect gain enhancement, we used the measured reflection data from the focused arch system as an input to a simple MATLAB script named SCHERPA (SCHloer Effective Reflection Plane Analysis, see Appendix D). The principle is simple: having empirically observed the apparent reflection depth within the reflector and using a known thickness and permittivity for our antenna substrate, we calculate the total electrical distance from the antenna to the reflection plane. We express this distance in wavelengths because the desire is that we maintain as close to a $1/4$ wavelength distance as possible to obtain constructive interference at the antenna.

As two benchmarks, we model a PEC reflector and a perfect absorber beneath the antenna. The PEC is treated as having a reflection coefficient of -1.0, while the absorber is assumed to reflect no energy at all. The antenna is treated as radiating a unit field toward the reflector/PEC plane/absorber and a unit field away, in the desired radiation direction. Total fields at the antenna are found by coherently summing the reflected and direct fields in each case, and the PBG reflector's performance is characterized by dividing the PBG reflector power by the other two configurations' power. The results are output as four subplots (Figure 21) showing (a) the electrical depth of the reflection plane within the PBG, (b) the total electrical distance from the antenna to the reflection plane, including the substrate, (c) PBG reflector gain versus the perfect absorbing boundary, and (d) PBG reflector gain versus the PEC ground plane.

A further explanation of certain features of Figure 22 is in order. The first subplot (upper left) shows the measured value of L_{eff} , the reflection plane distance behind the reflector's surface (Equation (2), p. 13), in wavelengths. One can regard the plot as sitting in the x-z plane of Figure 21 with the viewer looking in the -y direction. The surface of the PBG reflector then corresponds with the horizontal axis of the plot. The second subplot is just a plot of L_{eff} plus $h(f)$,

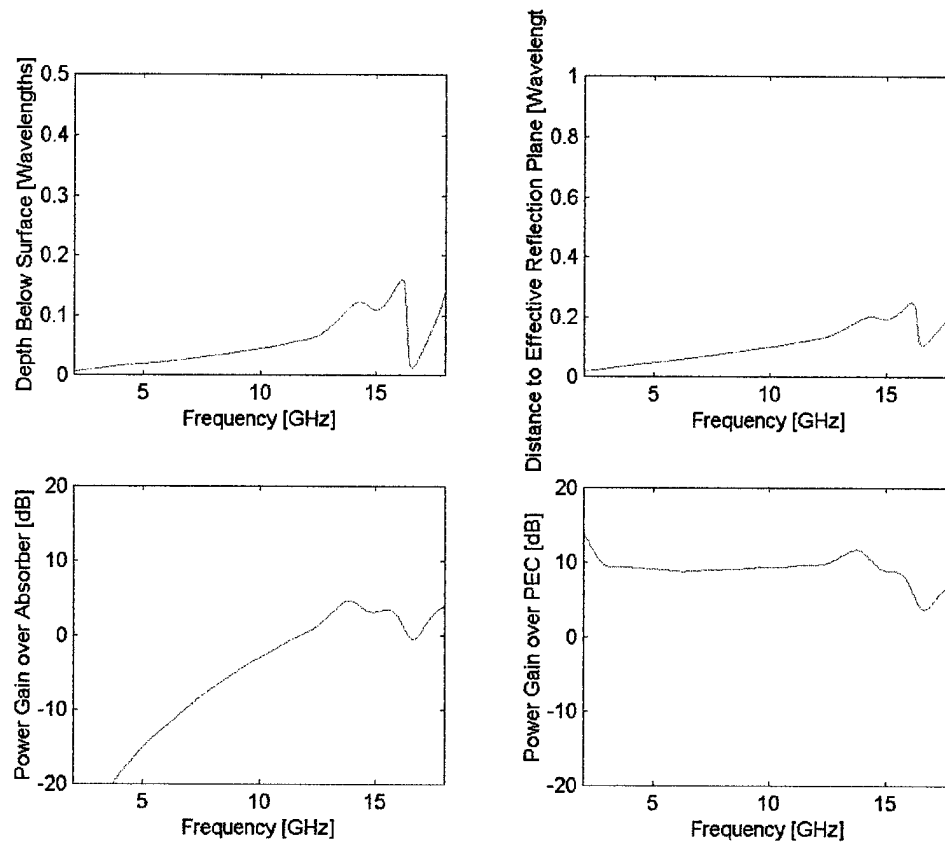


Figure 22. SCHERPA Output for Normal Incidence, Zero Azimuth, Vertical Polarization

the electrical thickness of the microstrip antenna substrate. Here, the horizontal axis corresponds to the plane of the antenna itself (assuming a planar antenna). On this plot, an ideal reflector-substrate pair would plot out at a constant value of 0.25, corresponding with the appropriate effective reflection distance for perfect constructive interference. The third subplot shows the power gain of the PBG reflector system in dB over an ideal absorber-loaded cavity benchmark. Here, the theoretical maximum gain is 6dB, since perfect constructive interference implies doubled field strength and quadrupled power relative to the idealized absorber-backed antenna that has no interference of any kind. The final subplot shows power gain for the PBG reflector over an ideal PEC benchmark located at the same position as the front face of the PBG reflector.

Here, there is no theoretical maximum, since the PEC reflector can cause destructive interference and thereby increase the *relative* power of the fields coming from the PBG reflector. Note that if the PEC plane were placed a quarter-wavelength behind the antenna at a desired operating frequency, the theoretical maximum *at that frequency* would be 0 dB.

This approach is too simplistic for a high accuracy prediction; it does not account for surface waves, losses, preferential radiation into a dielectric substrate, or any of the other factors that make microstrip antennas challenging to design. Furthermore, it implicitly assumes plane wave illumination because that is the illumination provided by the focused arch system used to collect the reflection data. The code is also set up only for normal incidence. Still, we intended the model solely as a first-order approximation to the real physical problem.

For a direct comparison, in Figure 23 we overlay the predictions from SCHERPA with plots of the measured relative gain for the zero azimuth, vertical polarization case. The upper plot shows the absorber comparison, the lower shows the PEC comparison. Any detailed comparison is difficult because of the very noisy nature of the measured data. A more useful comparison comes from examining contour plots like those in Figure 24. Each plot shows the contours for regions where we measured gain with the PBG reflector versus one of the other boundaries at a particular azimuth and polarization. The lowest contour is at zero dB (equal power) with subsequent contours at intervals of 3 dB up to 21 dB gain. The first example is for the vertically polarized case at normal incidence, with the absorber comparison on top and the PEC comparison below. The main difference is that this plot provides the data for all measured incident angles rather than just normal incidence.

Interestingly, even though it was only developed for normal incidence, the SCHERPA prediction accurately captures the overall behavior and main trend in each of the plots across the

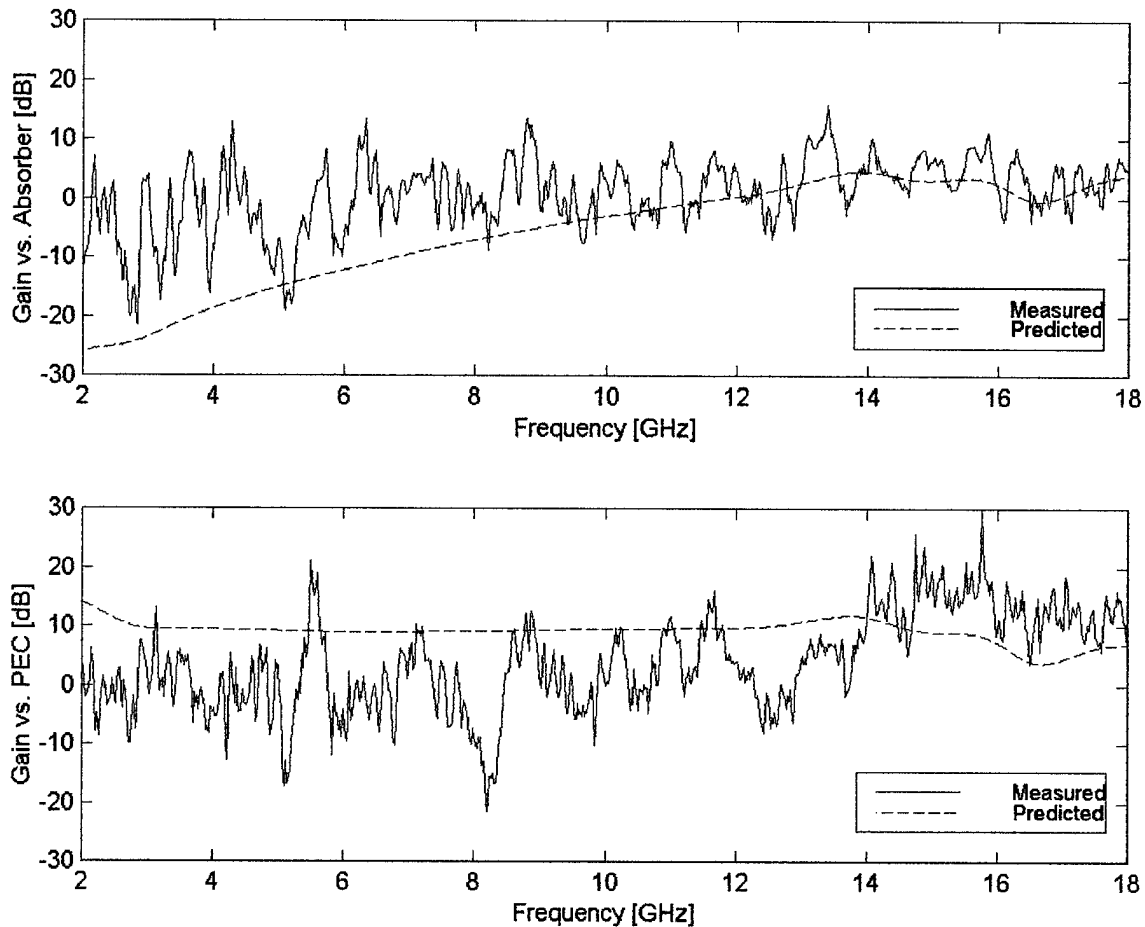
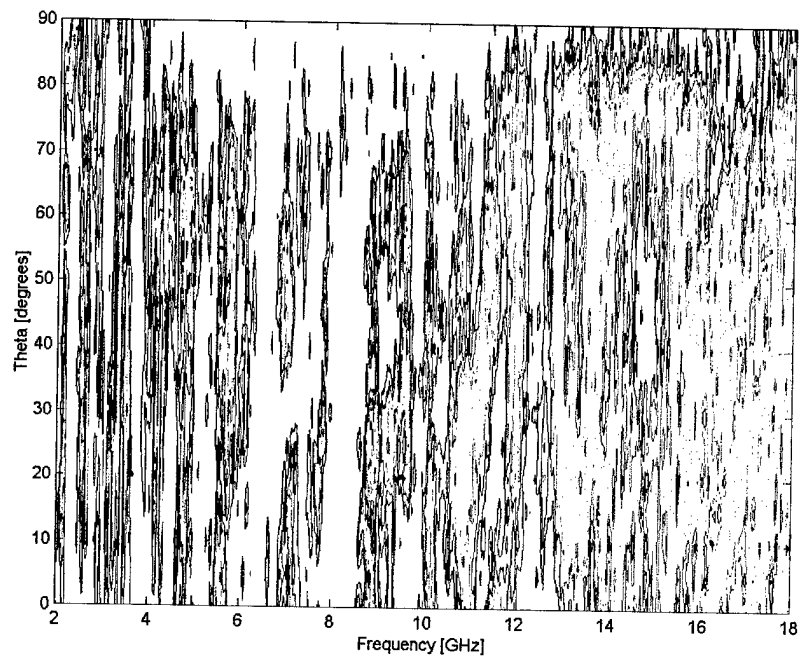
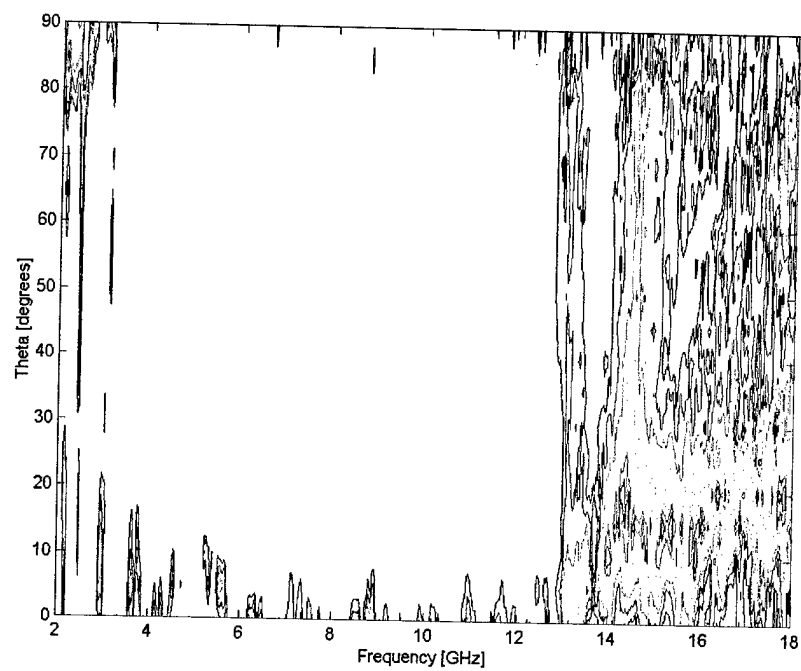


Figure 23. Comparison of SCHERPA Prediction with Measured Relative Gain at Normal Incidence (top) Gain Versus Absorber (bottom) Gain Versus Ground Plane

full range from normal to grazing incidence. Predicted and measured relative gains generally increase with frequency for the absorber comparison and are roughly level for the PEC comparison. Considering the noise present in the measurements due to the shorting effect of the reflection plane's proximity to the antenna (p. 57), the model seems to provide a useful first-order approximation of gain enhancement. The implication of this is that, given accurate reflection phase predictions from a computational analysis of a candidate reflector, one can estimate the potential for gain enhancement across a particular bandwidth without having to rely solely on



**Figure 24. Contour Plots of PBG Reflector Performance, Vertical Polarization
(top) Gain Versus Absorber (bottom) Gain Versus Ground Plane**

measurements. We conclude from this portion of the analysis that even a simple effective reflection plane model may be valid for describing the general behavior of a PBG reflector. A better model that accounts for realistic radiation could serve well as a 'back-of-the-envelope' design tool in PBG applications. The reader may further assess the utility of the effective reflection plane analysis used here by comparing the SCHERPA outputs in Appendix D with the corresponding relative gain contours in Appendix C.

Antenna Gain Pattern Analysis

We have already described some of the salient features of our gain comparison contours, including the reflector's generally superior performance against the ground plane and its inferior performance against the absorber loaded cavity. This relationship holds over the entire range of our data and is most likely due to the previously mentioned problem of the antenna's proximity to the ground plane. The PBG reflector partially alleviates this trouble, but still produces enough destructive interference that it does not perform particularly well against the absorber-loaded cavity. This assessment is also supported by the fact that almost everywhere in the experimentally confirmed stop band of the reflector, the absorber outperforms it. The most likely explanation for this is that the PBG reflector does not allow sufficient EM penetration and still behaves like a ground plane when compared with the absorber.

Conclusions

Looking back at our experiment, what can we deduce about engineering a photonic band gap reflector? First, the computational aspect of design is clearly non-trivial. This is probably the main reason that so many PBG experiments have adopted the 'try it and see' approach that we ended up using. Automated PBG design, "solving the inverse problem," and other similar goals are worthy but still far from completion and are likely to remain that way.

We therefore look for useful design inferences we can draw from the work just concluded. Among our most useful findings is the fact that a MPBG structure can have significant ($>10\%$) irregular lattice distortions and still exhibit the expected cutoff behavior. We have also provided further evidence that a three-unit cell structure is more than adequate to produce a sharp, deep stop band. In fact, our effective reflection plane analysis indicates that the reflection within the PBG occurs in the first unit cell of depth; it may well be that one can remove the other two unit cells' depth with little or no performance penalty. We have measured an approximately linear reflected phase within the stop band, indicating a possible suitability of this type of PBGS to use as an antenna reflector. We have assembled a large volume of bulk reflection data, rare in PBG research, and determined that the roughly linear phase behavior persists over a wide range of incident angles and complementing polarizations. We have also observed that even though our pattern elements are very electrically small, they can exert a profound influence on the polarization behavior of the crystal if they are not arranged symmetrically. We are also optimistic that a simple redesign of our structure - perhaps as basic as including a thicker dielectric substrate between the antenna and reflector - could provide significant gain enhancement over either of the comparison benchmarks.

We met with partial success in our research goals. We were able to run through all steps of a PBG design problem in a workstation environment, but were unable to solve the specific problem we wanted as a validation benchmark. The TMM technique appears to offer a solution to this shortcoming. We succeeded in developing a photonic crystal on a wire mesh design with an apparently complete stop band in a 150% fractional bandwidth spanning the S - to K_x -band frequencies, nearly meeting our 2-18GHz goal. We also demonstrated wideband (25% fractional bandwidth) gain enhancement of well over 10 dB for a frequency-independent microstrip antenna, though not over the range of incident angles we desired.

On the way to achieving these successes, we passed several side roads that presented interesting research challenges. Due to the constraints of finite time and energy, we were forced to leave them to other researchers, who will find them listed in the final chapter of this document.

VI. Suggestions for Further Work

Characterization and Refinement of the AFIT PBG Structure

Defect Studies. Much of the effort in PBG research is directed at creating very highly localized modes by introducing defects within the structure. This is due largely to the emphasis on finding PBGs for use in semiconductor lasers and other IR or optical applications. In the RF regime, defects could allow the propagation of selected frequencies within the stop band in an application such as a scan-independent PBG radome (Collins, 1997).

Although it was not intended as part of this research, we ended up studying the effect of a 2D defect on our structure. We strongly suspect that the polarization sensitivity of the structure is partially due to the extra half-sheet of 'atoms' on the incident face. Removing the pattern on the two outside faces should establish the true 'control' case for comparison. The ability to readily change our stack of circuit boards makes studying other defect structures straightforward (disassemble the stack, introduce the defect, reassemble and measure). Without any alteration of the circuit boards, one can investigate the effects of stacking defects:

- (1) Incorrect stacking sequence (ACBD-ACBD-ABCD)
- (2) Missing layer (ABCD-ABD-ABCD)
- (3) Layer replaced with dielectric (ABCD-AB ϵ D-ABCD)

Alteration of the existing boards could introduce other classes of defects:

- (4) Removal of individual atoms within the structure (point/zero dimensional defects)
- (5) Removal of a line of atoms within the structure (line/1D defects)

- (6) Removal of entire sheets of atoms or parts thereof (layer/2D defects)
- (7) Removal of adjacent atoms in successive layers (volumetric/3D defects)

Such studies could point the way toward other defects that could be integrated in a redesign of the structure for a different application. In an extreme case, one could combine a useful defect type with effective medium theory to create a periodic superlattice of defects with its own associated band structure.

Effective Reflection Plane Engineering. Can we control the effective reflection plane depth within the confines of the present design? There is no published research indicating what effect a change in the structure may have on the value of L_{eff} . As an example, one might consider changing the photonic crystal's thickness. Ample data exists to show that adding layers deepens the stop band in transmission (Özbay *et al.*, 1996:3798). But what happens to L_{eff} when we add or remove layers? We could assume that if L_{eff} is already far less than the thickness of the structure, it will not change simply because we add "extra" structure somewhere behind it. Yet the *effective* reflection plane location is only the observable result of scattering from the structure and does not necessarily correspond to an actual physical reflection at that depth. Further work on the effect of removing layers could be performed immediately with the present structure because the stack of circuit boards is not permanently bonded.

Method of Assembly. Our unbonded stack has the advantage of easy reconfiguration for further study on variables such as defect structures and changing the total number of layers. Yet it is not practical because of the need to use a vacuum to maintain pressure in the boards. Other assembly methods would have to preserve the electrical continuity between layers. Such methods might include using a conducting adhesive at each lattice position or 'sandwiching' the structure between two highly rigid plates clamped in compression. Finding an assembly method

that is practical and maintains electrical contact between layers would make this type of PBG structure far more flexible in its potential use. Alternatively, research could focus on using a capacitive bonding interlayer like the one used in the UCLA MDPC (Sievenpiper *et al.*, 1998) and studying the behavior of the resulting structure.

Minimum Size Requirement. The PBG substrate used in these measurements was large compared to the antenna. Investigation of the minimum size (in unit cells) of substrate required to open a sufficiently deep band gap would be useful in determining the feasibility of PBG substrates for various applications.

Antenna Type and Mounting. Leung *et al.* noted that a slot antenna performed better on a PBG substrate than did a dipole because the slot's own ground plane eliminated sidelobes due to the multiple scattering from the PBG material. Yet the PBG behind the slot still rejected radiation into its hemisphere and increased the power radiated into the forward hemisphere (Leung *et al.*, 1997:1569). Replacing our microstrip antenna with a log-periodic slot antenna (like that shown in Balanis, 1997:554) might improve the chances of demonstrating the wideband gain we sought in this experiment.

As described earlier, some researchers have studied the effects of placement relative to the PBG lattice on the measured patterns of highly resonant antennas. The question of how placement affects broadband antenna performance on a PBG substrate remains unresolved. In this research, we assumed that a frequency-independent antenna would be relatively insensitive to placement in relation to a lattice much smaller than the antenna itself. We were also not able to readily change the antenna's position because of the hole we had to drill for the coaxial feeds. A substantial additional project could address the sensitivity of our or a similar frequency-independent antenna to its position within the unit cell of a PBG structure.

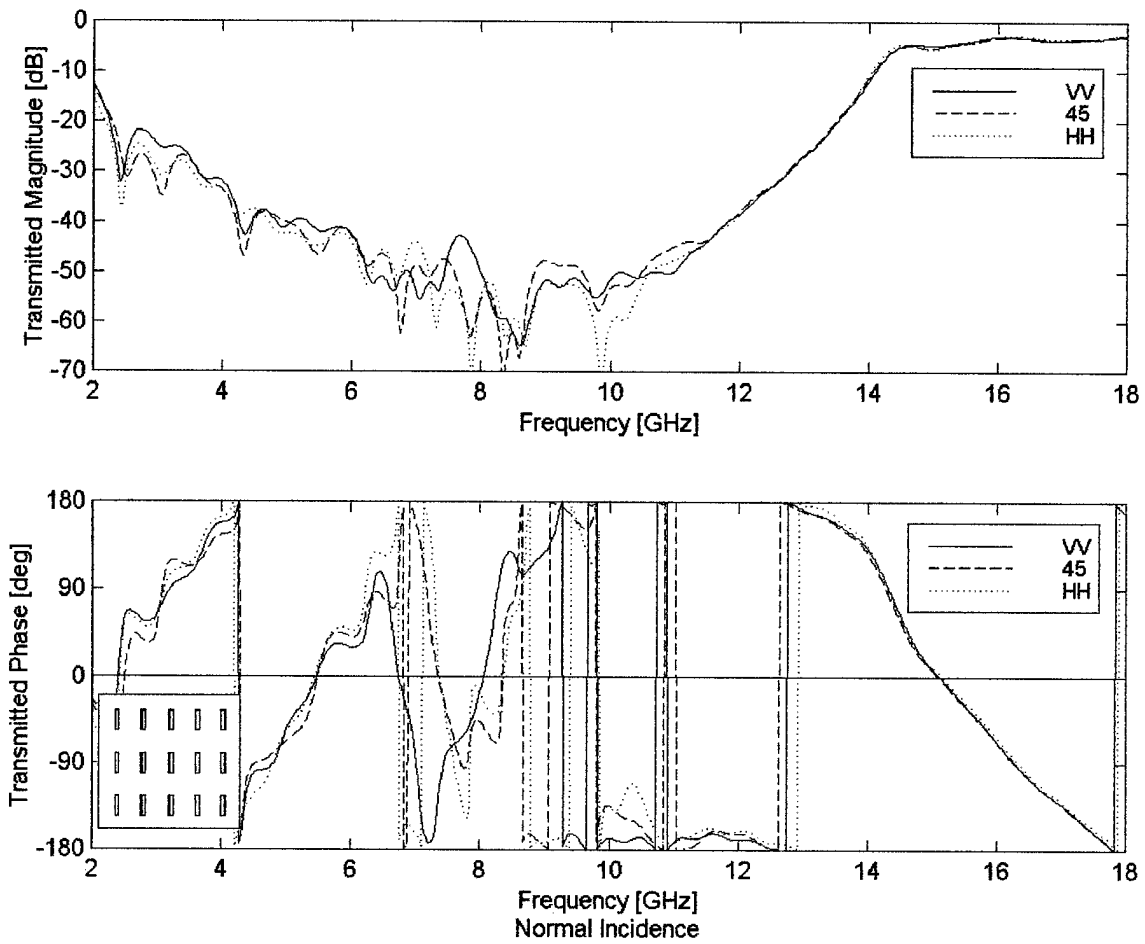
Computational Electromagnetics

Research in computational electromagnetics can support development of PBG structures of all types. As our own experience indicates, the computational aspects of a PBG problem can be some of the most vexing issues that arise. Any research that contributes to the ability to conduct reliable analysis, even in a low-order approximation, might be useful in narrowing the scope of a particular PBG design problem.

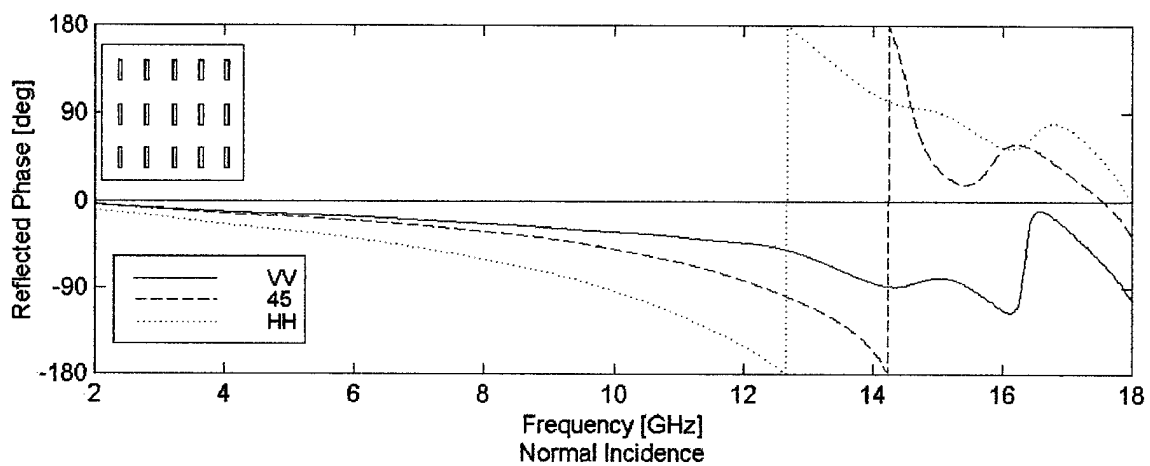
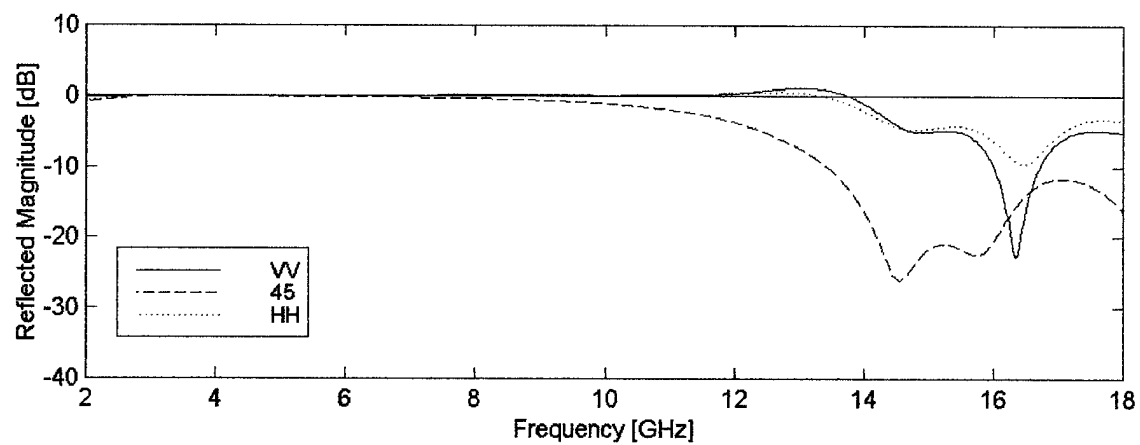
According to the MURI Interim Report for 1998, the finite difference time domain (FDTD) approach has been the "workhorse" among numerical techniques in PBG analysis. Finite element method (FEM) and moment method (MM) approaches have also seen significant use (U.S. Army Research Office, 1998:19). Among the papers reviewed for the present work, FDTD, and FEM methods each account for about 30% of the calculations with the remaining 40% covered by MM/plane wave approaches.

Appendix A. Reflection/Transmission Data

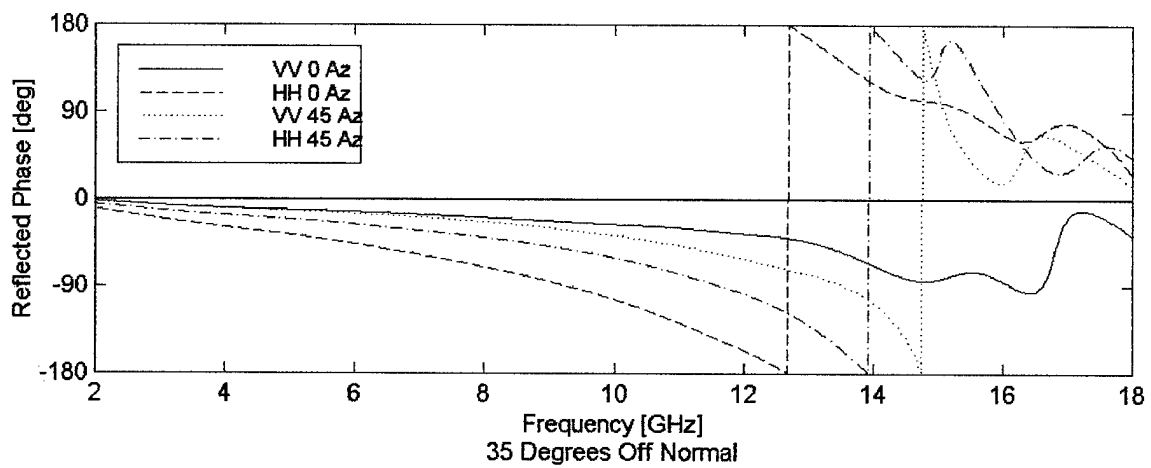
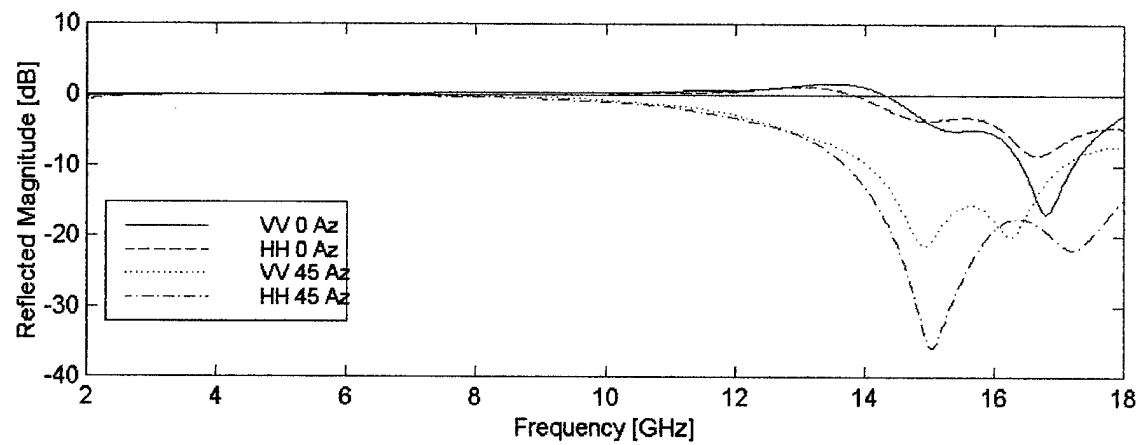
This appendix contains the plotted data for all of the 'bulk properties' measurements taken in the AFRL/XPN focused arch system. We present the data as paired plots of magnitude and phase. To facilitate analysis, data is presented in several combinations of 'constant' and 'variable' factors. For cases where the sample orientation is constant, we have included reference diagrams of the incident face of the sample as viewed along the incident wave vector. Depending upon the data presented, polarization is labeled either in the plot legend or in the overall figure caption. 'Zero azimuth' is defined as the orientation in which the sample is square with the page and the pattern elements on the incident face are vertically oriented. Ninety degrees azimuth is then square orientation with horizontal pattern elements on the incident face, and 45° azimuth is the case midway between the other two. These are the only azimuth angles used in our measurements. Elevation angle is defined with normal incidence as zero degrees (spherical-type coordinates). The sample rotation for elevation measurements was made about a vertical axis, so that at 90° elevation, the sample appears as a vertical line.



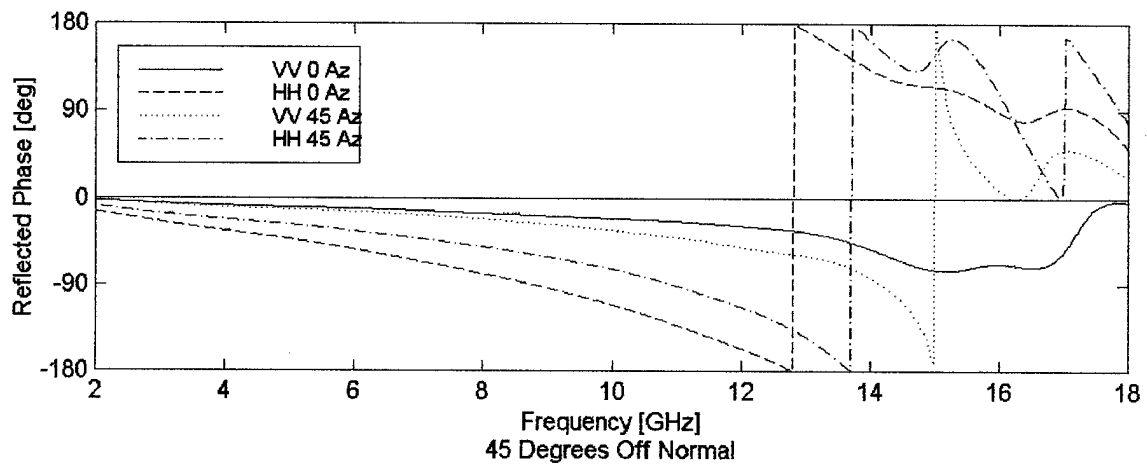
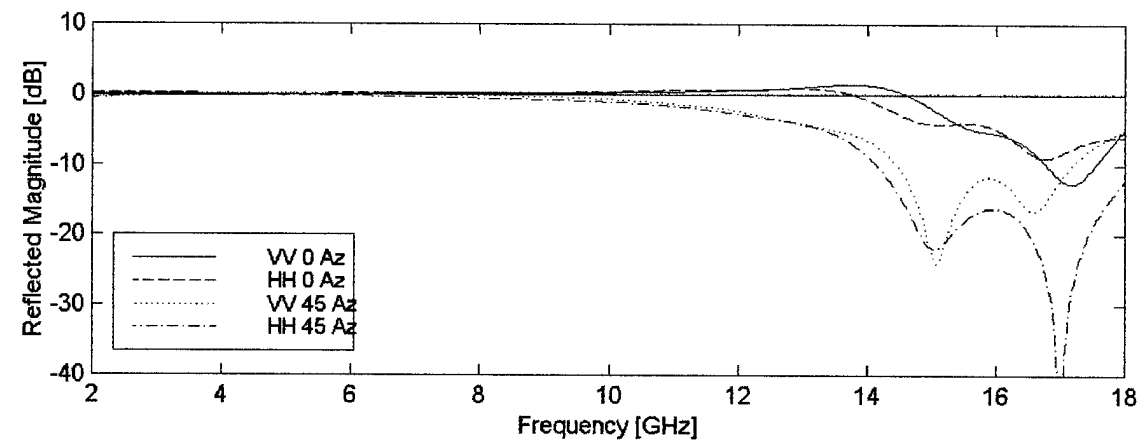
Bulk Transmission at Normal Incidence Showing Effect of Polarization



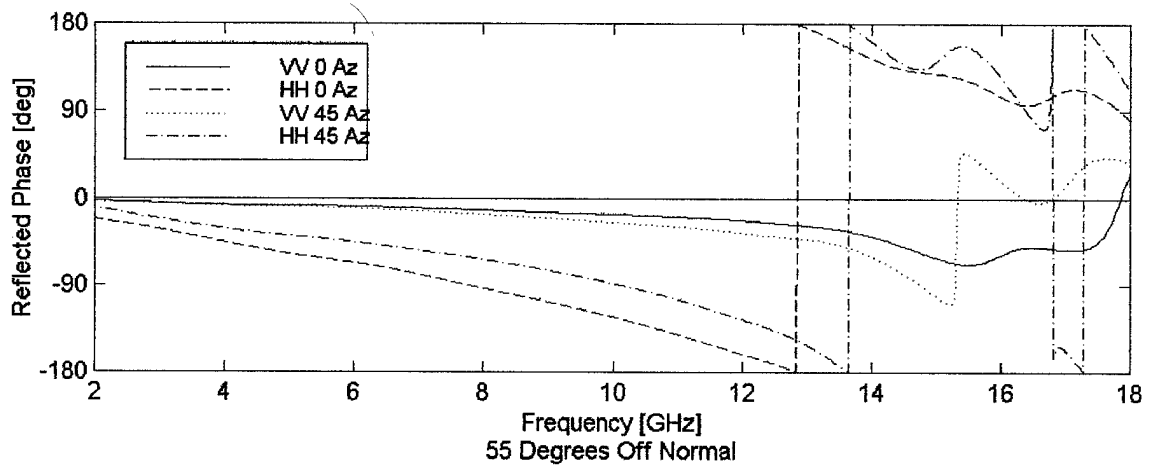
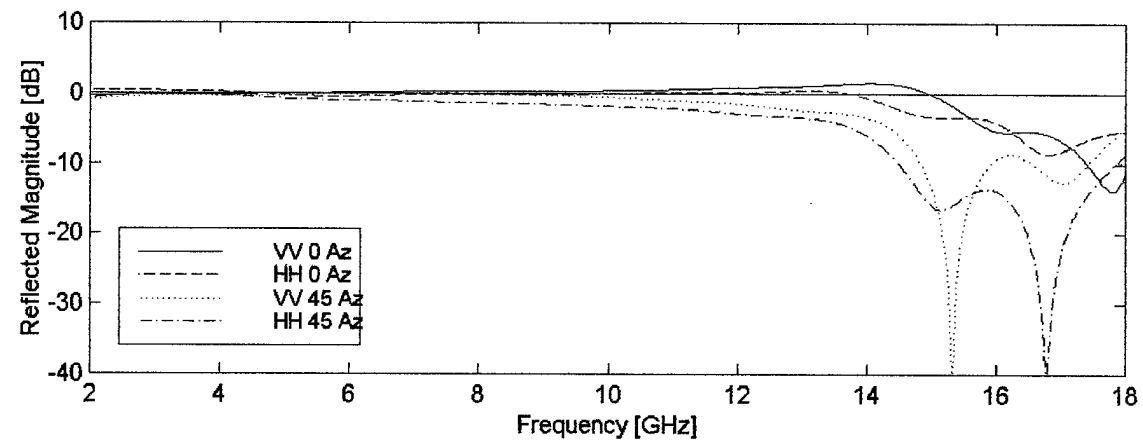
Bulk Reflection at Normal Incidence Showing Effect of Polarization



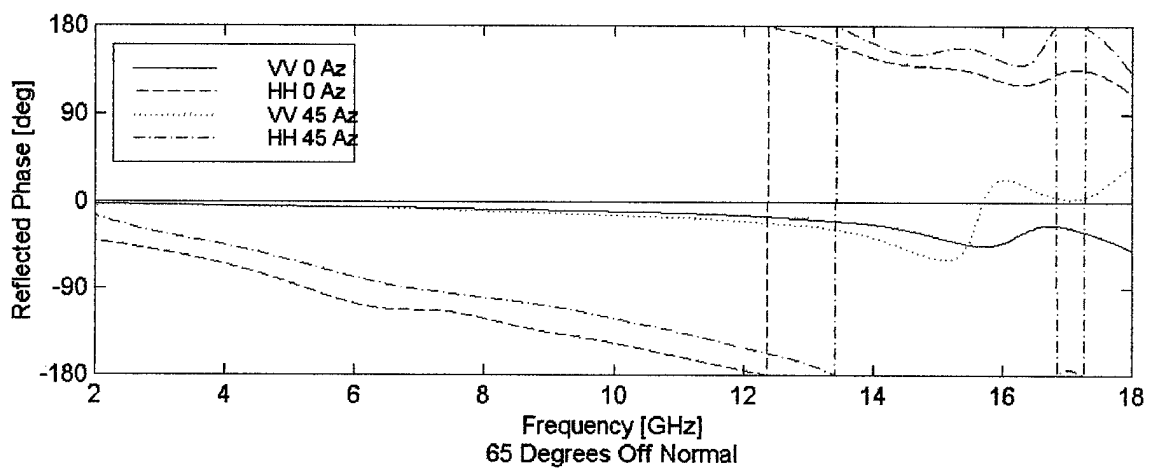
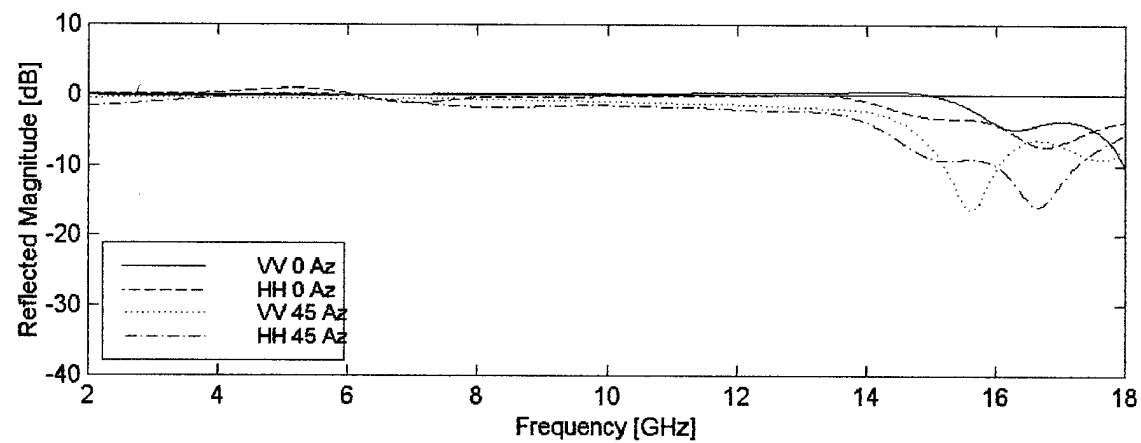
Bulk Reflection at 35° Incidence Showing Effect of Polarization



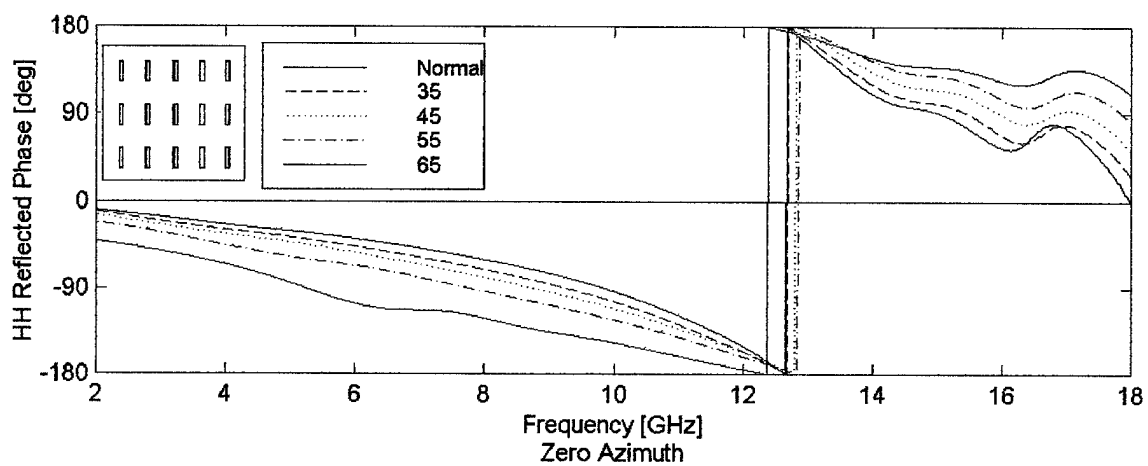
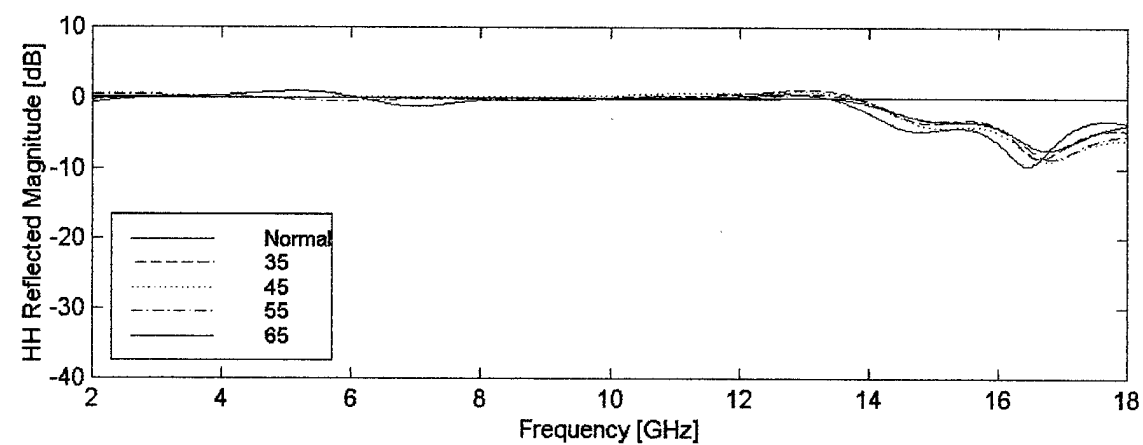
Bulk Reflection at 45° Incidence Showing Effect of Polarization



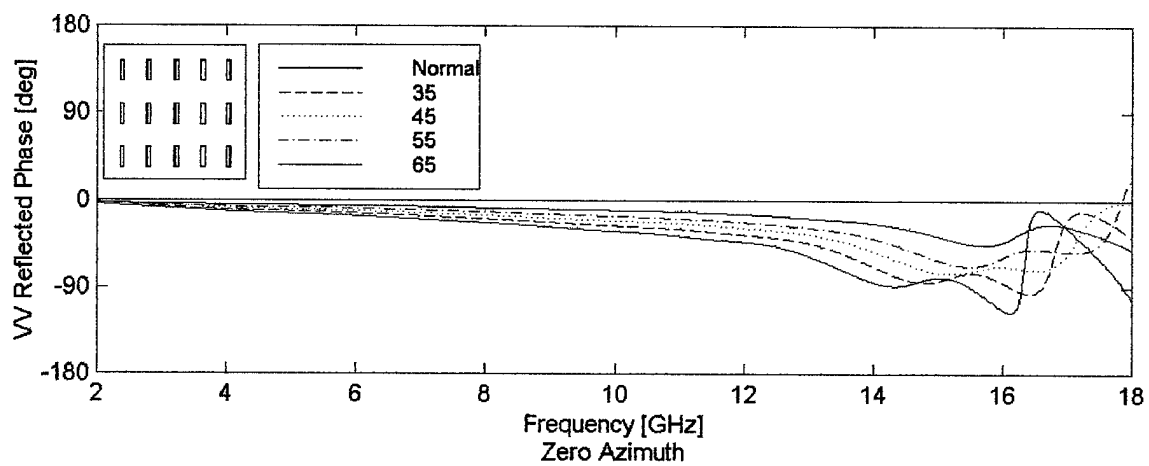
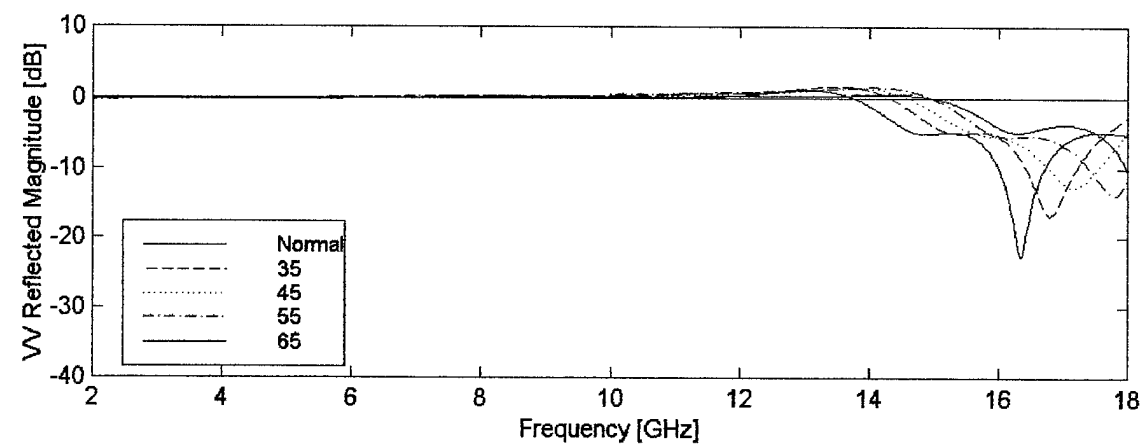
Bulk Reflection at 55° Incidence Showing Effect of Polarization



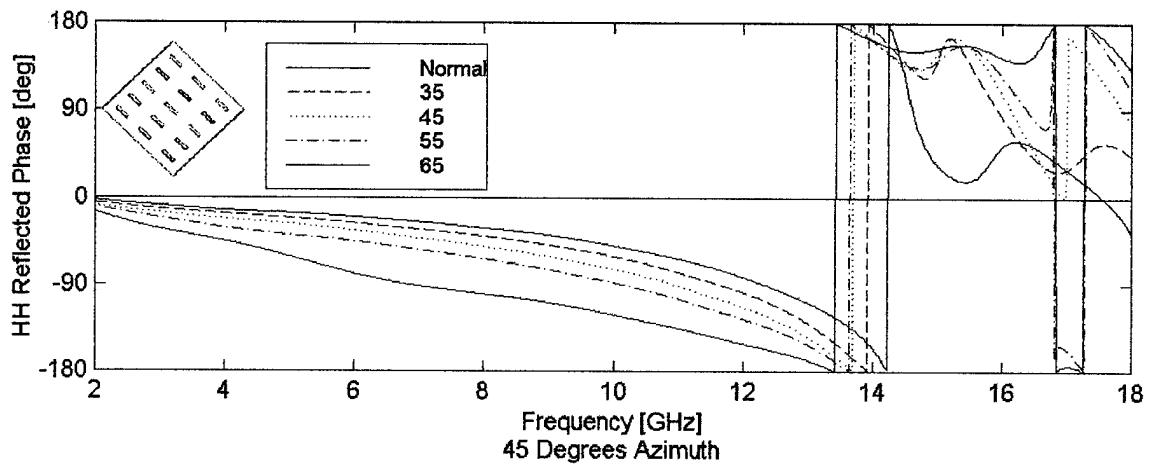
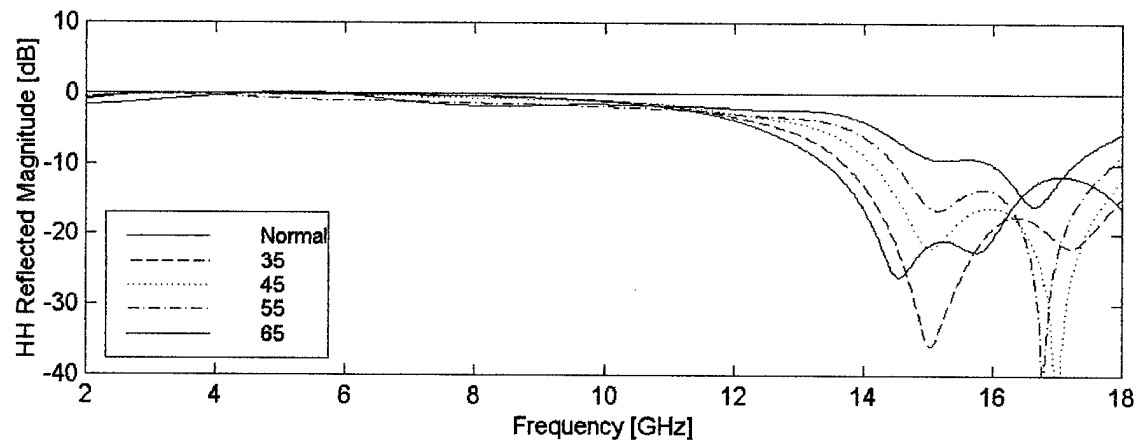
Bulk Reflection at 65° Incidence Showing Effect of Polarization



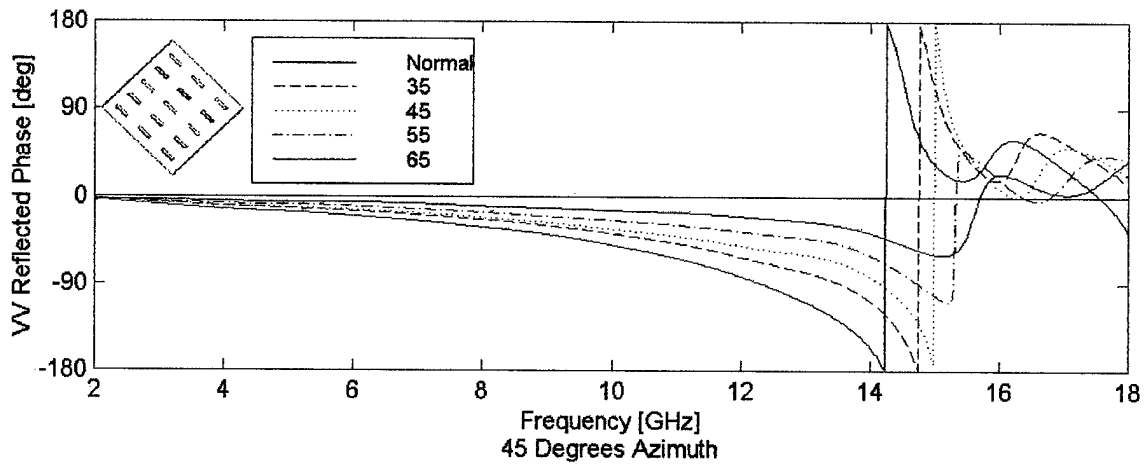
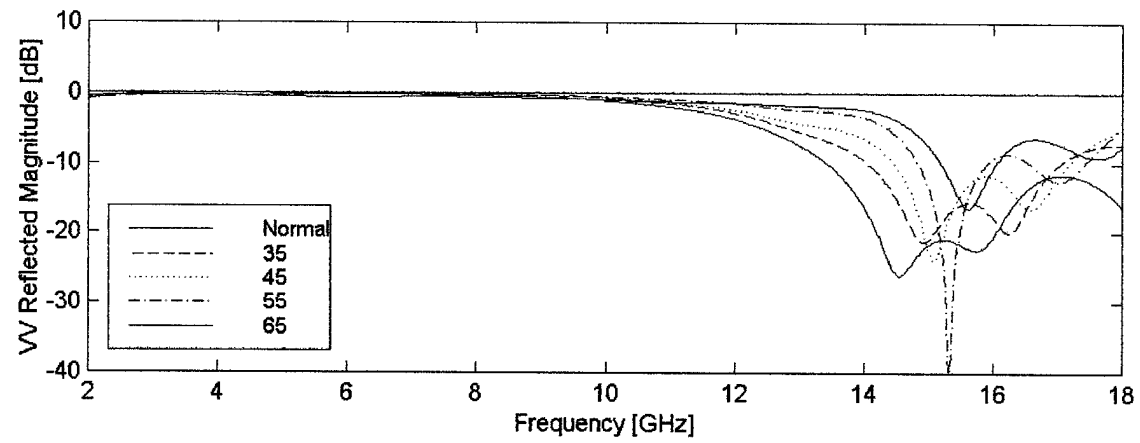
Bulk Reflection at Zero Azimuth, H/Parallel Polarization, Showing Effect of Elevation



Bulk Reflection at Zero Azimuth, V/Orthogonal Polarization, Showing Effect of Elevation



Bulk Reflection at 45° Azimuth, H/Parallel Polarization, Showing Effect of Elevation

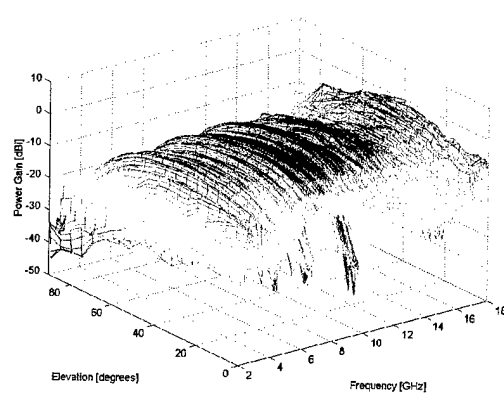
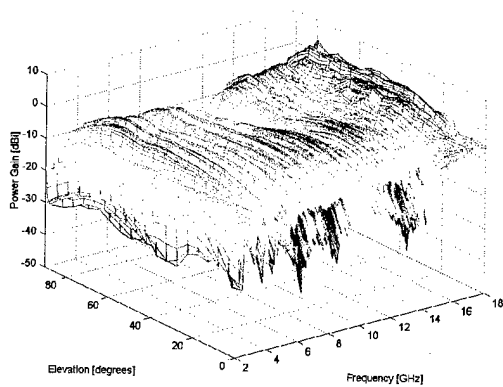
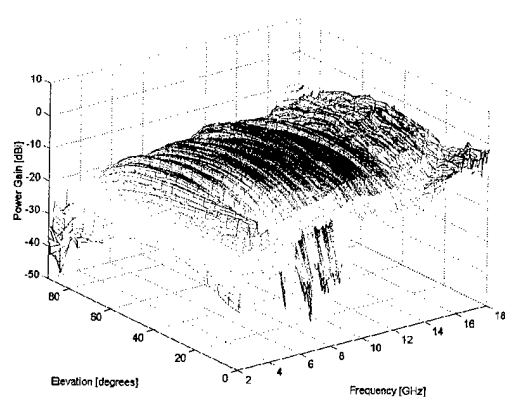
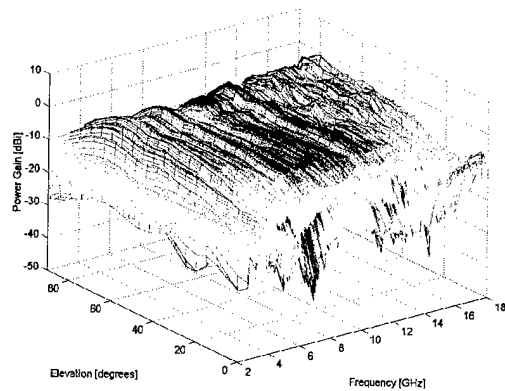
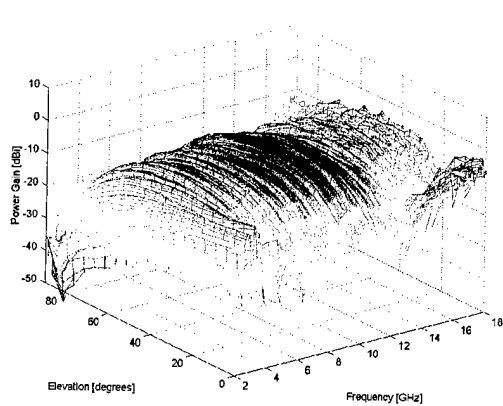
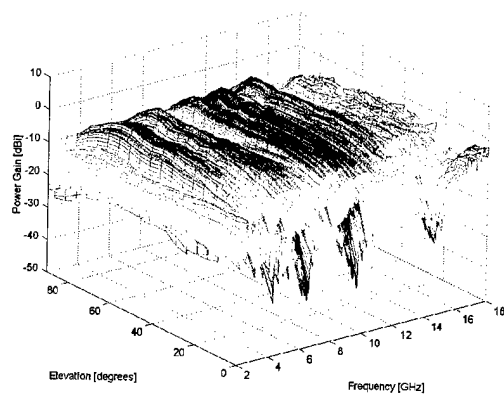


Bulk Reflection at 45° Azimuth, V/Orthogonal Polarization, Showing Effect of Elevation

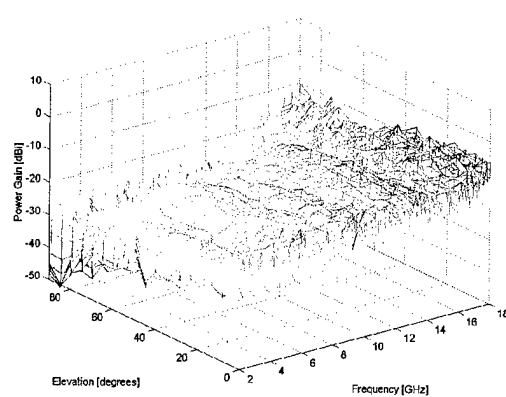
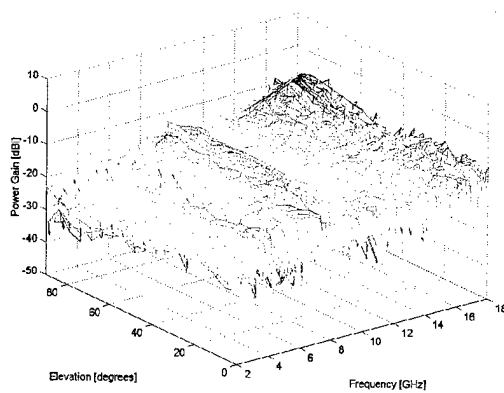
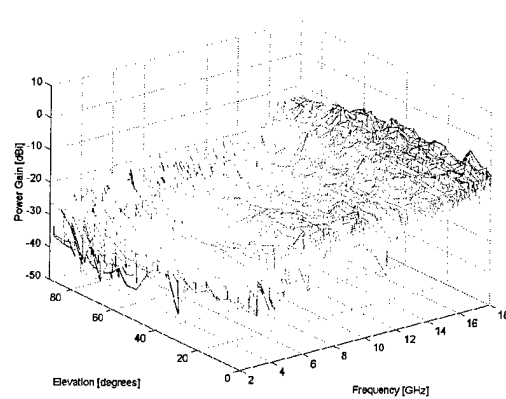
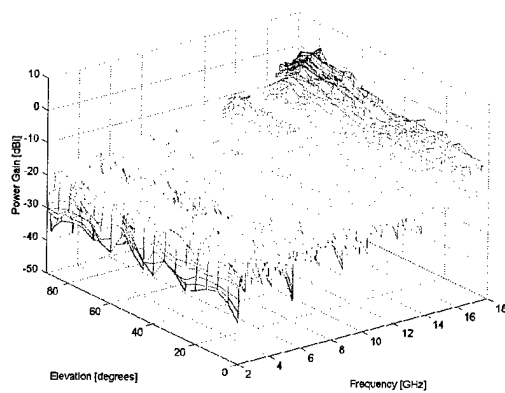
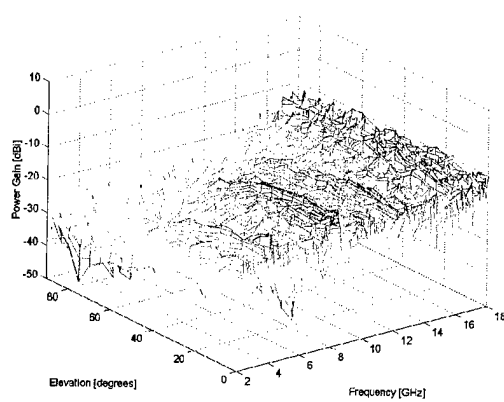
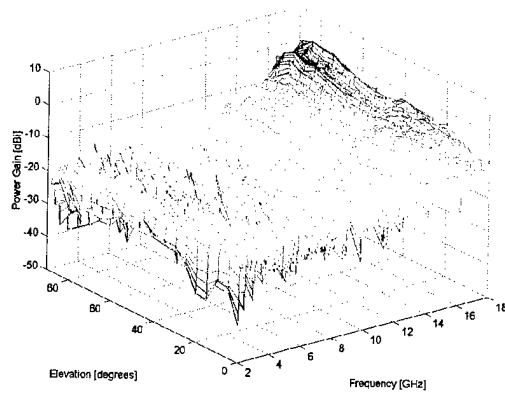
Appendix B. Antenna Pattern Cuts

This appendix contains the antenna pattern cuts measured in the AFIT Microwave Laboratory's anechoic chamber. The data is presented in a three-dimensional plotted format, with antenna gain in dB over isotropic plotted against both frequency and elevation. Plots are placed in pairs on each page, with the top plot showing horizontal/TM/parallel polarization and the bottom showing vertical/TE/orthogonal polarization. Each pair of plots is for a single azimuth angle. 'Zero azimuth' is defined as the orientation in which the reflector edges are vertical and horizontal and, for the PBG reflector, the pattern elements on the incident face are vertically oriented. Ninety degrees azimuth is then square orientation with horizontal pattern elements on the incident face of the PBG, and 45° azimuth is the case midway between the other two. These are the only azimuth angles used in our measurements. Elevation angle is defined with normal incidence as zero degrees (spherical-type coordinates), with data taken every five degrees. The rotation for elevation measurements was made about a vertical axis, so that at 90° elevation, the sample appears as a vertical line. Frequency sampling is every 20 MHz from 2 GHz to 18 GHz.

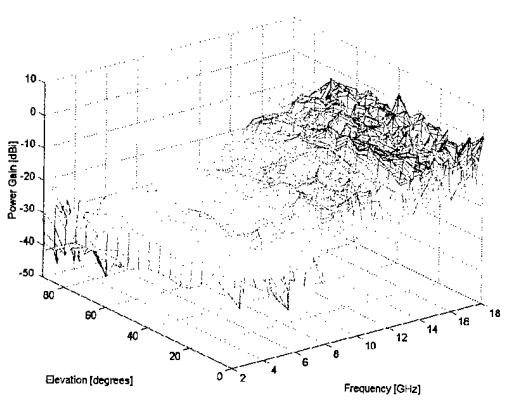
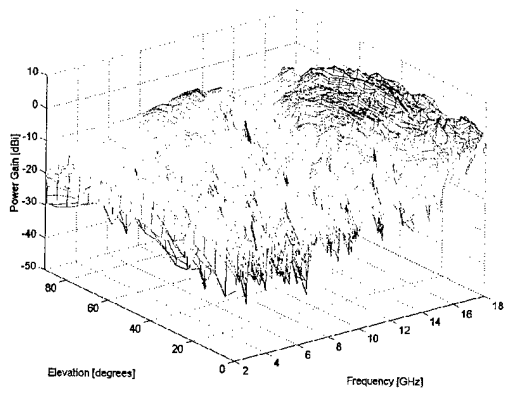
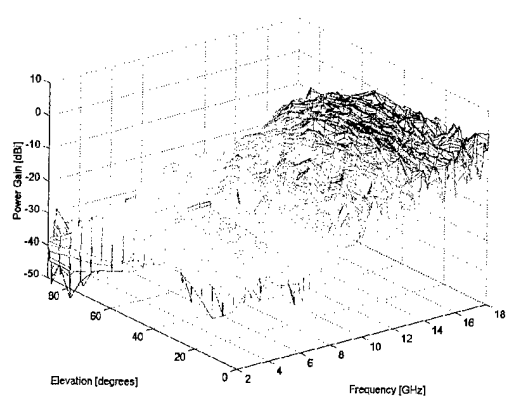
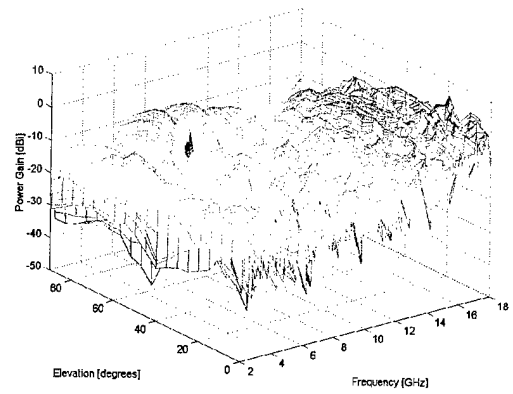
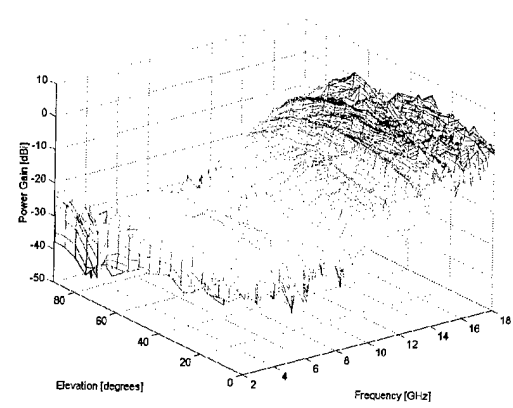
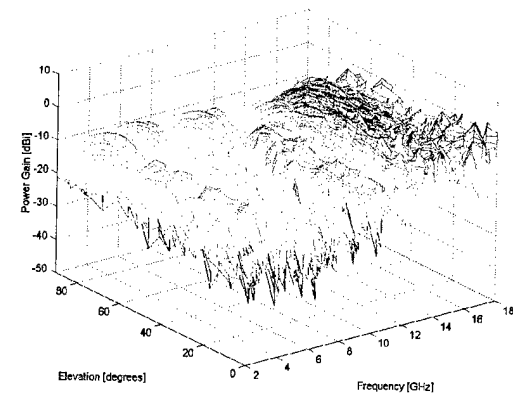
The plots have been reduced in size to allow comparison of all patterns for one configuration on a single page. Axes are identical on all plots, with the 2 GHz/0° incidence point at the front corner, incident angle on the left axis, and frequency on the right. The vertical axis runs from -50 to +10 dBi in 10 dB increments.



Pattern Cuts for Absorber Loaded Cavity Backed Antenna for (top) 0° Azimuth (middle) 45° Azimuth (bottom) 90° Azimuth; Orthogonal/TE Polarization on Right, Parallel/TM Polarization on Left



Pattern Cuts for Ground Plane Backed Antenna for (top) 0° Azimuth (middle) 45° Azimuth (bottom) 90° Azimuth; Orthogonal/TE Polarization on Right, Parallel/TM Polarization on Left

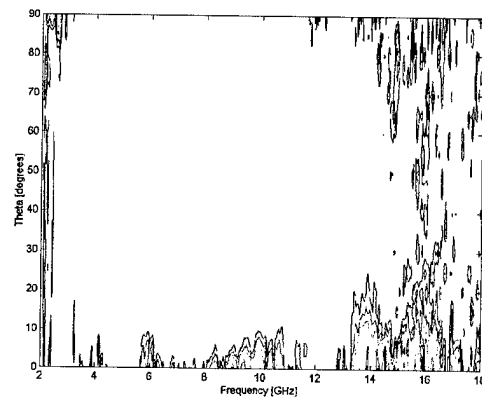
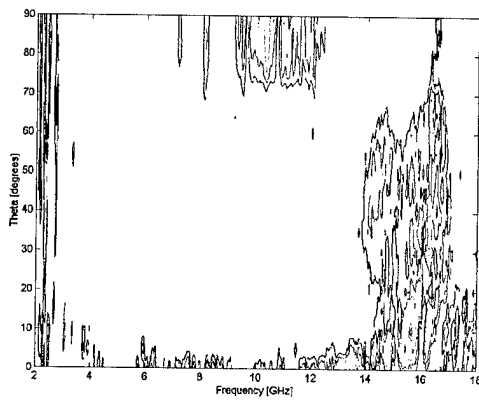
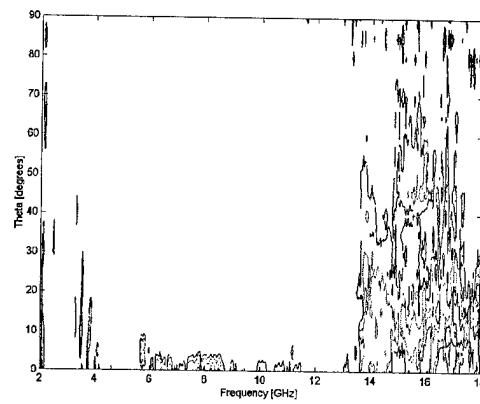
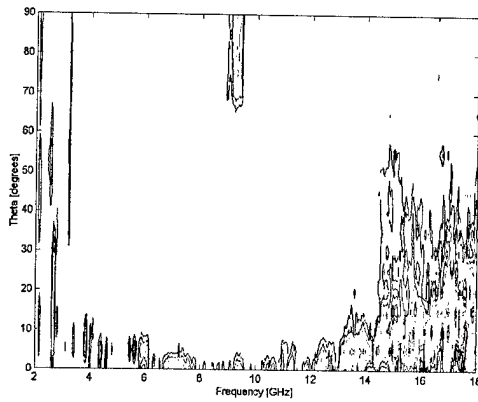
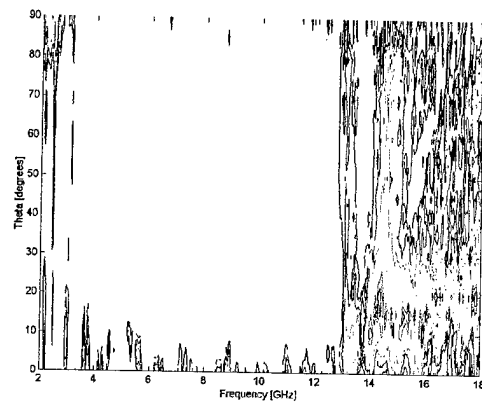
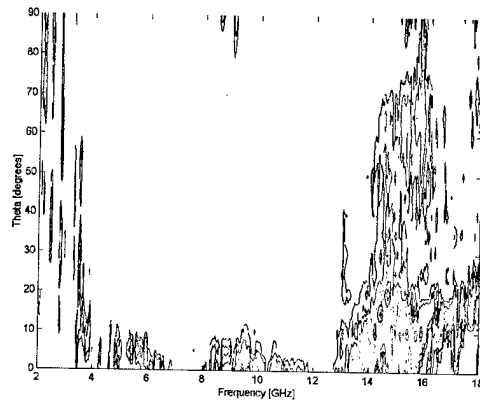


Pattern Cuts for PBG Reflector Backed Antenna for (top) 0° Azimuth (middle) 45° Azimuth (bottom) 90° Azimuth; Orthogonal/TE Polarization on Right, Parallel/TM Polarization on Left

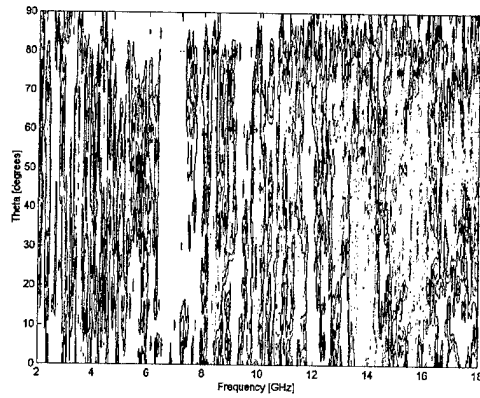
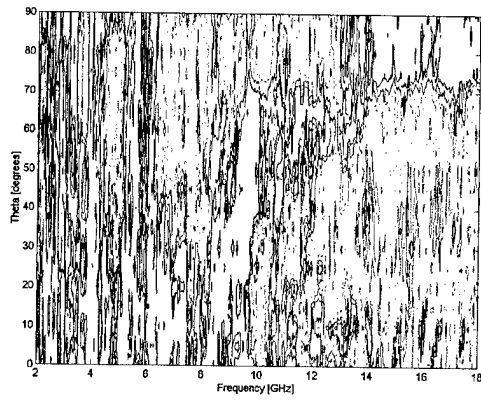
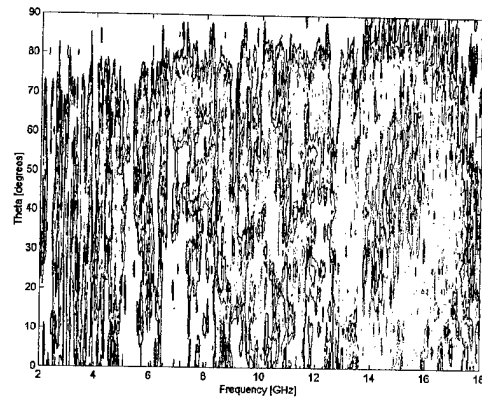
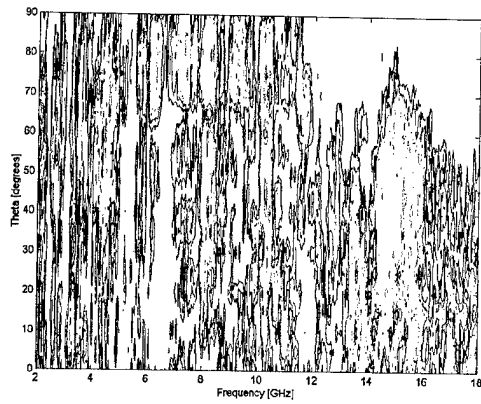
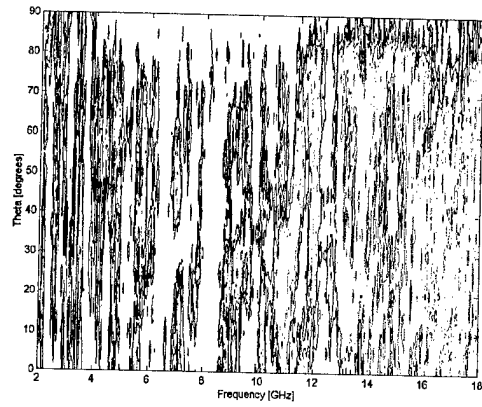
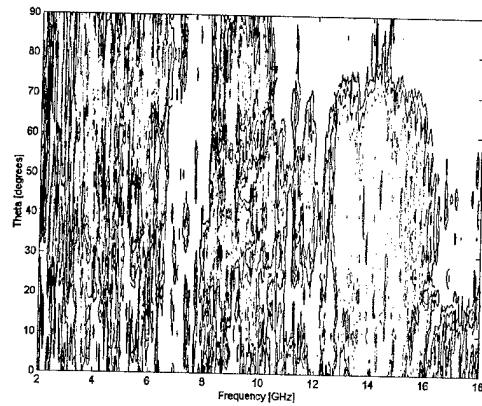
Appendix C. Gain Enhancement Contours

This appendix contains the relative antenna gain contours derived from the antenna pattern cuts of Appendix B. The data is presented in two-dimensional contour plots, with relative gain in dB over each reference case (the absorber loaded cavity and the reflecting ground plane) plotted against both frequency and elevation. The relative gain is plotted with starting with the 0 dB (no gain) contour at 3 dB intervals. Contours for negative values (i.e., *loss* versus the reference case) are left out for clarity, thus any large white space represents a region in which the antenna gain on the PBG reflector is inferior to the reference case. Plots are placed in pairs on each page, with the top plot showing TM/parallel polarization and the bottom showing TE/orthogonal polarization. Each pair of plots is for a single azimuth angle and reference case. 'Zero azimuth' is defined as the orientation in which the reflector edges are vertical and horizontal and, for the PBG reflector, the pattern elements on the incident face are vertically oriented. Ninety degrees azimuth is then square orientation with horizontal pattern elements on the incident face of the PBG, and 45° azimuth is the case midway between the other two. These are the only azimuth angles used in our measurements. Elevation angle is defined with normal incidence as zero degrees (spherical-type coordinates), with data taken every five degrees. The rotation for elevation measurements was made about a vertical axis, so that at 90° elevation, the sample appears as a vertical line. Frequency sampling is every 20 MHz from 2 GHz to 18 GHz.

Plots have been reduced so that all the comparisons against a given benchmark are on the same page. The vertical axis is incident angle and the horizontal axis is frequency.



**Relative Gain Contours for PBG Reflector Versus Absorber Loaded Cavity for
(top) 0° Azimuth (middle) 45° Azimuth (bottom) 90° Azimuth; Orthogonal/TE
Polarization on Right, Parallel/TM Polarization on Left**



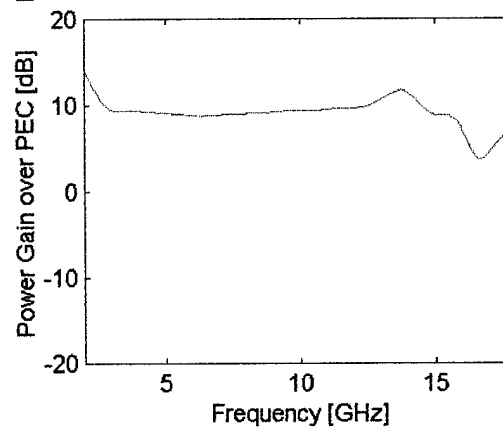
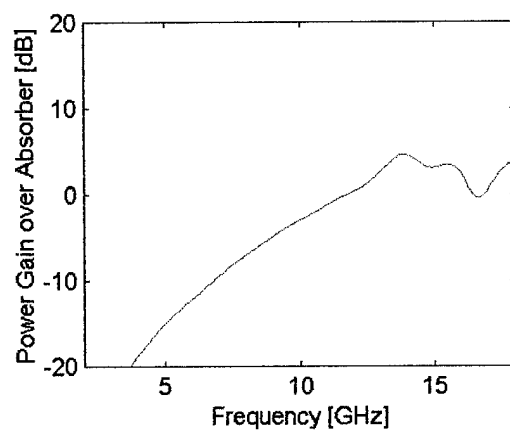
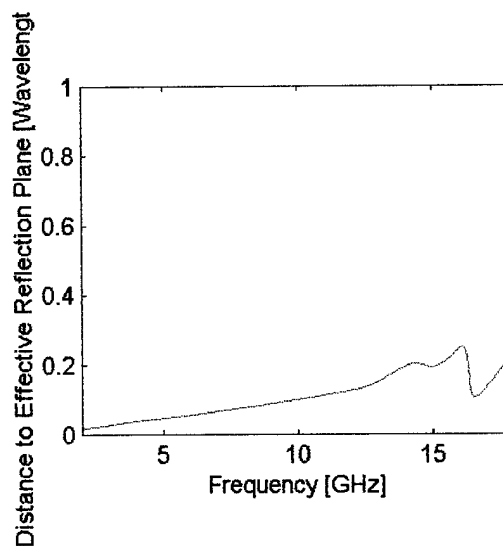
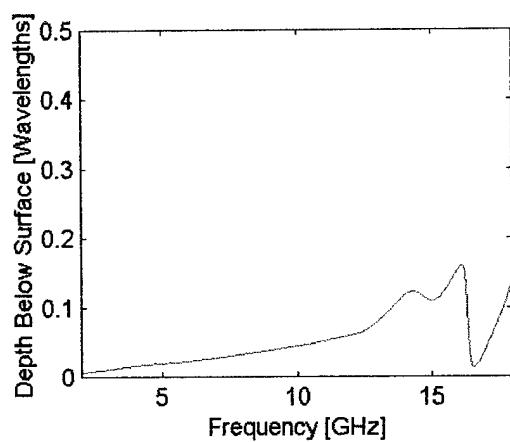
**Relative Gain Contours for PBG Reflector Versus Absorber Loaded Cavity for
(top) 0° Azimuth (middle) 45° Azimuth (bottom) 90° Azimuth; Orthogonal/TE
Polarization on Right, Parallel/TM Polarization on Left**

Appendix D. Effective Reflection Plane Analysis

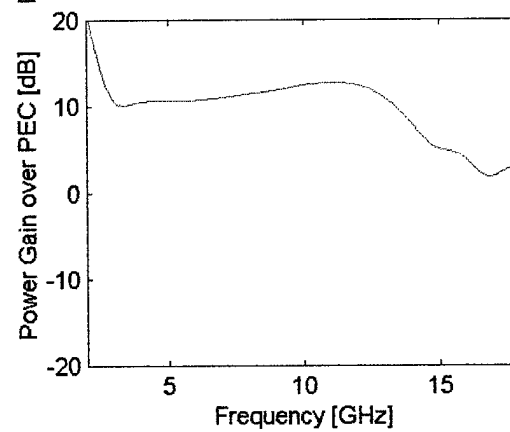
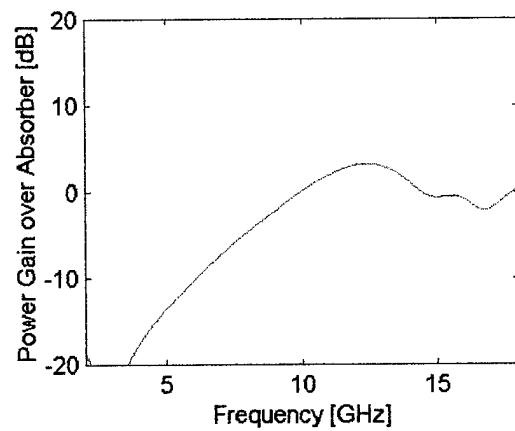
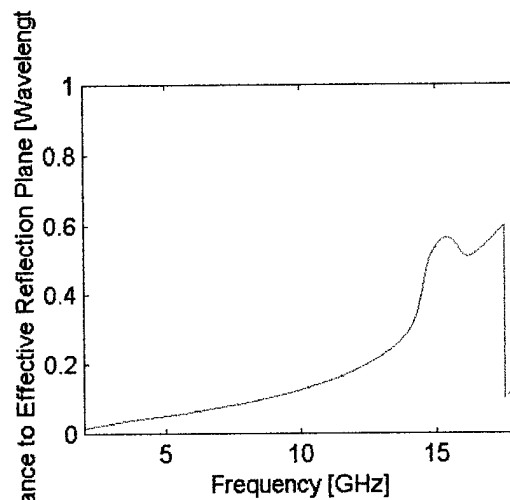
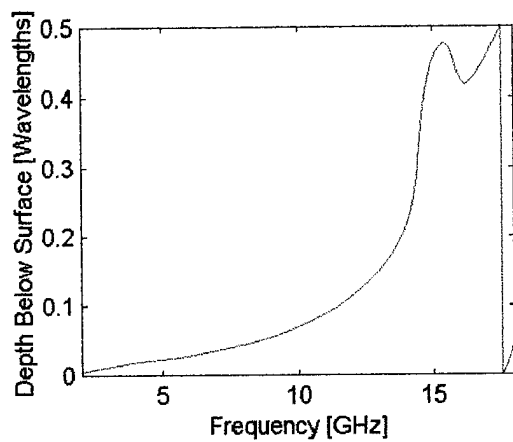
This appendix consists of a brief description of the Schloer Effective Reflection Plane Analysis (SCHERPA) code, sample outputs from the analysis in Chapter V, and a copy of the code itself. SCHERPA was written in MATLAB™ Version 5.2.

SCHERPA is a simple implementation, for normal incidence, of the effective reflection plane (ERP) concept described in Chapter II. It requires measured (or predicted) data for the magnitude and phase of fields reflected by a PBG structure as a function of frequency. It converts the phase information into an effective reflection depth within the structure. This information is used with the magnitude data to generate a reflected field which is coherently summed with a unit strength 'direct' field to obtain a total field for an idealized antenna above the PBG reflector. Comparisons are then made with fields radiated from the idealized antenna above (1) a perfectly conducting ground plane optimized for a user-specified operating wavelength and (2) a perfect absorber.

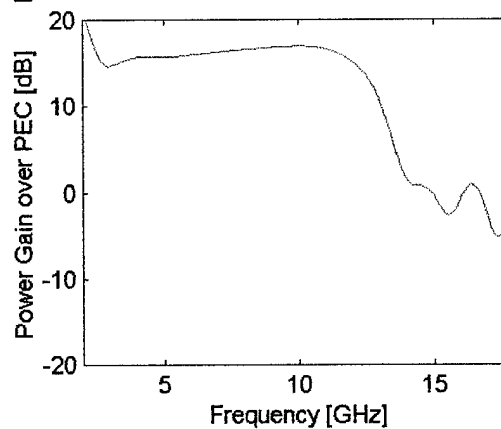
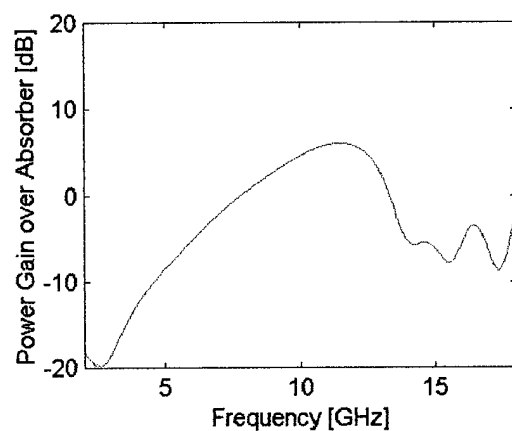
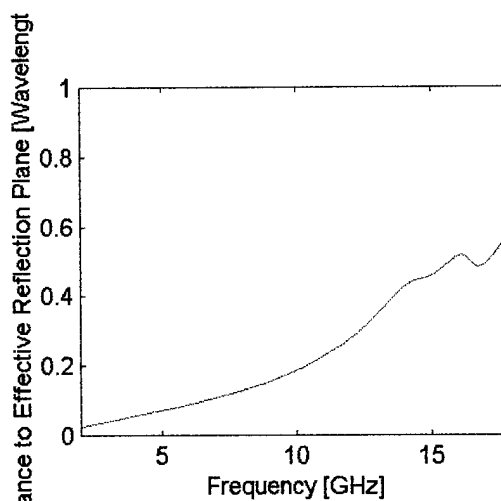
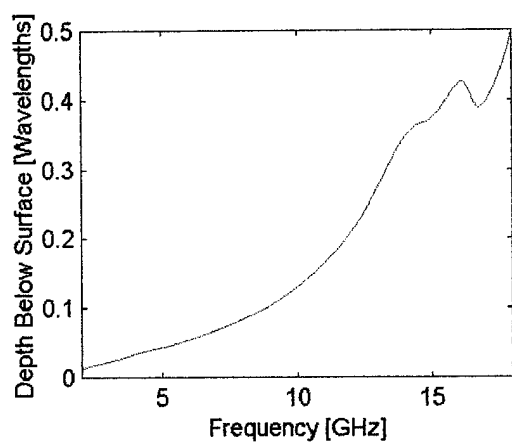
In slightly modified form, the code was used to generate the plots in this appendix showing the SCHERPA prediction of our PBG reflector's performance against the perfect absorber and perfect reflector reference cases. To generate these plots, we replaced the user-specified desired center frequency with a user-specified antenna substrate thickness matching our measured substrate dimensions. The resulting output plots are in four parts, showing (a) the electrical distance of the ERP beneath the PBG reflector's surface, (b) the total electrical distance from the antenna through the substrate to the ERP, (c) the predicted performance of the PBG reflector versus the perfect absorber, and (d) predicted PBG performance versus the PEC reflector.



**SCHERPA Output for 0° Azimuth, Vertical Polarization
(Limiting Case of Orthogonal Polarization)**



**SCHERPA Output for 45° Azimuth, Vertical Polarization
(Limiting Case of Orthogonal and Parallel Polarizations)**



**SCHERPA Output for 0° Azimuth, Horizontal Polarization
(Limiting Case of Parallel Polarization)**

```

%Schloer Effective Reflection Plane Analysis Version 1.0
%Capt Karl C. Schloer, Air Force Institute of Technology

c=3E8;

%Read in data file 'rt4500h' as the matrix 'tmp' and construct
the freq, mag & phase vectors
tmp = rt4500h;
freq=1E9*tmp(:,1); freqGHz=tmp(:,1); mag=tmp(:,2); phs=tmp(:,3);

%Adjust for phase rollover and nonphysical gains (S11>0)
for n=1:801,
    if phs(n)>0,
        phs(n)=phs(n)-360;
    end
    if mag(n)>0,
        mag(n)=0;
    end
end

%Calculate Leff, the distance of the effective reflection plane
beneath the PBG surface, in wavelengths and plot
Leff=-phs./720;

%Query for desired center frequency at which antenna will be 1/4
wave above reflection plane
hinmm=input('Enter substrate thickness in mm: ');
hinm = hinmm./1000;
epsiin=input('\nEnter epsilon of dielectric slab: ');
n=50*(centin-2.0); cent=freq(n+1); centGHz=(1E-9)*cent;
h=(.25-Leff(n+1)).*(c./(cent.*sqrt(epsiin))); hmm=1000*h;

```

```

%fprintf('\n%s %s %s\n\n','Antenna will be placed',hmm,'mm above
surface.')

%Calculate total electrical distance from reflection plane
aird=hinm*sqrt(epsiin)*freq(:,1)./c; totd=aird+Leff;

%Use an idealized antenna that radiates in only two directions,
directly toward and directly away from the reflector, with unit
field magnitude in each direction. Take coherent sum of reflected
and direct waves at the antenna and compare with perfect
absorbing and perfect reflecting substrates
PBGrefmag=10.^(mag./20);
PBGref=PBGrefmag.*cos((pi./180)*(720*totd+180));
PBGtot=PBGref+1;

%Absorbing substrate comparison - assume no reflected field
gain=20*log10(PBGtot);

%PEC substrate comparison - assume reflection coefficient = -1
h2=.25.*(c./(cent.*sqrt(epsiin)));
PECphs=(720.*hinm./(c./(freq.*sqrt(epsiin))))+180;
PECref=cos((pi./180).*PECphs); PECtot=PECref+1;
loss=20*log10(PBGtot./PECTot);

figure
set(gcf,'Color',[1 1 1],'Colormap',gray)
subplot(2,2,1), plot(freqGHz,d), xlabel('Frequency [GHz]'),
ylabel('Leff Depth Below Surface [Wavelengths]'), axis([2 18 0
0.5])
subplot(2,2,2), plot(freqGHz,totd), axis([2 18 0 1]),
xlabel('Frequency [GHz]'), ylabel('Electrical Distance to
Effective Reflection Plane [Wavelengths]')

```



```
subplot(2,2,3), plot(freqGHz,gain), xlabel('Frequency [GHz]'),  
ylabel('Power Gain over Absorber [dB]'), axis([2 18 -20 20])  
subplot(2,2,4), plot(freqGHz,loss), xlabel('Frequency [GHz]'),  
ylabel('Power Gain over PEC [dB]'), axis([2 18 -20 20])
```

Bibliography

- Agi, K., E. R. Brown, O. B. McMahon, C. Dill III and K. J. Malloy. "Design of ultrawideband photonic crystals for broadband antenna applications," Electronics Letters 30: 2166-2167 (8 December 1994).
- Balanis, Constantine A. Advanced Engineering Electromagnetics. New York: John Wiley & Sons, 1989.
- , Antenna Theory: Analysis and Design, Second Edition. New York: John Wiley & Sons, 1997.
- Barlevy, Alon S., Daniel F. Sievenpiper, and Yahya Rahmat-Samii. "Photonic Bandgap (PBG) Structures of Multiple Metallic Periodic Screens: Efficient Electromagnetic Characterization," IEEE Antennas & Propagation Symposium Proceedings, 1998, 1216-1219.
- Bouckaert, L. P. *et al.* "Theory of Brillouin Zones and Symmetry Properties of Wave Functions in Crystals," Physical Review 50: 58-67 (1936).
- Bowden, C. M., J. P. Dowling, and H. O. Everitt, Feature Editors. "Development and Applications of Materials Exhibiting Photonic Band Gaps," Special Feature in Journal of the Optical Society of America B 10: 280 (February 1993).
- Brillouin, Léon. Wave Propagation in Periodic Structures: Electric Filters and Crystal Lattices. New York: McGraw-Hill Book Company, 1946.
- Brown, E. R., C. D. Parker, and E. Yablonovitch. "Radiation properties of a planar antenna on a photonic-crystal substrate," Journal of the Optical Society of America B 10: 404-407 (February 1993).
- , -----, and O.B. McMahon. "Effect of surface composition on the radiation pattern from a photonic-crystal planar-dipole antenna," Applied Physics Letters 64: 3345-3347 (13 June 1994).
- and O.B. McMahon. "Large electromagnetic stop bands in metallodielectric photonic crystals," Applied Physics Letters 67: 2138-2140 (9 October 1995).
- Coccioli, R., W. R. Deal, and T. Itoh. "Radiation characteristics of a patch antenna on a thin PBG substrate," IEEE Antennas & Propagation Symposium Proceedings, 1998, 656-657.

- Collins, Peter J. Class handout, EENG 700, Seminar in Remote Sensing and Communications. School of Engineering, Air Force Institute of Technology, Wright-Patterson AFB OH, 23 October 1997.
- Eibert, Thomas F. and John L. Volakis. "Hybrid FE/BI Modeling of Commensurate and Non-Commensurate 3D Doubly Periodic Structures," IEEE Antennas & Propagation Symposium Proceedings, 1998, 414-417.
- Ellis, Thomas J. and Gabriel M. Rebeiz. "MM-Wave Tapered Slot Antennas on Micromachined Photonic Bandgap Dielectrics," IEEE Microwave Theory & Techniques Symposium Digest, 1996, 1157-1160.
- Everitt, Henry O. "Applications of Photonic Band Gap Structures," Optics & Photonics News, November 1992, 20-23.
- Hecht, Eugene. Optics, Second Edition. Reading, Massachusetts: Addison Wesley Publishing Company, 1987.
- Hewlett-Packard Company. Student Guide, HP Course Number HP8510B+24D, Basic Network Measurements Using the HP 8510B Network Analyzer System (Edition 3.0). Hewlett-Packard Company, January 1988.
- Ho, K. M., C. T. Chan, and C. M. Soukoulis. "Existence of a Photonic Gap in Periodic Dielectric Structures," Physical Review Letters 65: 3152-3155 (17 December 1990).
- Jasper, L. J. and G. T. Tran. "Photonic band gap (PBG) technology for antennas," SPIE 2843: 80-89 (1996).
- Joannopoulos, John D., Robert D. Meade, and Joshua N. Winn. Photonic Crystals: Molding the Flow of Light. Princeton: Princeton University Press, 1995.
- Kelly, P. K., J. G. Maloney, B. L. Shirley, and R. L. Moore. "Photonic Band Structures of Finite Thickness: Theory and Experiment," IEEE Antennas & Propagation Symposium Proceedings 1994, 718-721.
- Kesler, M. P., J. G. Maloney, and B. L. Shirley. "Antenna design with the use of photonic bandgap materials as all dielectric planar reflectors," Microwave and Optical Technology Letters 11: 169-174 (March 1996).
- Kirkpatrick, Scott. "Classical Transport in Disordered Media: Scaling and Effective-Medium Theories," Physical Review Letters 27: 1722-1725 (20 December 1971).
- Landauer, Rolf. "The Electrical Resistance of Binary Metallic Mixtures," Journal of Applied Physics 23: 779-784 (July 1952).
- Leung, K. M. "Diamondlike photonic band-gap crystal with a sizable band gap," Physical Review B 56: 3517-3519 (15 August 1997).

- and Y.F. Liu. "Full vector calculations of photonic band structures in face-centered cubic dielectric media," Physical Review Letters 65: 2646-2649 (date?).
- Leung, W.Y., R. Biswas, Shi-Di Cheng, M. M. Sigalas, J. S. McCalmont, G. Tuttle, and K.-M. Ho. "Slot Antennas on Photonic Bad Gap Crystals," IEEE Transactions on Antennas and Propagation 45: 1569-1570 (October 1997).
- McCalmont, J. S., M. M. Sigalas, G. Tuttle, K.-M. Ho, and C. M. Soukoulis. "A layer-by-layer metallic photonic band-gap structure," Applied Physics Letters 68: 2759-2761 (6 May 1996).
- McGrath, Daniel T. PARANA Version 2 Users' Guide: A Hybrid Finite Element Code for Phased Array Antenna, Periodic Structure, and Waveguide Device Analysis. Report Number PL-TR--97-1087. Kirtland AFB NM: Advanced Weapons and Survivability Directorate, Phillips Laboratory, 20 May 1997.
- McIntosh, K. A., L. J. Mahoney, K. M. Molvar, O.B. McMahon, S. Verghese, M. Rothschild, and E. R. Brown. "Three-dimensional metallodielectric photonic crystals exhibiting resonant infrared stop bands," Applied Physics Letters 70: 2937-2939 (2 June 1997).
- Moore, Ricky Lamar, Morris Philip Kesler, James Geoffrey Maloney, and Brian Leon Shirley. "Electromagnetic Antenna and Transmission Line Utilizing Photonic Bandgap Material," United States Patent Number 5,689,275 (18 November 1997).
- Nyhoff, Larry R. and Sanford Leestma. FORTRAN 77 for Engineers and Scientists Second Edition. New York: Macmillan Publishing Company, 1988.
- Özbay, E., A. Abeyta, G. Tuttle, M. Tringides, R. Biswas, C. T. Chan, C. M. Soukoulis, and K. M. Ho. "Measurement of a three-dimensional photonic band gap in a crystal structure made of dielectric rods," Physical Review B 50: 1945-1948 (15 July 1994).
- Özbay, E., B. Temelkuran, M. Sigalas, G. Tuttle, C. M. Soukoulis, and K. M. Ho. "Defect structures in metallic photonic crystals," Applied Physics Letters 69: 3797-3799 (16 December 1996).
- Pendry, J. B. and A. MacKinnon. "Calculation of Photon Dispersion Relations," Physical Review Letters 69: 2772-2775 (9 November 1992).
- Pendry, J. B., A. J. Holden, W. J. Stewart, and I. Youngs. "Extremely Low Frequency Plasmons in Metallic Mesostructures," Physical Review Letters 76: 4773-4776 (17 June 1996).
- Poilasne, G., J. Lenormand, P. Pouligen, K. Mahdjoubi, C. Terret, and Ph. Gelin. "Theoretical Study of Interactions Between Antennas and Metallic Photonic Band-Gap Materials," Microwave and Optical Technology Letters 15: 384-389 (20 August 1997).

- Poilasne, G., P. Pouligen, K. Mahdjoubi, C. Terret, Ph. Gelin, and L. Desclos. "Radiation Characteristics of a Half Wavelength Dipole Inside Metallic Photonic Band-Gap Structures," IEEE Antennas & Propagation Symposium Proceedings, 1998, 170-173.
- Radisic, Vesna, Yongxi Qian, Roberto Coccioli, and Tatsuo Itoh. "Novel 2-D Photonic Bandgap Structure for Microstrip Lines," IEEE Microwave and Guided Wave Letters 8: 69-71 (February 1998).
- Schultz, John W. Focused Arch Measurement System User's Manual. Signature Technology Branch, Air Force Research Laboratory, Wright-Patterson AFB OH, November 1998.
- Sievenpiper, D. F., M. E. Sickmiller, and E. Yablonovitch. "3D Wire Mesh Photonic Crystals," Physical Review Letters 76: 2480-2483 (1 April 1996).
- Sievenpiper, D. F., E. Yablonovitch, J. N. Winn, S. Fan, P. R. Villeneuve, and J. D. Joannopoulos, "3D Metallo-Dielectric Photonic Crystals with Strong Capacitive Coupling between Metallic Islands," Physical Review Letters 80: 2829-2832 (30 March 1998).
- Sigalas, M. M., C. T. Chan, K. M. Ho, and C. M. Soukoulis. "Electromagnetic Wave Propagation Through Dispersive and Absorptive Photonic Band-Gap Materials," Physical Review B 49: 11080-11087 (15 April 1994).
- Sigalas, M. M., C. T. Chan, K. M. Ho, and C. M. Soukoulis. "Metallic photonic band-gap materials," Physical Review B 52: 11744-11751 (15 October 1995).
- Sigalas, M. M., R. Biswas, Q. Li, D. Crouch, W. Leung, R. Jacobs-Woodbury, B. Lough, S. Nielsen, S. McCalmont, G. Tuttle, and K.M. Ho. "Dipole Antennas on Photonic Band-Gap Crystals - Experiment and Simulation," Microwave and Optical Technology Letters 15: 153-158 (20 June 1997).
- Smith, Glenn S., Morris P. Kesler, and James G. Maloney. "Dipole antennas used with all-dielectric, woodpile photonic-bandgap reflectors: gain, field patterns, and input impedance," scheduled for publication in Microwave and Optical Technology Letters (May 1999).
- Solymar, L. and D. Walsh. Lectures on the Electrical Properties of Materials (Fourth Edition). Oxford: Oxford University Press, 1988.
- Stoytchev, M. and A. Z. Genack. "Microwave transmission through a periodic three-dimensional metal-wire network containing random scatterers," Physical Review B 55: R8617-R8619 (1 April 1997).
- Temelkuran, B., E. Ozbay, M. Sigalas, G. Tuttle, C. M. Soukoulis, and K. M. Ho. "Reflection properties of metallic photonic crystals," Applied Physics A 66: 363-365 (1998).

- U.S. Army Research Office. Photonic Band Engineering Interim Progress Report. USARO Award Number DAAH04-96-1-0389, 1 January 1998 - 31 December 1998.
- Vassallo, C. "Effective Dielectric Tensor for Electromagnetic Waves in Weakly Inhomogeneous Media," Journal of Applied Physics 43: 892-897 (March 1972).
- Verdeyen, Joseph T. Laser Electronics (Third Edition). Englewood Cliffs, NJ: Prentice-Hall, Inc., 1995.
- Yablonovitch, E. "Inhibited Spontaneous Emission in Solid State Physics and Electronics," Physical Review Letters 58: 2059-2062 (18 May 1987).
- and T. J. Gmitter. "Photonic band structures: The face-centered cubic case," Physical Review Letters 63: 1950-1953 (30 October 1989).
- , T. J. Gmitter, and K. M. Leung. "Photonic Band Structure: The Face-Centered Cubic Case Employing Nonspherical Atoms," Physical Review Letters 67: 2295-2298 (21 October 1991).
- , T. J. Gmitter, R. D. Meade, K. D. Brommer, and J. D. Joannopoulos. "Donor and Acceptor Modes in Photonic Band Structure," Physical Review Letters 67: 3380-3383 (9 December 1991).
- , "Photonic band-gap structures," Journal of the Optical Society of America B 10: 283-295 (2 February 1993).
- Yang, Hung-Yu David, Nicolaos G. Alexopoulos, and Eli Yablonovitch. "Photonic Band-Gap Materials for High-Gain Printed Circuit Antennas," IEEE Transactions on Antennas and Propagation 45: 185-187 (January 1997).
- Yang, D. H. and K. Agi, Session Chairs. "Antenna Applications of Photonic-Band-Gap Materials," Special Session in USNC/URSI National Radio Science Meeting Digest. 113-123 (21-26 June 1998).
- Zhang, Lijun, Harry Contopanagos, Nicolaos G. Alexopoulos, and Eli Yablonovitch. "Cavity Backed Antennas with PBG-Like Substrate or Superstrate Materials," IEEE Antennas & Propagation Symposium Proceedings, 1998, 186-189.
- Zhang, Ze and Sashi Satpathy. "Electromagnetic wave propagation in periodic structures: Bloch wave solutions of Maxwell's equations," Physical Review Letters 65: 2650-2653 (19 November 1990).
- , "Analysis of Frequency Selective Layers via a Combined Finite-Element Integral-Equation Method (FE-IEM)," IEEE Antennas & Propagation Symposium Proceedings, 1998, 398-401.

Vita

Capt Karl C. Schloer was born 20 August 1972 in Redlands, California. His family moved to Oregon in 1980 and he graduated from Bend High School in 1989. He earned a Bachelor of Science in Materials Science and Engineering from the Massachusetts Institute of Technology in 1993. His thesis was entitled "Transient Liquid Phase Diffusion Bonding of Ti-6Al-4V Alloy" and his undergraduate record earned him membership in Sigma Xi, the scientific research honor society. Capt Schloer was also a Distinguished Graduate of the Air Force Reserve Officer Training Corps, Detachment 365, at MIT and was awarded a Regular Commission on 28 May 1993.

Capt Schloer completed USAF Intelligence Applications Officer technical training at Goodfellow Air Force Base, Texas in 1994 and proceeded to the 354th Fighter Wing at Eielson Air Force Base, Alaska. There he served as Chief of Intelligence, 355th Fighter Squadron; Chief of Space Applications Training & Integration, 353rd Combat Training Squadron; and Chief of Intelligence Systems, 354th Operations Support Squadron. For his work he was named the 1995 11th Air Force Intelligence Officer of the Year.

In August 1997, Capt Schloer entered the School of Engineering, Air Force Institute of Technology, to begin a Master of Science program in Low Observables. While there, he was inducted into the Tau Beta Pi and Eta Kappa Nu honor societies. Upon graduation on 23 March 1999, he proceeded to the Air Force Research Laboratory's Signature Technology Branch (AFRL/XPN) at Wright-Patterson Air Force Base, Ohio.